INVESTIGATING THE KINETICS OF THYMUS RECOVERY FOLLOWING ACUTE DAMAGE AND BONE MARROW TRANSPLANTATION

by

ABDULLAH SULTAN ALAWAM

A thesis submitted to The University of Birmingham

for the Degree of DOCTOR OF PHILOSOPHY

Institute of Immunology and Immunotherapy

College of Medical and Dental Science

University of Birmingham

January 2021

ABSTRACT

Following ablative therapies used for different diseases such as cancer, damage to the thymus disrupts its ability to support T-cell development. Restoration of thymus function, either endogenously or after transplant, is critical in re-establishing the peripheral T cell compartment. Although the thymus has capability to repair following damage, the ability of the thymus to impose tolerance on newly developing thymocytes is poorly understood. Initially, Sub-Lethal Irradiation (SLI) was used as a model of thymic injury and endogenous thymus regeneration. Post SLI, it was found that the thymus recovers in two distinct phases where an early phase depends upon an intrathymic radioresistant progenitor. Furthermore, analysis of thymic microenvironments revealed that the cTEC compartment was maintained and able to support thymocyte development. However, the mTEC and intrathymic DC compartment were significantly impaired. Consequently, post SLI, Treg selection was reduced and the negative selection process was impaired as revealed by the development of 'forbidden' self-antigen specific thymocytes. Following BMT, cTEC numbers were also maintained while the mTEC and DC compartment sustained long term decline. While conventional $CD4^+$ and $CD8^+$ single positive thymocyte recovery was rapid, the kinetics of medulla-dependent $Foxp3^+$ Treg was slower in comparison. Furthermore, analysis of negative selection through endogenously expressed self-antigens and active Caspase3 expression revealed that negative selection was impaired post BMT. Importantly, transfer of $CD4^+$ thymocytes from BMT mice into nude hosts generated autoimmune symptoms including lymphocytic infiltrates and auto-antibodies. Collectively, these findings indicate that following thymus damage, the thymic microenvironment has differential recovery kinetics that impacts the quality of newly produced T cells, with defects in medullary recovery leading to a loss of immune tolerance and autoimmunity.

<u>**TABLE OF CONTENTS**</u>

LIST OF FIGURES

LIST OF TABLES

ABBREVIATIONS

αβTCR	alpha beta T cell receptor
AIDs	acquired immunodeficiency syndrome
Aire	Autoimmune regulator
APC	Antigen Presenting Cell
APECED	autoimmune polyendocinopathy-candidiasis-ectodermal dystrophy
APS1	Autoimmune polyendocrine syndrome type 1
Atg5	autophagy related gene 5
BM	bone marrow
BMC	bone marrow chimeras
BMSU	Biomedical Service Unit
BMT	bone marrow transplant
BSA	Bovine Serum Albumin
CCL	C-C chemokine ligand
CCR	C-C chemokine receptor
CD	Cluster of differentiation
cDC	Conventional dendritic cell
cDC1	Conventional dendritic cell 1
cDC2	Conventional dendritic cell 2
Cld3	Claudin-3
Cld4	Claudin-4
CLP	Common lymphoid progenitors
CMJ	Cortical medullary junction
CMP	Common myeloid progenitors
CT	Computerized tomography
cTEC	Cortical thymic epithelial cells
CXCL	CXC chemokine ligand
CXCR	CXC chemokine receptor
DC	Dendritic cells
Dex	Dexamethasone
DLL4	Delta like-ligand 4
DN	Double negative
Dox	Doxycycline
DP	Double positive
ETP	Early T-cell progenitors
eYFP	Enhanced yellow fluorescent protein
FCS	Fetal calf serum
Fezf2	FEZ family zinc-finger 2
Foxn1	Forkhead box protein 1
Foxp3	Forkhead box protein 3

Gcm2	Glial cells missing 2
GFP	Green fluorescent protein
H&E	Hematoxylin and Eosin
H2AX	H2A histone family member X
HIV	Human immunodeficiency virus
HSC	Hematopoietic stem cells
ICAM-1	Intracellular adhesion molecule 1
IFNγ	Interferon gamma
IL	Interleukin
IL-R	Interleukin receptor
iNKT	Invariant natural killer T cells
IP	Intraperitoneal
IV	Intravenous
KLF2	Kruppel-like factor 2
LSK	Lineage, stem cell antigen 1, cKit
Ltα	Lymphotoxin alpha
LTβR	Lymphotoxin beta receptor
LTi	Lymphoid tissue induced cells
M1	Mature 1
M2	Mature 2
MHC	Major Histocompatibility Complex
MPP	Multipotent progenitors
mTEC	Medullary thymic epithelial cells
MTS20	Mono clonal antibody 20
MTS24	Mono clonal antibody 24
NFκB	Nuclear factor kappa-light-chain-enhancer
NIK	NFκB inducing kinase
nTreg	Natural T Regulatory
OCT	Optimal Cutting Temperature compound
PBS	Phosphate Buffered Saline
PCR	Polymerase chain reaction
pDC	Plasmacytoid Dendritic cell
PSGL1	P-selectin glycoprotein ligand 1
PVS	Perivascular space
RAG1	Recombination-activating genes 1
RAG2	Recombination-activating genes 2
RANK	Receptor Activator for NF-kb
RBC	Red blood cell
RORγ	Orphan nuclear hormone receptor
RTE	Recent thymic emigrant
S1PR1	Sphingosine 1 phosphate receptor 1
SCZ	Subcapsular zone

SLI	Sublethal irradiation
Sm	Immature stage
SSEA-1	Embryonic stem cell marker
TBI	Total body irradiation
TCR	T cell receptor
TEC	Thymic epithelial cells
TEPC	Thymic epithelial progenitor cells
TGFβ	Transforming growth factor
Th	T helper
TNC	Thymic nurse cells
TNFRSF	Tumor Necrosis Factor Receptor Superfamily
TRA	Tissue restricted antigen
TRECs	T cell receptor excision circles
Treg	T regulatory
TSSP	Thymus specific serine proteases
UEA-1	Ulex europeaus agglutin 1
VCAM-1	Vascular adhesion molecule 1
VDJ	Variable diversity and joining
WT	Wildtype
XCL1	X-C chemokine ligand 1

1 CHAPTER 1: INTRODUCTION

1.1 Immune System Overview

1.1.1 T-cells and Their Response

As part of the adaptive immune response, αβT-cells play an important part in recognizing and targeting foreign pathogens. Following their development in the thymus and entry into the bloodstream, αβT-cells travel to, and recirculate within secondary lymphoid tissues that include spleen and lymph nodes. Those αβT-cells that do not encounter specific foreign antigens recirculate between blood and lymphoid tissues via lymphatics and are termed naïve αβT-cells. Once antigen is presented to antigen-specific αβT-cells as peptide fragments bound to either MHC class I or MHC class II complexes by antigen presenting cells (APCs), αβTCR signaling, together with co-stimulation, results in proliferation and differentiation to an effector stage where antigen-specific αβT-cells can participate in an immune response. This differentiation process can give rise to multiple kinds of functional effector T-cells, including Th1 and Th2 cells that secrete specific cytokines and acquire specific effector functions that depend on the type of antigen being recognized (Otagiri *et al.*, 2017).

1.1.1.1 CD4 αβT-cells and Subsets

CD4 αβT-cells recognize antigen presented by MHC class II (MHCII) molecules can differentiate into different effector types that include different T helper (Th) subsets such as Th1, Th2, and Th17. The different Th classes define the specific functional direction the αβT-cell takes. For a Th1 phenotype, αβT-cells produce interferon γ (IFNγ) and production of this cytokine is controlled by expression of the transcription factor T-bet (Szabo *et al.*, 2000). In contrast, expression of the transcription factor GATA-3 is associated with differentiation towards a Th2 subset that is defined by the production of IL-4. The Th17 phenotype, defined by IL-17 production, is associated with RORγt expression, with differentiation into the

phenotype requiring co-exposure to Transforming Growth Factor β (TGFβ) as well as IL-6 (Zhu and Paul, 2008). In addition to Th1, Th2 and Th17 subsets, CD4 αβT-cells also include a T regulatory (Treg) subset. Functionally, Treg act as a regulator that suppress self-reactive immune responses. While Treg can be both generated in the periphery from naïve T cell (induced Treg), perhaps the most well-defined subset is natural Treg that are generated intrathymically during T-cell development. Natural Treg (nTreg) express the Forkhead box protein 3 (Foxp3) transcription factor that distinguishes them from other CD4 αβT cell subsets. (Chen *et al.*, 2003; Vignali, Collison and Workman, 2008). Unlike conventional T cell development, nTreg are dependent on the medulla for selection and development through the precursor population present in the thymus (Cowan *et al.*, 2013).

1.1.1.2   CD8 T-cells

Unlike CD4 T-cells, CD8 T-cells recognize antigen presented by MHC class I (MHCI). Once activated the cells take on a cytotoxic effector T-cell phenotype and are able to identify and kill infected cells. As with CD4 αβT-cells, CD8 αβT-cell activation involves both αβTCR-peptide/MHC interactions and costimulatory interactions (e.g., CD28-CD80/CD86) with dendritic cells. This initiates cellular expansion and differentiation towards a CD8 effector phenotype (Obar and Lefranois, 2010), which allows antigen-specific cells to travel to sites of infection, where they produce cytokines such as IFNγ and TNFα, and secrete cytolytic factors such as Granzyme B and perforin that target infected cells (Bannard, Kraman and Fearon, 2009)

1.1.1.3   T-cell Activation

The T-cell activation process is governed by antigen presentation in the form of MHC/peptide complexes. αβT-cells do not bind antigen alone, but instead utilize their αβT-cell receptors

(αβTCR) to identify antigen fragments presented by the MHC complexes. As previously stated, CD4 T-cells recognize MHCII molecules, while CD8 T-cells recognize MHCI molecules (Otagiri *et al.*, 2017). When patrolling T-cells encounter APCs, if αβTCR-foreign peptide/MHC interactions occur alongside CD28-CC80/CD86 co-stimulation, this triggers the differentiation and expansion process into T helper subsets for CD4 αβT-cells and cytotoxic phenotype for CD8 αβT-cells.

1.2   T-cell Development

1.2.1   Thymus Development and Overview

The thymus stems from two components: the third pharyngeal pouch endoderm that gives rise to thymic epithelial cells (TEC) and neural crest derived mesenchyme. Thymus development is closely related to that of the parathyroid glands, as both organs develop from the primordia of the pharyngeal pouch. As the separation of the thymus occurs from the parathyroid, the thymus moves to the anterior chest cavity with aid of neural crest cells to form a distinct bilobed organ (Blackburn and Manley, 2004). Having these two organs rise from common primordia, thymus identity has been suggested to be marked by expression of the forkhead transcription factor 1 (Foxn1), while Glial cells missing 2 (Gcm2) is expressed in a complimentary fashion that marks the parathyroid (Gordon *et al.*, 2001).

The thymus is a primary lymphoid organ that functions within the immune system by supporting the development of naïve αβT-cells and their export into the periphery. The thymus is dependent on continuous seeding of lymphoid precursors to support new cohorts of αβT-cell development. Lymphoid precursors are generated in the bone marrow (BM) and migrate to the thymus to undertake differential developmental steps. The important role of thymus in the

immune system was highlighted in the early 1960s, where surgical removal of the thymus in neonatal mice resulted in lymphocyte depletion was observed alongside increased mortality caused by an inability to fight infections (Miller, 1961).

1.2.2   Progenitor Colonization and Lineage Commitment

As the thymus lacks self-renewing stem cells that can be used to generate new cohorts of αβT-cells, it is dependent on colonization from bone marrow (BM) precursors. Hematopoietic stem cells (HSCs) that reside in the BM have the ability to differentiate into all different blood cell lineages. Downstream of HSCs, multiple immature progenitors exist, including Lineage⁻ Scal1⁺cKIT⁺ LSK cells. Some LSK cells also express FLT3 and are commonly known as multipotent progenitors (MPP) that lack self-renewing ability and are able to differentiate into common myeloid progenitors (CMP) and common lymphoid progenitor (CLP). CLPs express high levels of both FLT3 and IL-7Ra and have the ability to give rise to T and B cells (Bhandoola and Sambandam, 2006). Despite an understanding of haemopoietic progenitors in the bone marrow, the nature of thymus colonising lymphoid progenitors remains unclear. However, early T-cell progenitors (ETP) are generally accepted as the earliest lymphoid progenitors that reside in the thymus, and their frequencies are used as a surrogate for thymus colonization (Allman *et al.*, 2003) (Benz *et al.*, 2008). Following their entry into the thymus, the commitment of lymphoid progenitors to the T-cell lineage is mediated by the Notch signaling pathway. The importance of this was shown by inactivation of Notch1 function in neonatal mice that showed severe loss of thymocytes. In addition, reconstitution of lethally irradiated mice with Notch1 deficient BM resulted in a block of early T cell development but spared other lineages (Radtke *et al.*, 1999).

In relation to mechanisms of thymic colonisation, studies have suggested that chemokine receptor activity is critical for the selective entry of lymphoid progenitors into the thymus. For example, C-C chemokine receptor type 9 (CCR9) and 7 (CCR7) and CXCR4 have all been shown to play a role in the regulation of progenitor entry (Calderón and Boehm, 2011). For example, CCR7 has been shown to be selectively expressed on thymus colonizing progenitors, and CCR9/CCR7 double deficient mice express a phenotype in which ETP are significantly reduced (Liu *et al.*, 2006; Zlotoff *et al.*, 2010). Embryonic mice that lack CCR9/CCR7/CXCR4 show a further reduction in thymus colonisation (Calderón and Boehm, 2011). However, progenitors still colonise the thymus under these conditions, raising the possibility of additional chemokine receptors and/or mechanisms. For example, thymic endothelium expresses P-selectin, and lymphoid progenitors express P-selectin glycoprotein ligand 1 (PSGL1) that binds P-selectin. Mice deficient in PSGL1 were shown to have reduced ETP, suggested as a consequence of reduced progenitor entry (Rossi *et al.*, 2005). Having highlighted the importance of the thymic endothelium and its role in the regulation of progenitor entry, a specific type of thymic endothelial cell, known as thymic portal endothelial cells, has recently been identified. Lymphotoxin beta receptor (LTβR) has been implicated in regulating thymic portal endothelial cells and mice deficient in LTβR have reduced ETP (Shi *et al.*, 2016). LTβR regulation of progenitor entry to thymus also extends to expression of adhesion molecules such as intracellular adhesion molecule 1 (ICAM-1) and vascular adhesion molecule 1 (VCAM-1). LTβR deficient mice show decreased expression of these adhesion molecules within the thymic endothelium and as a result reduced ETP in the steady state. Importantly, in a bone marrow transplant (BMT) setting, exogenous antibody-mediated stimulation of LTβR improved thymus recovery and increased expression of VCAM1 and ICAM1 (Lucas *et al.*, 2016). All together,

these studies highlight different mechanisms that regulate thymus colonization to ensure proper T-cell development.

1.2.3   ETP and DN Population Transition

ETP are identified by their expression of cluster of differentiation (CD) markers. Phenotypic characterization of ETP shows that they are CD4$^-$CD8$^-$ and subsequently are termed double negative (DN). This population can be subdivided by their differential expression of CD44 and CD25. DN1 cells, classified by their expression of CD44, are a heterogenous population and have the ability to give rise to different cells types that include T-cells, B-cells, and dendritic cells (DC) (Shah and Zúñiga-Pflücker, 2014). Further characterization of the DN1 populations can be seen by the differential expression of CD24 and CD117. The DN1 population can be split into five subsets, where cells that express CD117 are known to be particularly effective $\alpha\beta$T-cell progenitors (Porritt *et al.*, 2004). DN1 cells then transit to the DN2 stage defined by co-expression of CD44 and CD25. Similar to DN1, DN2 can be further split into 2 different populations, DN2a and DN2b. While DN2a can give rise to DC, the DN2b have lost that potential (Masuda *et al.*, 2007). Transition from DN2 to DN3 is defined by loss of CD44 as well as successful rearrangement of the TCRβ chain (Dudley *et al.*, 1994). This process is accomplished by the generation of Variable, Diversity, and Joining, V(D)J, segments and is mediated by the recombination-activating genes 1 and 2 (RAG1 and RAG2) (Shinkai *et al.*, 1992). Following successful TCRβ chain rearrangement, cells express the pre-TCR at their cell surface. This consists of TCRβ, preTα and CD3 components, and signaling through this complex triggers proliferation together with downregulation of CD25, TCRα chain rearrangement, and expression of both CD4 and CD8 that results in the formation of CD4$^+$CD8$^+$ to transition to the double positive (DP) thymocytes (Fehling *et al.*, 1995). In

contrast, thymocytes that fail to rearrange TCRβ successfully cannot express the pre-TCR, and are directed towards apoptosis (Falk *et al.*, 2001).

ETP entry to thymus has been investigated and in adult mice this is thought to occur at the cortico-medullary junction. Following this, some evidence suggests that ETP undergo the differential transition stages, and at each stage travel through the cortical regions of the thymus to reach the subcapsular zone (SCZ) (Lind *et al.*, 2001). Migration of developing thymocytes through different cortical regions is mediated by CXC chemokine ligand 12 (CXCL12) that binds the receptor CXC chemokine receptor 4 (CXCR4). Expression of CXCR4 is crucial for successful DN transition as it was shown that CXCR4 deletion in thymocytes results in a block at the DN stage (Plotkin *et al.*, 2003). During these DN stages and their movement across the cortex, immature thymocytes proliferate extensively which is a process mediated by Notch and Interleukin 7 (IL-7) signaling (Balciunaite *et al.*, 2005). In addition, CXCR4 has also been shown to act in concert with the pre-TCR, where it acts as a costimulatory molecule required for transition to the DP stage (Janas *et al.*, 2010; Trampont *et al.*, 2010).

1.2.4   Positive Selection

After rearrangement of TCRα chain and following β selection, the TCRα and TCRβ chain pair to generate a functional αβTCR. It is following this process that the DP undergo a process known as positive selection in the cortical region of the thymus. DP migrate from the SCZ and distribute randomly with in the cortical region. Indeed, studies have shown that although DP are confined to the cortical region of the thymus, they are able to move freely within this region. This free movement allows DP thymocytes to engage with other cell types in the cortex (Bousso *et al.*, 2002). In the cortex, DP thymocytes interact with cortical thymic epithelial cells (cTEC;

will be discussed in detail in section 1.3.2) that express MHCI and MHCII molecules. The functional αβTCR generated will be tested for affinity and those cells that are not capable of TCR-MHC interactions will undergo death by neglect (Dzhagalov and Phee, 2012). This is a fundamental process in development, as ensures that newly generated αβT-cells are biased towards MHC recognition and are able to respond to antigen presentation by MHC complexes in the periphery. As a result of positive selection, successful TCR-MHC interactions result in downregulation of Rag1 and Rag2 expression, which prevents further TCR rearrangement (Brandle *et al.*, 1992). Furthermore, it has been suggested that orphan nuclear hormone receptor (RORγ) mediates this process as DP thymocytes express RORγ which in turn activates anti-apoptotic factor, Bcl-xL. Indeed, mice deficient for RORγ show no expression of Bcl-xL and thus suggesting that RORγ regulates survival of DP population (Sun, Unutmaz and Zou, 2000).

Lineage commitment to either the CD4 or CD8 phenotype is the result of the positive selection process. DP thymocyte interactions with cTEC that involve MHCII will lead to developing thymocytes acquiring a CD4 phenotype, while interactions with MHCI will eventually result in a CD8 phenotype. The mechanism that explains the process of commitment to either the CD4 or CD8 lineage remain incompletely understood. However, there is currently evidence for a model in which αβTCR signaling results in the generation of CD4 SP thymocytes, irrespective of whether the αβTCR was ligated by MHCI or MHCII. Following this, further recognition of MHCII then re-enforces the CD4 SP phenotype, while recognition of MHCI results in co-receptor reversal, and the re-expression of CD8 which generates DP thymocytes that ultimately downregulate CD4 to become MHCI-restricted SP8 cells (Singer, 2002). Following TCR engagement and commitment to either the CD4 or CD8 phenotype, thymocytes upregulate their expression of CCR7 to begin their migration towards the medullary region of the thymus for

further development. This is an essential process as the next step in T-cell development is the negative selection process that occurs in the medulla region of the thymus. The importance of this process was shown by analysis of mice deficient in CCR7, where the accumulation of mature SP thymocytes in the cortical region of the thymus is accompanied by a failure in T-cell tolerance (Ueno *et al.*, 2004; Kurobe *et al.*, 2006; Nitta *et al.*, 2009).

1.2.5   Negative Selection

The random rearrangement of TCRα and TCRβ genes generate a diverse range of specificity among the developing thymocytes. While this is beneficial for the generation of a diverse repertoire it does not select for cells that are only capable of recognizing foreign antigenic peptides. Thus, the negative selection process that occurs in the medulla region of the thymus acts to ensure that the developing thymocytes do not initiate self-reactive immune responses against self-tissue. This process is mediated by the interactions of the newly committed CD4 or CD8 cells that have migrated from the cortex to the medulla with medullary thymic epithelial cells (mTEC; **will be discussed in detail in section 1.3.3**), and dendritic cells (DC). Here, mTEC act as effective antigen presenting cells (APCs) to test the affinity of the TCR for self-antigens. mTEC can screen the developing SP thymocytes in several ways. For example, while mTEC have the ability to autonomously present self-antigens they have themselves produced, mTEC-derived antigens can also be cross-presented by nearby DC that play a role in negative selection (Klein *et al.*, 2014).

Interestingly, while cTEC have been mainly implicated in facilitating the positive selection process, studies have shown the negative selection and clonal deletion can also occur within the thymic cortical region. Indeed, a study by McCaughtry et al. showed using the HY[cd4] model

where negative selection occurs at the DP thymocyte stage, clonal deletion occurs within the cortex to ubiquitous self-antigens (McCaughtry *et al.*, 2008). Furthermore it was shown that cells undergoing clonal deletion through their identification by Caspase-3 expression localized within cortical regions (McCaughtry *et al.*, 2008). Additionally, in a different study where transgenic mice that responded to antigens under the K14 promoter were used to study clonal deletion, it was shown that clonal deletion occurred even if antigen presentation was restricted to cTEC, thus suggesting that cTEC play a role in the negative selection process (Mayerova and Hogquist, 2004). Altogether, these studies highlight that negative selection is not limited to medullary regions and can occur within the thymic cortex.

TCR signals that have high affinity interactions with self-peptide are directed towards apoptosis. This is to ensure that potential self-reactive cells do not escape into the periphery. A pathway that is suggested to initiate programmed cell death in negative selection is Bim, which is part of the pro-apoptotic Bcl-2 family. It was shown that high TCR affinity resulted in the upregulation of Bim which in turn inhibited Bcl-xL. In a transgenic mouse model that expressed high TCR affinity towards self-peptide, the deficiency of Bim resulted in inability to kill the autoreactive cells (Bouillet *et al.*, 2002). However, deficiency in Bim alone did not result in autoimmune disease, suggesting that other molecules play a critical role in apoptosis during negative selection. In support of this, mice deficient in both Bim and Puma showed signs of autoimmunity as well as an accumulation of mature thymocytes, suggesting an impairment in negative selection (Gray *et al.*, 2012).
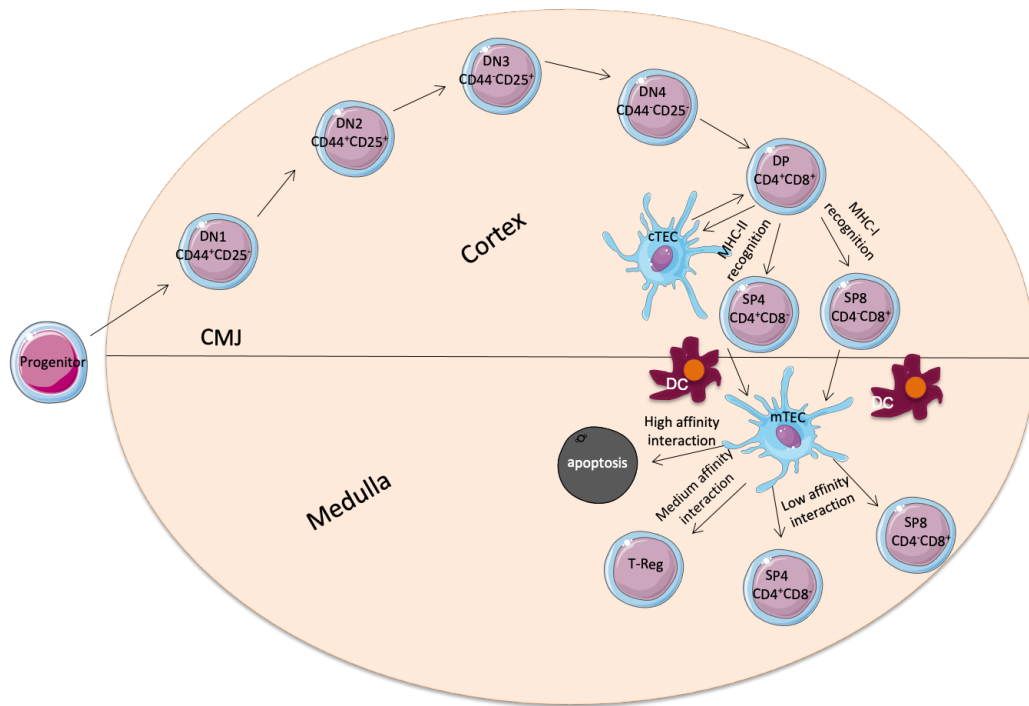
Figure 1.1. T cell Development.

Progenitors colonise the thymus and enter at the CMJ to undergo T cell development. Migration of progenitors to the cortical region to undergo differential maturational steps based on their expression of CD44 and CD25. Following rearrangement of TCR genes during the DN stages, thymocytes upregulate CD4 and CD8 and become DP thymocytes. DP thymocytes then interact with self-peptides in the form of MHC complexes presented by cTEC to undergo positive selection. Following successful positive selection, thymocytes transition to become either CD4$^+$ or CD8$^+$ thymocytes and upregulate CCR7 to enter the medulla. Upon entry to the medulla, thymocytes interact with mTEC to facilitate negative selection. Thymocytes that have low affinity to self-peptide continue maturation while thymocytes that have high affinity binding to self-peptides are directed towards cell apoptosis. Thymocytes that have medium binding affinity are directed towards a Treg phenotype.

1.2.6 Thymus Egress

Following thymic selection, developing thymocytes require further maturation to acquire a phenotype that will allow them to egress from the thymus into the periphery. These phases can be subdivided on the basis of expression of CD69 and CD62L. SP thymocytes that are still egress incompetent are $CD69^+$ while those that are more mature and represent egress competent cells are $CD62L^+$. Thus, immature thymocytes are phenotypically characterized as $CD69^+CD62L^-$, while mature thymocytes are $CD69^-CD62L^+$. Other studies have shown that SP thymocytes can be divided into three stages with expression markers of CD69, CD62L, and MHCI. The least immature stage, termed SM, have a $CD69^+MHCI^-$ phenotype. The second stage can be defined as double positive for CD69 and MHCI and are termed mature 1 (M1) (Xing *et al.*, 2016). The final stage is determined by the loss of CD69 expression and continued expression of MHCI and are termed mature 2 (M2). Further maturation markers were investigated, such as Kruppel-like factor 2 (KLF2) and sphingosine 1 phosphate receptor 1 (S1PR1) which are known to be required for thymocyte egress from the thymus. Unlike SM and M1, the M2 population expressed high levels of S1PR1 and KLF2, suggesting M2 represent egress-competent SP thymocytes (Xing *et al.*, 2016).

In relation to mechanisms of egress, S1P is the ligand for the G protein-coupled receptor that is expressed on SP thymocytes. Blood concentrations of S1P are high and it is thought that mature SP thymocytes migrate towards the S1P gradient following S1PR1 expression. This was demonstrated when S1PR1 was specifically deleted on T-cells which resulted in block of mature cells from leaving the thymus into the periphery (Allende *et al.*, 2004). Further studies have been conducted to explain the mechanism governing T-cell egress. The type 2 IL-4R complex is expressed by stromal cells within the thymus. IL-4Rα, which is a component of this receptor, has been shown to mediate thymus egress in a process that is independent from the

S1PR1 mechanism. IL-4Rα deficiency resulted in the accumulation of mature cells and reduced number of cells in the periphery. Furthermore it was shown that iNKT cells provide the IL-4 and IL-13 ligands that initiate this signaling pathway, thus implicating iNKT cells in the control of thymus egress (White *et al.*, 2017).

LTβR has also been implicated in the regulation of thymocyte egress by the control of mature cell entry into the perivascular space (PVS) (Boehm, Scheu, Pfeffer and Conrad C Bleul, 2003). Additionally, it was suggested that the process of thymus egress is not random and instead is controlled by LTβR which allows only the most mature SP thymocytes to leave the thymus (James *et al.*, 2018). Here, three populations of CD62L$^+$ CD4 SP were described; M2a that expressed low levels of CD62L, M2b that expressed intermediate levels of CD62L, and finally M2c that expressed high levels of CD62L. Using Rag2GFP mice as a molecular timer to define which cells had spent the longest in the thymus (Boursalian *et al.*, 2004) it was shown that M2a had the highest level of GFP and M2c had the lowest with in this group. In contrast, S1PR1 expression was highest on the M2c population, however the M2a and M2b populations did also express levels of S1PR1(James *et al.*, 2018). Moreover, analysis of cells that resided in the PVS following iv injection of anti-CD4, showed that these cells were biased towards M2c, indicating a conveyor belt mechanism of thymus emigration, which biases thymus migrants towards the most mature cells.

1.3 Thymic Microenvironment

1.3.1 Development of Thymic Epithelial Cells

The thymic microenvironment has an essential role in the function of the thymus and in the support of T-cell development. This microenvironment is composed of multiple cell types that aid in the development process, and in this thesis the focus will be on thymic epithelial cells (TEC). The TEC population is composed of cortical TEC (cTEC) and medullary TEC (mTEC) that support T-cell development and regulate positive and negative selection in the different regions of the thymus as discussed earlier. The location of the cTEC and mTEC is distinct, as cTEC are confined to the cortex region of the thymus, while mTEC are found in the medulla. While both types are anatomically different, they possess shared expression of markers such as MHCI and MHCII. cTEC and mTEC are also identified by their differential expression of multiple markers: cTEC express Ly51, cytokeratin 8, CD205, and β5t, and mTEC are identified by the expression of cytokeratin 5, Ulex europeaus agglutinin 1 (UEA-1), and ER-TR5. Furthermore the mTEC population can further subdivided by the expression of MHCII, CD80 and Aire that identifies heterogeneity within the mTEC population (Alves *et al.*, 2014; Sansom *et al.*, 2014; Bornstein *et al.*, 2018).

During thymus organogenesis TEC are generated from third pharyngeal pouch endoderm (Blackburn and Manley, 2004). Around Day 12 of gestation, an influx of hematopoietic precursors into the thymus shapes and influences the thymic epithelial microenvironment and TEC developmental pathways are initiated. This is facilitated by Foxn1, which facilitates the differentiation and growth of TEC. The importance of Foxn1 is seen in studies of Foxn1 deficient nude mice, where there is a failure of thymus development without the impairment in attracting bone marrow derived cells (Blackburn *et al.*, 1996; Balciunaite *et al.*, 2002; Hetzer-Egger *et al.*, 2002). In the embryonic thymus, the two different primary types of TEC are known

to arise from a common progenitor that is dependent on Foxn-1 expression (Bleul *et al.*, 2006). In agreement with this, single eYFP^{+} cells from E12 thymus lobes were shown to generate both cTEC and mTEC (Rossi *et al.*, 2006). However, it was also shown that Foxn-1 deficient mice contain thymic epithelial progenitor cells (TEPC), but these cells cannot differentiate into further developmental stages. It was also suggested that Foxn-1 does not determine the fate of the cell, but is involved in the latter stages of differentiation into either cTEC or mTEC (Nowell *et al.*, 2011). While the phenotype of bipotent TEPC is not fully clear, earlier studies have shown that they may be identified by their expression of MTS20 and MTS24. Here, purification and grafting of MTS20^{+}MTS24^{+} TEC from embryonic mice into nude mice showed they could differentiate into both types of TEC, suggesting that the initiation of the TEC development occurs from a single TEPC type (Bennett *et al.*, 2002; Gill *et al.*, 2002). Interestingly, later studies suggested that TEPC also expressed cTEC markers. For example, CD205^{+} embryonic TEC developed into both cTEC and mTEC progeny (Baik *et al.*, 2013). Similarly, IL-7YFP^{+} cells with a cTEC phenotype generated cTEC and mTEC (Alves *et al.*, 2009), while fate mapping studies with β5t-cre transgenic mice showed essentially all TEC arise from a β5t[+] progenitor (Ohigashi *et al.*, 2013). This model of development is referred to as the "serial progression model" where both cTEC and mTEC arise from a common cell type with cTEC features (Alves *et al.*, 2014).

The existence of cTEC-like bipotent progenitors has limited the ability to definitely identify and study the cTEC development pathway. Interestingly however cTEC maturation can be distinguished by the expression of CD40 and MHCII, and cTEC-like progenitors may lack expression of these markers (Shakib *et al.*, 2009). Importantly, it is not clear whether such a pathway exists in the adult thymus, as most of the studies described above focus on embryonic

thymus. Interestingly, it was observed that in a young mouse, β5t cTEC that were positioned near the CMJ can give rise to the mTEC population (Mayer *et al.*, 2016), suggesting that β5t[+] cTEC can serve as precursors for mTEC in the postnatal thymus. This was confirmed through the generation of β5t reporter mice where β5t[+] cTEC were identified as ZsGreen[+] and grafting of ZsGreen[+] cTEC under the kidney capsule resulted in ZsGreen[+] mTEC (Mayer *et al.*, 2016). Similarly, in a mouse model where doxycycline (Dox) induces EGFP expression in β5t expressing cells (Ohigashi *et al.*, 2015) , it was suggested that the maintenance of the mTEC population through adulthood is achieved by a β5t[+] neonatal progenitor. In contrast, the cTEC population is thought to be maintained for non-β5t expressing progenitor, as a big percentage of the cTEC population did not express EGFP (Ohigashi *et al.*, 2015) .

Studies have also examined stages in TEC development downstream of bipotent progenitors. Evidence for Claudin-3 and claudin-4 (Cld3,Cld4) expression in mTEC restricted progenitors suggests a route of development for mTEC that is unipotent and is able to only maintain the mTEC population (Hamazaki *et al.*, 2007). Indeed, isolation and grafting of Cld3/4[+] embryonic TEC into nude mice specifically generated mTEC clusters, identifying this subset as an mTEC progenitor population (Hamazaki *et al.*, 2007). This was further expanded to identify a population that expressed the embryonic stem cell marker (SSEA-1) that was also Cld3/4[+] which was found to be self-renewable and able to maintain the mTEC population postnatally. Interestingly, these mTEC progenitors were found to decrease in wild type (WT) mice when compared to *Rag2* deficient mice, suggesting that T-cell development contributes to this decrease (Sekai, Hamazaki and Minato, 2014).

Furthermore, the Cld3/4$^+$ mTEC progenitor population was found to be dependent on NFκB signaling for their differentiation capability. Thus, aly/aly mice (deficient in NFκB-inducing kinase NIK) and *Traf*6 were shown to lack Cld3/4$^+$ progenitor cell at the embryonic stage (Hamazaki *et al.*, 2007). Interestingly, and in support of a role for NFκB signaling in mTEC development, multiple members of the Tumor Necrosis Factor Receptors superfamily (TNFRSF) have been shown to have mTEC defects. For example, Relb$^{-/-}$ mice lack mTEC (Burkly *et al.*, 1995; Weih *et al.*, 1995), while RANK$^{-/-}$ mice (Rossi *et al.*, 2007; Akiyama *et al.*, 2008; Hikosaka *et al.*, 2008) and LTβR$^{-/-}$ mice has reduced mTEC numbers. Regarding RANK, further heterogeneity was found within the Cld3/4$^+$ progenitor population where they can be split on the basis of RANK expression in RANK^{Venus} reporter mice. This phenotypical analysis identified a progenitor population that resided with in Cld3/4$^+$ cells that lacked the expression of SSEA-1 but expressed RANK, perhaps identifying a stage of mTEC development that is downstream of SSEA-1$^+$ Cld3/4$^+$ progenitors. Furthermore, RANK$^+$ progenitor cells depend on Relb for their emergence, as Relb$^{-/-}$ mice showed a complete absence of RANK^{Venus+} progenitors but retained normal numbers of the SSEA-1$^+$ progenitors (Baik *et al.*, 2016).

For LTβR involvement in mTEC development, initial studies demonstrated a significant reduction in mTEC in germline LTβR$^{-/-}$ mice (Boehm *et al.*, 2003). More recent studies using Foxn1^{Cre} (Cosway *et al.*, 2017) or K14^{Cre} (Wu *et al.*, 2017) have shown that LTβR expression by TEC is directly involved in regulation of their numbers. Significantly, the numbers of Cld3/4$^+$SSEA-1$^+$ mTEC progenitors in the neonatal stage of development was also found to be reduced when LTβR expression was targeted with K14^{Cre,} suggesting that LTβR plays a role not only in maintenance of mTEC progenitors (Wu *et al.*, 2017).
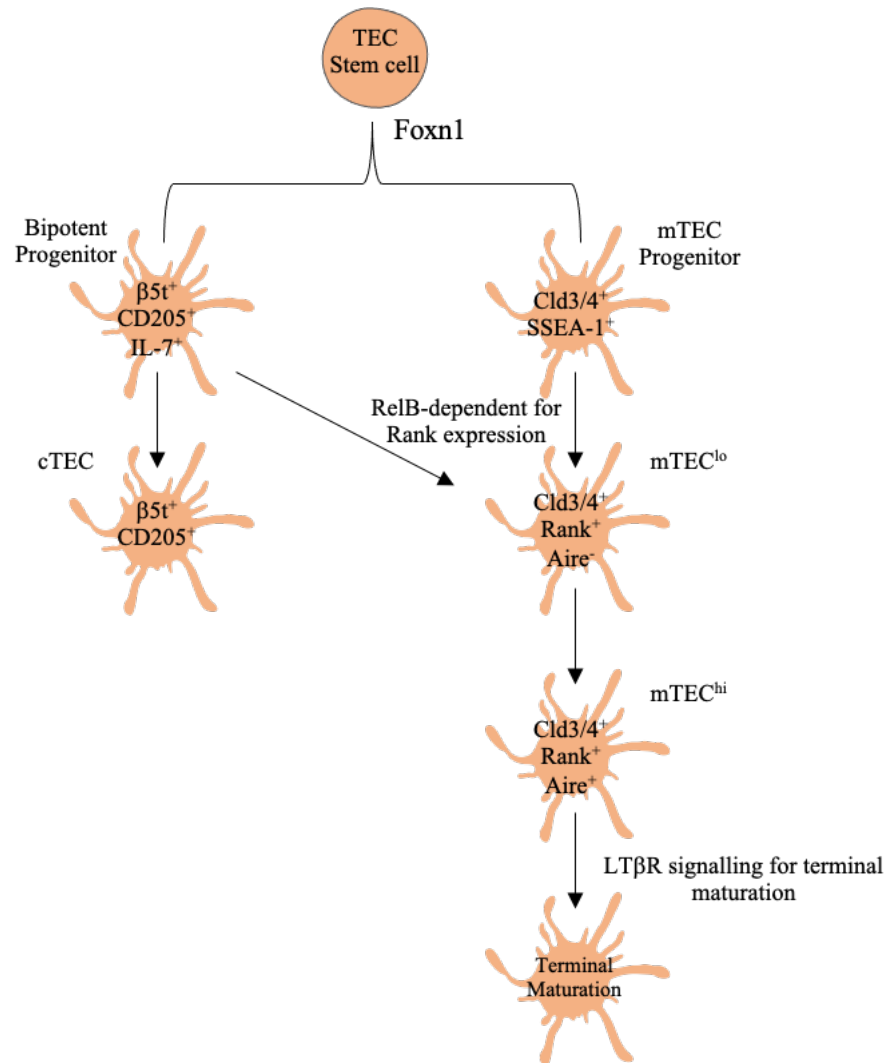
Figure 1.2. Thymic Epithelial Cell Development.

Thymic epithelial cell development occurs with a TEC progenitor that expresses the transcription factor Foxn1. Development can then occur through two pathways. A bipotent TEC progenitor maturates into either mature cTEC and mTEC progenitor. Similarly, an mTEC progenitor also drives mTEC development where it develops into mTEC^{lo}. The mTEC^{lo} population develops into mTEC^{hi}. However, following terminal differentiation mTEC^{hi} become mTEC^{lo} suggesting that not all mTEC^{lo} develop into mTEC^{hi}.

1.3.2   Function of Cortical Thymic Epithelial Cells (cTEC)

As discussed in section 1.2.4, cTEC play an essential role in the positive selection process by screening developing thymocytes to ensure that they have a functional αβTCR that is able to recognize MHC-peptide complexes. A critical aspect of cTEC function has recently been shown to involve their specialized antigen processing properties. For MHCI recognition, this is accomplished by cTEC specific expression of the β5t proteasomal subunit encoded by *Psmb11* (Murata *et al.*, 2007). Indeed, it was shown that β5t deficient mice have a defect in CD8$^+$ αβT-development in the thymus, identifying this molecule as a key regulator of cTEC function (Murata *et al.*, 2007). For MHCII recognition, cTEC also express cathepsin L and thymus specific serine proteases (TSSP) which have been implicated in the generation of the peptide fragments presented by the MHC II on cTEC during the positive selection of CD4$^+$ T-cells. Cathepsin L deficient mice display a phenotype that shows reduced CD4$^+$ T-cell selection and no impairment in the CD8$^+$ T-cell selection. In agreement with this, the generation of bone marrow chimaeras using WT bone marrow and lethally irradiated Cathepsin L deficient hosts showed that CD4$^+$ T-cell selection was significantly impaired, highlighting the need for Cathepsin L expression by radioresistant stroma, likely TEC (Honey *et al.*, 2002).

Interestingly, cTEC may function during positive selection by engulfing of DP thymocytes, which results in the formation of multi-cell complexes termed thymic nurse cells (TNC). This occurs by the formation of complexes between the epithelial cell and the thymocyte that allows for the engulfment of the developing thymocyte to facilitate further differentiation (Wekerle, Ketelsen and Ernst, 1980) . However recent research have proposed that TNC and this mechanism of positive selection allows the developing DP that is undergoing positive selection to undergo secondary TCR rearrangements, which may enhance opportunities for the selection

process (Nakagawa *et al.*, 2012). Again in relation to the role of cTEC in positive selection, cTEC express CD83, which regulates the ubiquitin ligase MARCH 8 which in turn regulates expression of MHCII on TEC. MARCH 8 deficient mice have elevated cTEC expression of MHCII, yet CD4^{+} T-cell numbers are unaffected (Liu *et al.*, 2016). In the same study, a mutated form of CD83 was expressed that resulted in impaired CD4^{+} T-cell selection that could be rescued by MARCH 8 deletion. This data suggests that regulation of CD4^{+} T-cell selection can be maintained by the regulation of MHC-II complexes through MARCH 8 and CD83 expression (Liu *et al.*, 2016). cTEC function and its regulation in the selection of CD4+ T-cells can also occur through formation of autophagosomes, and this process has been shown to be a mechanism for MHCII loading. Indeed, it was shown that autophagy related gene 5 (Atg5) deficient mice show a reduction in CD4^{+} T-cells in MHCII restricted TCR transgenic mice. However, this deficiency also led to decreased TRA expression that contributed to manifestations of autoimmunity. This data suggests that the process of autophagy plays a role in cTEC function but it is not an exclusive mechanism to cTEC (Nedjic *et al.*, 2008).

cTEC function can also extend to developmental stages that occur prior to the positive selection process. cTEC express the Notch ligand delta-like ligand 4 (DLL4) that aids in the commitment of lymphoid progenitors to the T-cell lineage by the progenitor cell. Thus, the specific deletion of DLL4 in TEC using Foxn1[Cre] resulted in an early block in T-cell development and the increased presence of immature B cells in the thymus (Koch *et al.*, 2008). Interestingly, it has been proposed that thymocytes regulate the expression of DLL4 by cTEC to maintain and facilitate thymopoiesis (Fiorini *et al.*, 2008). Indeed, it was shown that during the neonatal period, expression of DLL4 on cTEC was significantly higher than in adult age. This could be because thymocyte expansion in the neonatal period is at its peak, while during the adult age it

has reached equilibrium and these interactions regulate the DLL4 expression by cTEC (Fiorini *et al.*, 2008).

CXCR4 is a chemokine expressed by majority of progenitors in the cortex of the thymus, and it was shown that its ligand, CXCL12, is expressed by cTEC (Plotkin *et al.*, 2003) . CXCL12 plays an important role in directing the entering progenitors through the cortex for further development. Indeed, it was shown that after targeted deletion of CXCR4 on thymus progenitors, progenitors were found to be immobile and stuck at the CMJ. This provides evidence that CXCL12 allows progenitors to migrate through different cortical regions for further development, as CXCR4 deficient progenitors were not able to differentiate into the DP or SP progeny (Plotkin *et al.*, 2003). Furthermore, the CXCR4-CXCL12 signaling pathway has also been implicated in survival of DN thymocytes (Janas *et al.*, 2010). Cultured sorted DN3 thymocytes were unable to differentiate into DP thymocytes in the presence of the CXCR4 antagonist, AMD3100. The number of recovered DP thymocytes following three days of culture was reduced, suggesting that CXCR4/CXCL12 play a role in the differentiation and proliferation of developing thymocytes (Janas *et al.*, 2010). Interestingly, the role of CXCR4/CXCL12 in the maturation of thymocytes is not essential after the DN stages, as loss of CXCR4 on DP thymocytes shows normal development and correct localization (Lucas *et al.*, 2017).

1.3.3 Function of Medullary Thymic Epithelial Cells (mTEC)

mTEC are confined to the medulla region of the thymus, an area that is required for the negative selection process and central tolerance induction. As previously mentioned, unlike cTEC, mTEC can be separated into subsets based on expression of MHCII and CD80 into mTEC^{lo} and mTEC^{hi}. Thus, mTEC^{lo} are identified as CD80$^-$MHCII^{lo} and the mTEC^{hi} are identified as

CD80$^+$MHCII^{hi}. The mTEC^{hi} subset in particular has been shown to play an important role in the process of negative selection and central tolerance induction. This involves their ability to support a process termed promiscuous gene expression, that allows the mTEC population to express a vast array of tissue restricted self-antigens (TRA) (Derbinski *et al.*, 2001). The ability of mTEC to express TRA to screen newly produced T-cells before thymus egress is controlled at least in part by Aire, which in thymus is only expressed in the mTEC^{hi} population (Anderson *et al.*, 2002). In humans, mutations in Aire result in a multiorgan autoimmune disease termed APS1 or APECED (Nagamine *et al.*, 1997; Wang *et al.*, 1999). Furthermore, mice deficient in Aire also exhibited autoimmune disease with a reduction in peripheral antigen presentation by mTEC (Anderson *et al.*, 2002; Gavanescu *et al.*, 2007; Meredith *et al.*, 2015; Oftedal *et al.*, 2015). Interestingly, while there is strong evidence that Aire plays a major role in control of TRA by mTEC, not all TRA are controlled by Aire, suggested additional regulators also exist. Thus, in addition to Aire, the transcription factor Fez family zinc-finger 2 (Fezf2) was also reported to be associated with regulating and presenting TRAs during the negative selection process (Takaba *et al.*, 2015). While Fezf2 deficient mice show a different phenotype to Aire deficient mice, they still exhibited peripheral organ cell infiltration and autoantibody production that are indictive of autoimmune disease. Interestingly, Fezf2 expression does not seem to be restricted to a specific mTEC type and was also found to be expressed within the Aire$^+$ mTEC fraction. Collectively, these studies suggest that the intrathymic expression of TRAs is regulated by at least two different factors to ensure effective negative selection and central tolerance induction (Takaba *et al.*, 2015).

In addition to playing a direct role in tolerance induction through self-peptide presentation, mTEC are also involved in other aspects of T cell development, including the positioning of

positively selected thymocytes within the thymus. For example, the mTEC^{lo} population expresses the CCR7 chemokine ligand CCL21, which is essential in regulating the migration of positively selected thymocytes from the cortex into the medulla. Consistent with this, mice lacking CCR7 or CCL21 both show defects in thymic tolerance (Kurobe *et al.*, 2006; Nitta *et al.*, 2009; Kozai *et al.*, 2017). In addition to CCL21, mTEC also express the chemokine XCL1, that regulates the intrathymic positioning of thymic XCR1$^+$ DC (Lei *et al.*, 2011). Interestingly, XCL1 expression by mTEC is controlled by Aire, and XCL1 deficiency results in an autoimmune phenotype. Thus, mTEC express multiple chemokines that underpins their ability to mediate intrathymic tolerance mechanisms.

1.3.4 Dendritic Cells

In addition to mTEC, thymic DC represent an important antigen presenting cell population in the thymus for the negative selection process. Thymic DC represent a heterogenous population and can be split into two main types: plasmacytoid (pDC) and conventional (cDC) dendritic cells. The cDC population can be further broken down by their relative expression of Signal regulatory protein α (Sirpα), where Sirpα$^-$ cDC are identified as cDC1 and Sirpα$^+$ cDC are identified as cDC2 (Wu and Shortman, 2005).

Furthermore, a recent study has shown the important role thymic DC impose on tolerance induction. This was emphasized by the deletion of LTβR and subsequently the altered cDC1 compartment that led to autoimmune manifestations. This study provides a mechanism of tolerance induction that is independent of mTEC availability that directly implicates the role of cDC1 in the negative selection process (Cosway *et al.*, 2017).

1.3.4.1 Intrathymic cDC1

In studies investigating the origins of thymic DC, evidence suggests that cDC1 development occurs via an intrathymic precursor (Luche *et al.*, 2011). There has been some speculation that thymic DC arise from a T cell progenitor that colonizes the thymus, however IL-7R fate mapping studies suggest that DC rise from a separate population (Schlenner *et al.*, 2010). Thus, while approximately 85% of all T cell progenitor cells expressed IL-7R^{Cre}, the speculation was that the remaining 15% could be responsible for the myeloid lineage in the thymus. However, fate mapping of IL-7R showed that all myeloid lineages in the thymus were IL-7R$^-$, and that this pathway was restricted to T cell precursors (Schlenner *et al.*, 2010). In CCR7 deficient mice, it was shown that the population of cDC1 was reduced (Cosway *et al.*, 2018). This was attributed to the reduction of the migrating cDC1 progenitors that failed to enter the thymus as a result of CCR7 deficiency. Furthermore, CCL21 was identified as an essential ligand for the intrathymic development of the cDC1 population as CCL21 deficient mice showed clear reductions in this population (Cosway *et al.*, 2018).

Functional capabilities of cDC1 in the thymus include antigen presentation during negative selection as well as Treg selection in a mechanism that is dependent on Aire (Perry *et al.*, 2014). This was concluded by direct comparison of GFP acquisition. Chimeras were generated where mTEC were GFP$^+$, and the ability of labelled DC to acquire GFP was measured as a means of antigen transfer. Indeed, it was shown the Sirpa$^-$ cDC1, referred to as CD8α^+ DC in this study, acquired higher GFP levels than the Sirpα^+ cDC2 population, indicating their higher efficacy of antigen acquisition (Perry *et al.*, 2014).

1.3.4.2 Migratory cDC2 and pDC

Some conventional DC that reside in peripheral tissues have been shown to migrate to the thymus (Bonasio *et al.*, 2006). Unlike the intrathymic cDC1 population and its role in tolerance induction, migratory cDC2 have been suggested to circulate the periphery, collect antigen and then enter to the thymus where they can present peripheral antigens during negative selection of developing thymocytes (Bonasio *et al.*, 2006). The intrathymic localization of cDC2 has been shown to be confined to the perivascular space around thymus vessels where they are capable of capturing antigens and aiding the antigen presentation process. This was shown to involve a CCR2 dependent mechanism, where CCR2 deficient mice exhibited reduced cDC2 composition and altered thymic tolerance as there was accumulation of self-reactive T cells in the periphery (Baba, Nakamoto and Mukaida, 2009). Although CCR2 deficient mice did not display signs of autoimmune disease at an early age, the presence of autoreactive cells implicates the role of antigen presentation that is mediated by cDC2 (Baba, Nakamoto and Mukaida, 2009).

In addition to migratory cDC, pDC can also regulate tolerance induction in a similar way to the cDC2 population. Immature pDC, that have not been activated by Toll-like receptors (TLR), are able to migrate to thymus to present peripheral antigens. This was shown by uptake of fluorescence labelled antigens by pDC and their migration to the thymus via CCR9 mechanism (Hadeiba *et al.*, 2012). Indeed, transfer of CCR9 deficient pDCs did not result in migration to thymus and in a competitive BM chimaera assay, the frequency of CCR9 deficient pDCs was significantly reduced in the thymus (Hadeiba *et al.*, 2012). These studies highlight the essential role of migratory DC and their role in capturing peripheral antigens for screening purposes during T cell development as well as their role in maintaining tolerance induction.

1.4 Thymus Damage and Regeneration

1.4.1 Thymus Involution

The thymus requires continuous seeding by lymphoid progenitors to generate new cohorts of naïve T cells. This continuous process is affected by multiple factors that cause either transient or long-lasting degenerative effects on the rates of thymus function. Subsequently, both acute and chronic mechanisms of thymus involution disrupt intrathymic T-cell development and influence the way in which new T cells are produced. This disruption has potentially severe consequences, including immunodeficiencies that may compromise an individual's immune system, which collectively highlights the importance to investigate such degenerative pathways. Important aspects of multiple types of thymus involution, both natural and acquired, are summarized below.

1.4.1.1 Natural Chronic Thymus Involution: Impact of Ageing on Thymus Function

The thymus is susceptible to natural occurring degeneration as a result of ageing. This process of thymus involution significantly impairs the production of naïve T cells and their egress into the periphery. For example, Hale et al. (Hale *et al.*, 2006) used 12 month old RagGFP mice to study recent thymic emigrants (RTEs), which can be identified in peripheral tissues as GFP$^+$ cells (Hale *et al.*, 2006). They found that proliferation and IL2 production of CD4$^+$ and CD8$^+$ RTEs cells following anti-CD3 and anti-CD28 in aged mice was significantly impaired compared to young mice. Thus, in aged mice, RTEs appear to be functionally impaired compared to their counterparts in young mice, suggesting that intrathymic T-cell development in the aged thymus is impaired. Interestingly, an increase in GFP$^-$ T cells was also reported in aged mice compared to young mice, suggesting enhanced recirculation of peripheral T cells occurs during ageing (Hale *et al.*, 2006). Whether this represents a factor that might influence intrathymic T-cell development is not clear.

As continuous thymus seeding by lymphoid progenitors controls the generation of new cohorts of naïve T cells, this process has been examined in relation to the decline in thymus function during age-related involution. Interestingly, the young thymus and the aged thymus show similar levels and patterns of expression recruitment molecules, such as P-selectin and CCL25 (Gui *et al.*, 2007), suggesting that limited progenitor entry to the aged thymus may not account for declining rates of T-cell development. Furthermore, lymphoid progenitors isolated from both young and aged thymi and transplanted into fetal thymus under the kidney capsule shows similar seeding capabilities (Gui *et al.*, 2007), suggesting that age related thymus involution occurs independent of recruitment. In a similar study (Zhu *et al.*, 2007), intrathymic injection of progenitors from young thymi into an aged thymus did not restore thymic function, suggesting that changes in lymphoid progenitors alone are not responsible for thymic involution. In addition, the transplantation of fetal thymus lobes in old mice showed normal thymus seeding by aged progenitors, confirming that progenitor colonization is not defective in aged thymi (Zhu *et al.*, 2007). Nevertheless, a recent study (Bredenkamp, Nowell and Clare Blackburn, 2014) has suggested that CCL25 expression by cTEC, which plays an important role in lymphoid progenitor recruitment, is significantly decreased during ageing. Whether this then impacts the nature of thymus colonizing progenitors (e.g., CCR9$^+$ versus CCR9$^-$ cells), is not clear.

Rather than alterations in haemopoietic cells, causes of age-related thymic involution have been suggested to include alterations in the thymic microenvironment, and changes in the numbers and properties of TEC that form these structures. Griffith et al. assessed the thymic microenvironment in an aged thymus and reported limited medullary areas (Griffith *et al.*, 2012). Furthermore, thymic size has been hypothesized to reach a peak at four weeks of age,

and analysis of thymi at twelve months has shown a significant decrease in cellularity. Keeping with the same pattern, TEC numbers have also shown to be significantly reduced at twelve months of age, which may contribute to progressive decline in thymus function that occurs during age related involution (Gray *et al.*, 2006). In the same study, using Ki67 as a maker for proliferation, the proliferation of TEC at twelve months of age was shown to be diminished, suggesting a reduction in TEC proliferation directly accounts for this decrease in TEC numbers. Interestingly the composition of thymic stroma is also significantly altered and shows different composition profiles between the non-aged and aged thymus that could also account for thymic function (Gray *et al.*, 2006). Most importantly, the reduced proliferation status of TEC was rescued by the induced upregulation of Foxn1 that resulted in increased TEC proliferation that increased thymus size (Bredenkamp, Nowell and Blackburn, 2014).

Recent studies have also attempted to dissect the molecular basis of age-related atrophy. (Cowan *et al.*, 2019) showed that the transcription factor Myc plays an essential role in controlling thymus size. Using transgenic mice where GFP is used to report Myc expression, it was shown that GFP levels were at the highest levels of expression during embryonic stages and had declined during adulthood. Using a $Foxn1^{Cre}/Myc^{fl/fl}$ transgenic mouse model to investigate forced expression of Myc in TEC, it was shown that there was a significant increase in thymus size as early as four weeks of age when compared to controls, and increased TEC numbers. Despite having an enlarged thymus, thymus architecture remained unchanged. Interestingly, it was also shown that thymus function was enhanced, by the measurement of the naïve T cell pool which suggested an increase in RTEs. With relation to the proliferative capacity of TEC, forced Myc expression also resulted in increased TEC proliferation with no effect on hematopoietic cell proliferation. Most importantly, following induced reduction of

TEC and subsequently thymus involution, induced expression of Myc by tamoxifen was able to generate significantly higher TEC numbers and promote increased thymic size (Cowan *et al.*, 2019).

These studies highlight the central role of TEC during thymus involution and support the idea that thymus involution is due at least in part to a declining TEC population. Indeed, it was shown by (Aw *et al.*, 2008) that following age related thymus involution, distinct cortical and medullary thymic compartments were less distinguishable in younger mice, which correlates with the degeneration of the TEC compartment (Aw *et al.*, 2008). Furthermore, analysis of senescent and apoptotic cells in the aged thymus revealed clear β-galactosidase activity within the aged thymus that was absent in the young thymi. Finally, staining for γH2AX to detect of cells with DNA damage, revealed co-staining of TEC markers and γH2AX in the aged thymus, further supporting the notion that a decline in TEC contributes to age related thymus involution (Aw *et al.*, 2008).

1.4.1.2 Multiple Stimuli Cause Acute Thymus Involution

In addition to the progressive chronic reduction in thymus size during ageing, the thymus also undergoes rapid and acute involution that is induced by multiple forms of stimulus that also impact thymus size and subsequently production of new T cells. For example, thymus weight was examined in a study that investigated the consequences of repeated stress by immobilization. Here, mice were subjected to immobilization for one hour a day for eight consecutive days and sacrificed under non-stress conditions. When compared to non-stressed mice, mice subjected to stress showed decreased thymus weight as well as decreased body weight (Rabasa *et al.*, 2015).

In addition to stress, infection also has a severe effect on the thymus (Savino *et al.*, 1986). In humans, thymus histology was investigated and has shown that acquired immunodeficiency syndrome (AIDs) patients undergo severe disruptions in TEC architecture as well as degeneration in the TEC population (Savino *et al.*, 1986). In addition, murine model studies have also investigated acute thymus involution caused by infection. It was shown by (Godfraind, Holmes and Coutelier, 1995) that transient thymus involution caused by hepatitis virus involved severe depletion of the DP thymocyte population, which was resolved by 2 weeks post-infection. It was hypothesized that this selective depletion was a result of TEC incorporation of the viral genome and that DP thymocyte interactions with the infected TEC population resulted in apoptosis (Godfraind, Holmes and Coutelier, 1995). Similarly, in a human immunodeficiency virus (HIV) murine model infection, where HIV resulted in inhibition and suppression of $CD4^+$ T cells, thymocyte development was investigated. It was shown the DP, SP4, and SP8 thymocytes contained viral burden. Interestingly, it was hypothesized that infection caused depletion of thymocytes through apoptosis and the TEC compartment showed a degenerative status (Stanley *et al.*, 1993). These different stimuli that induce thymus involution have a severe effect on thymus function. A study has shown that antigen that was intrathymically injected resulted in the pause of new T cell export (Uldrich *et al.*, 2006). Although the break in thymus export is not a result of an infection model, the presence of foreign antigens could resemble what occurs during infection and this resulted in impaired thymus function.

In contrast to an infection or stress model, thymus involution can also be caused by pregnancy (Zoller, Schnell and Kersh, 2007). This study investigated the effects of pregnancy on the thymus and showed a significant decrease in the presence of ETP, however analysis of the bone

marrow did not show a decline in the BM progenitors. Interestingly, the loss of ETP is also accompanied by loss of thymocyte proliferation and decreased RTE numbers. The ratio of Tconventional to Treg was also altered. The number of Treg was subsequently decreased because of the thymus size, however the percentage of Treg was significantly increased (Zoller, Schnell and Kersh, 2007) suggesting pregnancy can alter the makeup of the different thymocyte compartments.

1.4.2   Endogenous Thymus Regeneration

Endogenous thymus recovery is associated with acute thymus atrophy in which the thymus recovers its size and function without exogenous intervention. In a study conducted by Zubkova et al (Zubkova, Mostowski and Zaitseva, 2005) transient thymic atrophy was achieved by the administration of dexamethasone (Dex), a glucocorticoid. Shortly after Dex administration, total thymus cellularity significantly decreased, and cellularity then began to reach control numbers by day fourteen post treatment. Depletion of the DP thymocyte population was predominantly responsible for the overall decline in thymocyte numbers. However, the DN thymocyte population followed a similar pattern, and their numbers were also restored by day fourteen post Dex administration, which demonstrates that recovery of thymocyte populations involves both DN and DP thymocyte subsets (Zubkova, Mostowski and Zaitseva, 2005). Having been implicated in early thymocyte development, IL-7 levels were investigated following thymus damage. Post Dex administration, IL-7 mRNA levels significantly increased and returned to normal levels after recovery, demonstrating the potential importance of an IL-7 mediated recovery pathway. In the same study, another model of induced thymus atrophy was investigated, which was sub-lethal total body irradiation (TBI). Following such treatment, recovery kinetics followed a similar pattern to the Dex treated mice. Interestingly, levels of IL-7 alongside CCL25 and CXCL12 were found to be upregulated shortly following damage, again

highlighting their role in the mechanism of thymus recovery following acute damage (Zubkova, Mostowski and Zaitseva, 2005).

In earlier studies, the IL-2/IL2R pathway has been shown to be utilized during embryonic thymus generation to stimulate proliferation of colonizing progenitors (Jenkinson, Kingston and Owen, 1987). Further studies have shown (Zúñiga-Pflücker and Kruisbeek, 1990) that this pathway is also utilized following transient thymus recovery, suggesting that following damage the thymus follows a similar pattern to embryonic development in which IL-2R is expressed shortly after damage. Furthermore, endogenous thymus recovery is inhibited by anti-IL-2R blocking antibodies that stop the proliferation and differentiation of the progenitor population that is present post TBI. It was also demonstrated that following blockade of IL-2R after damage, there was a delay in the kinetics of the progenitors to generate DP thymocytes. Subsequently, this delay caused disruption in the regaining of thymus size, as thymic size following anti-IL-2R treatment did not recover compared to non-treated mice (Zúñiga-Pflücker and Kruisbeek, 1990).

A more recent study (Xiao *et al.*, 2017) also investigated endogenous thymus recovery, in which both male and female mice were subjected to TBI. Interestingly, it was shown that the thymus displayed biphasic recovery and in the case of female thymus recovery, the total thymus cellularity exceeded control numbers. The biphasic phenomenon was actually observed in an older study (Takada *et al.*, 1969). Here, the first drop in thymus cellularity was a result of depletion of cells induced by TBI, which was followed by a first phase of recovery attributed to an intrathymic precursor that survived the TBI damage and proliferated to develop the first cohort of T cells. Subsequently, the second drop in thymus cellularity was a result of insufficient

progenitor colonization from the bone marrow to drive the second phase of thymus regeneration. Interestingly in the same study, shielding the hind legs during TBI prevented the second drop in thymus cellularity suggesting that TBI directly impacts upon BM progenitors. Indeed, Xiao et al (Xiao *et al.*, 2017) reported a long term defect in the DN population that was linked to TBI damage to BM progenitors. Analysis of Lin$^-$Sca1$^+$cKIT$^+$ (LSK) cells following TBI showed a significant decrease in numbers even in mice subjected to lower doses of irradiation. While this reduction in LSK cells correlated with the long-term defect of the DN subsets during thymus recovery, the reduction was compensated by the expansion of the DN3 population to restore thymic size following damage. In other studies aimed at elucidating mechanisms of endogenous thymus recovery, IL-22 was identified as an essential driver following TBI (Dudakov *et al.*, 2012) . After observing DP thymocyte depletion, IL-22 levels in the thymus significantly increased during thymus recovery. This was confirmed by direct targeting of thymus radiation to confirm the increase in intrathymic IL-22 levels. Importantly, IL-22 deficient mice were subjected to TBI but failed to recover thymus size which supports a recovery mechanism via IL-22 upregulation. Indeed, the increase in levels of IL-22 correlated with reduced thymic size, and IL-22 upregulation was found to be attributed to the increase of an intrathymic lymphoid tissue inducer (LTi) cell population that survived TBI damage. In support of the this, mice that lacked LTi cells (RORγt$^{-/-}$) and subjected to TBI did not upregulate IL-22 following damage (Dudakov *et al.*, 2012). Altogether, these studies suggest following acute thymus atrophy, the thymus has the capability to recover thymus size and function through endogenous mechanisms.

1.4.3   Thymus Recovery and Bone Marrow Transplantation (BMT)

1.4.3.1   History and Importance of BMT

BMT is a mode of treatment that is utilized to regenerate the hematopoietic system following ablative therapy such as chemotherapy or radiotherapy. Following such therapies, individuals are left in an immunocompromised state until proper immune system regeneration is achieved. This process is aided by the infusion of donor cells into the patient to facilitate such regeneration. Older studies (Urso and Congdon, 1957) have examined the impact of BMT on the survival of irradiated mice. It was observed that to achieve recovery or survival following therapy, mice required a specific amount of bone marrow. Furthermore, it was shown that the number of bone marrow cells injected correlated with the leukocyte count suggesting that massive doses of bone marrow give rise to increased leukocytes. Interestingly, the dose of bone marrow did not have an effect on the thymus size as different doses regenerated the thymus to similar levels (Urso and Congdon, 1957). In contrast, a human study (Thomas *et al.*, 1957) where patients that were treated with ablative therapy and bone marrow infusion, did not result in the same positive results as compared to the murine model. Out of the six patients, only two had successful engraftment of the transplant and all patients did not survive beyond one hundred days. Nevertheless, this failure prompted increased research in this field and allowed for future trials to be conducted. Indeed, twenty years later, BMTs were conducted on one hundred patients that received ablative therapy and ninety-three successful engraftments were observed. Although the long term survival rate was low, this study highlighted the importance of BMT therapy early in the onset of the disease (Thomas *et al.*, 1977). Importantly, a key factor for generating successful engraftments and immunocompetence post BMT is the compatibility of the donor bone marrow (Zinkernagel *et al.*, 1980). This was shown by allogenic BMT, in which host and donor are incompatible, which resulted in a death rate of 85%.

Reconstitution of the immune system by BMT is widely accepted as an important determining factor in deciding the fate of patient. The reconstitution can occur via pre-existing donor T cells that are infused alongside haemopoietic progenitors, or via de novo T cell development from infused cells. A method to identify functional reconstitution by a thymus dependent pathway is the measurement of the T cell receptor excision circles (TRECs) that are present in RTE and can be used to distinguish peripheral T cell reconstitution by thymus from reconstitution by peripheral expansion (Weinberg *et al.*, 2001).

1.4.3.2 Conditioning and Depletion of Cells

Patients that undergo ablative therapies as a mode of treatment for different types of diseases have severe consequences in the depletion of their cells. In a study where patients were analyzed before and after intensive chemotherapy treatment show severe depletion in the CD4$^+$ T cell count following treatment (Mackall *et al.*, 1995). Importantly, it was shown that following treatment, the thymus dependent pathway is required for reconstitution of the CD4$^+$ T cell pool. As mentioned previously in section 1.4.1.1, age related thymus involution has a severe impact on the thymus function. With regards to the reconstitution of the T cell pool, patient age at the time of transplant has clear implications for the rate of rebound in T cell numbers. Patients that were under the age of 18 had successful regeneration of CD4$^+$ T cell count, suggesting efficient regeneration of intrathymic T-cell development. This was measured by the presence of CD45RA$^+$ T cells as a means to identify thymus dependent T cell reconstitution. Furthermore, the patients that showed higher CD45RA$^+$CD4$^+$ T cells also displayed enlarged thymus. This was shown by comparing computerized tomography (CT) scans before and after therapy and thus suggesting a thymus regenerative capability. Altogether this study highlights the essential role of the thymus in repopulating the T cell compartment following depletion as a consequence of treatment (Mackall *et al.*, 1995).

Murine models have been a useful means to study the beneficial impact of BMT post ablative therapy. In a study analyzing peripheral T cell reconstitution and thymus dependent/independent pathways (Mackall *et al.*, 1996), it was shown that in thymectomized mice the peripheral T cell pool is reconstituted mainly of homeostatic peripheral proliferation of mature T-cells present in the transplant. This has a severe consequence as the generated T cells have a limited T cell receptor repertoire. In contrast, thymus-bearing mice reconstituted the peripheral T cell pool in a thymus dependent pathway as indicated by the decreased proliferation of T cells from the transplant (Mackall *et al.*, 1996). Furthermore, the delay in T cell reconstitution post BMT has severe immunological consequences and thus studies have investigated treatments to enhance thymus function post BMT in murine models. For example, IL-7 was utilized to improve BMT reconstitution (Bolotin *et al.*, 1996). Here, lethally irradiated mice were subjected to exogenous IL-7 treatment post ablative therapy. It was shown that post treatment thymus function was comparable to non-irradiated mice suggesting enhanced thymopoiesis and improved immune reconstitution post BMT (Bolotin *et al.*, 1996). Similarly, and more recently, use of exogenous IL-21 in boosting thymus function to restore peripheral T cell populations has been assessed (Tormo *et al.*, 2017). Mice that received IL-21 treatment displayed complete reconstitution of the peripheral T cell pool that was not observed in the non-treated group. Importantly, IL-21 treatment was used in experiments involving humanized mice and showed improved T cell development (Tormo *et al.*, 2017), which could suggest that consequences of pre-treatment before BMT can be overcome by enhancing thymus function.

1.4.3.3 Thymus Regeneration and T cell Reconstitution

As discussed in the previous section, following ablative therapy the thymus and the periphery is depleted of T cells thus leaving individuals immunocompromised. To reach immunocompetence, BMT has been used as a mode of treatment to colonize the thymus by

donor progenitors to generate naïve T cells. Because the regeneration process requires infusion of cells and effective thymus colonization, studies have highlighted the effects of the ablative therapy on thymus function and the reconstitution of the T cell pool. Chemokine signaling has been shown to be essential for the recruitment of progenitors to seed the thymus through adulthood (Zlotoff *et al.*, 2010). Specifically, it was shown that CCR7 deficient progenitors were not able to colonize the thymus, nevertheless the mice had comparable thymus cellularity to control mice suggesting an intrathymic mechanism to compensate for the reduction in progenitors. Furthermore, in a different study and following BMT, the same group has shown that progenitor colonization is transiently independent of chemokine signaling and instead relied on the role of PSGL1 for thymus entry (Zlotoff *et al.*, 2011). Interestingly, it was suggested that following damage and during the reconstitution process, thymus colonization can be split into three stages; the first stage in which regeneration of the thymus is independent of chemokine signaling, the second stage in which the regeneration process is mostly dependent on chemokine signaling, and the last stage in which both CCR7 and CCR9 are strictly required at three weeks post BMT (Zlotoff *et al.*, 2011). The CCR7 and CCR9 ligands, CCL21 and CCL25 respectively, are expressed by mTEC and cTEC within the TEC population, demonstrating the importance of TEC microenvironments during early stages of thymus recovery post BMT. In another study (Kelly *et al.*, 2010) it was shown that following lethal irradiation and BMT, thymus cellularity is significantly decreased two weeks after damage. Importantly, analysis of thymus tissue four weeks post damage showed a clear reduction in total TEC that mapped to reductions in both cTEC and mTEC. Such reductions can have a direct impact on the ability of thymus progenitor recruitment post BMT. Indeed, other studies have also shown that following damage, TEC numbers are reduced (Zhang *et al.*, 2014). Here, while quantitative PCR (qPCR) analysis of sorted TEC populations from damaged thymi showed that

TEC continued to express mRNA levels of CCL21 and CCL25, however it was suggested that the reduction in TEC numbers accounted for impaired progenitor homing due to a reduction in chemokine availability.

From the studies described above, it is the clear that damage caused by lethal irradiation has a significant effect on TEC populations and progenitor colonization, which then has a direct impact on thymopoiesis. In relation to the recovery of TEC microenvironments, it was shown that following BMT, regenerative capabilities of TEC involves interplay between LTα and RANKL, that represent ligands for LTβR and RANK that are expressed by TEC (Lopes *et al.*, 2017). Indeed, the generation of bone marrow chimaeras in which LTα deficient mice were used as hosts, showed disruption in the regeneration of the TEC compartments when compared to WT hosts, however the TEC population in the damaged WT thymus remained decreased compared to non-damaged thymus. Moreover, LTα deficient hosts had disrupted T cell reconstitution post BMT as peripheral T cell counts were reduced up to one hundred days post BMT. A clear explanation for the impaired thymopoiesis was attributed to the decreased TEC population that had reduced expression of CCL21 mRNA. This reduction contributed to reduced progenitor colonisation in the LTα deficient host post BMT that resulted in incomplete T cell reconstitution. LTβR has also been implicated in the thymic regeneration process post BMT. For example, LTβR deficient mice have a clear reduction in the donor thymocyte population post BMT (Lucas *et al.*, 2016). Further analysis showed this mapped to a reduction in the ETP population, suggesting that LTβR operates during the recovery of thymus function by controlling progenitor entry to the thymus. Having observed the effect on T cell reconstitution post BMT in LTβR deficient mice, effects of agonistic anti-LTβR treatment on thymus recovery were assessed. Here, stimulation of LTβR post BMT showed increased donor

derived cells within the thymus, and enhanced peripheral T cell numbers, suggesting LTβR stimulation as a potential means to boost the recovery of thymus function post BMT.

1.5 General Aims

The thymus is the primary site for T cell development and the induction of central tolerance. Thus, damage to the thymus has a significant impact on this process. It is shown that following ablative therapies, damage to the thymus disrupts the thymic microenvironment which could impact the ability to support T cell development. Subsequently, this impact could result in delayed T-cell reconstitution. As a result, there is a period of immunodeficiency that leaves patients susceptible to potentially fatal infections. Thus, in this thesis we focus on examining the kinetics of thymus recovery following damage and we aim to answer the following questions:

1. We have used sub-lethal irradiation (SLI) in a mouse model of thymic injury and performed systematic examination of the recovery of both thymocytes and the thymic microenvironment and posed the following questions:

    a. What are the kinetics of endogenous thymus recovery following acute thymic damage?

    b. Are there qualitative changes that occur following acute thymus damage that affect overall thymus function?

2. Ablative therapies used in treatment of diseases such as cancer result in secondary immunodeficiency, leaving patients susceptible to potentially fatal infections. These ablative therapies deplete the immune system and consequently patients are dependent on bone marrow transplants (BMT) for immune reconstitution. As a result, we generated

bone marrow chimeras (BMC) and performed systematic examination of the recovery of thymus function following BMT and posed the following questions:

a. What are the kinetics of exogenous thymus recovery following BMT?

b. Following ablative therapy and BMT, does damage to the thymus impact the quality and balance of T cell development?

2   CHAPTER 2: MATERIALS AND METHODS

2.1 Mice

All mice were kept at the Biomedical Services Unit (BMSU) at the University of Birmingham. All animal use was performed in accordance with UK Home Office regulations and approved by the University of Birmingham Animal Welfare and Ethical Review Board. For experimental consistency tissue was harvested from mice that were 8-12wks of age. For further experimental consistency, female mice were used unless mouse limitations were present in which mixed gender was needed. For bone marrow chimeras (BMC) and sub-lethally irradiated (SLI) mice (Table 2.1), unmanipulated and unirradiated age matched controls were taken alongside as controls. All mice were sacrificed under schedule 1 procedure.

Table 2.1. Mouse Strains Used

Strain	Phenotype	Supplier
C57BL/6	Wildtype, CD45.2$^+$	External (Charles River)
BALB/c	Wildtype, CD45.2$^+$	External (Charles River)
BoyJ	Wildtype, CD45.1$^+$	BMSU
$TCR\alpha^{-/-}$	Loss of αβ T cell receptor. Mice lack CD4$^+$ and CD8$^+$ T cells	BMSU colony
RAG2^{GFP}	Green fluorescent protein (GFP) reporter expressed under the Rag-2 gene promotor	BMSU colony
RAG2^{GFP}Foxp3^{RFP}	Green fluorescent protein (GFP) reporter expressed under the Rag-2 gene promotor, and red fluorescent protein (RFP) that marks cells expressing the Foxp3 gene	BMSU colony
Nude	Natural mutation in Foxn1 that results in absence of thymus	BMSU colony
$Aire^{-/-}$	Gene knockout for Aire	BMSU colony
Kaede BALB/c	Transgenic mice carrying Kaede cDNA under the CAG promotor	Prof. David Withers University of Birmingham

2.2   Media

Following tissue dissection, RF10 media (Table 2.2) was used for *ex vivo* handling of tissue. Enzymatic digestion of tissue required RF10 as well as enzymes (Table 2.3). Mechanical disaggregation of tissue only required RF10 media. Following tissue preparation, cells were handled in MACS buffer (Table 2.4) or FACs buffer (Table 2.5). All media were stored at 4°C until used.

Table 2.2. RPMI-1640 Hepes Medium (RF10) Media Components

Medium and Additives	Volume	Supplier
RPMI 1640 + 20mM Hepes with L-Glutamine without bicarbonate	500ml	Sigma
200mM L-Glutamine	5ml	Sigma
5000 IU/ml Penicillin and Streptomycin	10ml	Sigma
Fetal Calf Serum (FCS)	50ml	Sigma

Table 2.3. Enzymatic Digestion Components

Medium and Additives	Volume	Supplier
RF10	1ml	Sigma
Deoxyribonuclease 1	2ul	Sigma
Collagenase Dispase or Collagenase D	25ul	Sigma

Table 2.4. MACS Buffer Components

Medium and Additives	Volume	Supplier
Dulbecco's phosphate buffered saline without calcium and magnesium	500ml	Sigma
Fetal Calf Serum (FCS)	2.5ml	Sigma
EDTA 0.05mM	2ml	Sigma

Table 2.5. FACS Buffer Components

Medium and Additives	Volume	Supplier
Dulbecco's phosphate buffered saline with calcium and magnesium	500ml	Sigma
Fetal Calf Serum (FCS)	15ml	Sigma

2.3   Tissue Preparation

Mice sacrificed after procedure were dissected at the BMSU facility. For most experiments, thymus and spleen were dissected. Other experiments also included different organs, liver, kidney, bone marrow. Isolated tissue from mice was placed in RF10 media. Any excess blood and fat were removed from all tissues prior to further processing.

2.3.1   Preparation of Tissue for T cell Development Analysis

For T cell development analysis, tissue was transferred to petri dishes containing RF10 media. Tissue was then mechanically disaggregated using frosted end glass slides (Thermo Scientific). Slides were washed with RF10 after tissue disaggregation was complete. Cells suspended in petri dishes were transferred to 15ml Falcon tubes (Corning Centistar) using a gauze filter. Cell suspensions were centrifuged for 4 minutes at 4 °C at 1400 rpm. Following centrifugation, thymic tissue was resuspended in FACS buffer, while splenic tissue was resuspended in 2ml

RBC lysis buffer (Sigma Aldrich) and left for 10 min at room temperature. Following lysis, RF10 was added to the cell suspension to neutralize the lysis reaction and then centrifuged and resuspended in FACS buffer.

2.3.2   Preparation of Tissue for Thymic Epithelial Cell Analysis

For the isolation of TEC, the thymus was transferred to a 1.5ml Eppendorf and incubated in an enzyme digestion solution (components in Table 2.3) using collagenase dispase. Tissue was cut into small pieces using fine scissors and transferred to a 5ml round bottom FACs tube. The tube was then placed in a thermo-mixer for 30 minutes and pipetted up and down in order to gently disaggregate the tissue. EDTA was subsequently added to stop any further enzymatic action and the tube was placed on ice. MACS buffer was added and then the sample was transferred to a 15ml tube via the use of a gauze filter to remove any undigested connective tissue. The sample was centrifuged for 4 minutes at 4 °C at 1400 rpm. Supernatant was removed and the resulting cell pellet was resuspended in MACs buffer. As the TEC population required enrichments, an additional step was required. The cell suspension was incubated with anti-CD45 beads (Miltenyi Biotech) for 20 minutes at 4°C. Following incubation, the cell suspension was passed through a column to magnetically separate $CD45^+$ cells from $CD45^-$ cells. LS columns (Miltenyi Biotech) were used and were activated by running 3mls of MACS buffer prior to adding the cell suspension. When the cell suspension was run through the column placed on a magnet, the labeled $CD45^+$ cells were trapped in the column, allowing the unlabeled cells to pass through, which were collected in 15ml Falcon tubes. This process allows for the enrichment of the TEC population that resided in the $CD45^-$ population.

2.3.3 Preparation of Tissue for Thymic Dendritic Cell Analysis

The thymus was transferred to a 1.5ml Eppendorf and incubated in an enzyme digestion solution (components in Table 2.3) using Collagenase D. Tissue was cut into small pieces using fine scissors and transferred to a 5ml round bottom FACs tube. The tube was then placed in a thermo-mixer for 30 minutes and pipetted up and down in order to gently disaggregate the tissue. EDTA was subsequently added to stop any further enzymatic action and the tube was placed on ice. MACS buffer was added and then the sample was transferred to a 15ml tube via the use of a gauze filter to remove any undigested connective tissue. The sample was centrifuged for 4 minutes at 4°C at 1400 rpm. Supernatant was removed and the resulting cell pellet was resuspended in MACs buffer.

2.3.4 Preparation of Lymphocytes from Liver Tissue

Liver tissue was dissected and weighed prior to disaggregation. A cell strainer was placed in a 50ml Falcon tube and liver was placed in a cell strainer and disaggregated with a syringe. The cell strainer was washed with FACS buffer to suspend any remaining cells. Cells were then centrifuged, and the resulting pellet was resuspended in 5ml RF10 media. In a separate 15ml falcon tube, 1.3ml of Optiprep (Sigma-Aldrich) and 3.7ml of PBS were mixed. The liver suspension was then slowly pipetted on top of the Optiprep mix. It was important to layer the liver suspension on top of the Optiprep mix for optimal results. The Falcon tube was then centrifuged for 25 minutes at room temperature (RT) at 1000RCF with brake speed at 1. Following centrifugation, lymphocytes were separated from other cell types and were isolated by careful pipetting into another 15ml falcon tube. The lymphocytes were washed in 10ml FACS and centrifuged again. The resulting pellet was resuspended in FACS buffer.

2.4   Cell Counts

Cell suspensions were counted using AccuCount Blank Beads (Spherotech Inc). All cell suspensions were resuspended in either 2ml FACS or MACS buffer depending on the disaggregation method. In a FACS tube, 100μl of buffer and 5μl of beads was added. From the cell suspension, 50μl of cells was added to the FACS tube. The FACS tube was then run-on BD LSR Fortessa Machine (BD) where the cells and beads were distinguished based on size and granularity. Because there was a known number of beads and volume of cells, the total cellularity of the cell suspension was calculated as shown in the equation below. This technique was consistent throughout all experiments.

$$\text{Total cellularity} = \left(\left(\frac{\# \text{ of cells}}{\# \text{ of beads}}\right) x \ 5000\right) x \ 40$$

2.5   Flow Cytometry

Antibodies used are outlined in Table 2.6. 5×10^6 of cells were placed in 96 well plate (Costar). The plate was then centrifuged to create cell pellets. The supernatant was removed, and 50μl of antibody (Table 2.6) was used to resuspend the pellet. Cells suspended in the antibody were then incubated for 30 minutes on ice. Cells were then washed with FACS/MACS buffer and centrifuged for 2 minutes at 4°C at 1400rpm.

Table 2.6. Flow Cytometry Immunolabelling

Specificity	Fluorochrome	Clone	Supplier
CD4	BV711	RM4-5	Biolegend
CD8	BV786	53-6-7	Biolegend
	Biotin	53-6-7	eBioscience
TCRβ	APCCY7	H57-597	Invitrogen
CD69	PECY7	H1-2F3	eBioscience
CD62L	APC	MEL-14	eBioscience
CD25	A700	PC61.5	eBioscience
	PB	ebio3C7	eBioscience
Foxp3	PE	FJK-165	eBioscience
CD45	BV605	30-F11	Biolegend
	PE	30-F11	
CD3	Biotin	145-2C11	BD Pharmingen
	APCCY7	17A2	eBioscience
TCRβ	Biotin	H57-597	eBioscience
CD45.1	APCCy7	A20	eBioscience
CD45.2	A700		eBioscience
TCRδ	Biotin	ebioGL3	eBioscience
NK1.1	Biotin	PK136	eBioscience
	APCCY7	PK136	eBioscience
TER119	Biotin	TER-119	eBioscience
Gr1	Biotin	RB6-8C5	eBioscience
CD11c	Biotin	N418	eBioscience
CD11b	Biotin	M1/70	Biolegend
B220	Biotin	RA3-6B2	eBioscience
Near IV Viability	APCCy7		
Cleaved Caspase-3	PE	5A1E	Cell Signaling Technology
CD44	PECY7	IM7	eBioscience
CD117	PercPcy5.5	2B8	eBioscience
Streptavidin	BV786	N/A	BD Pharmingen
	PECY7	N/A	eBioscience
CD11c	PECY7	N418	eBioscience
PDCA-1	PB	927	Biolegend
Sirpα	PE	P84	eBioscience
MHC-II	A700	M5/114.15.2	eBioscience
CD86	BV650	GL-1	Biolegend
CD19	APCCY7	ebio1D3	eBioscience
CD45	APCCY7	30-F11	eBioscience
EpCAM1	PercPcy5.5	G8.8	eBioscience
Ly51	PE	BP-1	BD Pharmingen
UEA-1	Biotin	B-1065	Vector
MHC-II	PB	M5/114.15.2	Biolegend
CD80	BV605	16-10A1	Biolegend
Anti-H2AX (Ser139)	Alexa Fluor 647	2F3	Biolegend

2.5.1   Intracellular Staining

Intracellular staining of transcription factors required a fixation/permeabilization step. The cells were stained for cell surface markers as described in Section 2.5. Following successful cell surface staining, the cells were washed and centrifuged and resuspended in fixation/permeabilization solution using the eBiosciences Foxp3/Transcription Factor Staining Buffer Set (Thermofisher). The set was used in accordance with the manufacturers protocol. Cells were incubated in the fixation/permeabilization solution for 45 minutes then washed twice with 10X permeabilization buffer that was made in distilled water. After the washing step, the intracellular antibody was diluted in permeabilization buffer and 50µl of the antibody mix was used. The cells were incubated for 30 minutes on ice then washed twice and centrifuged. The resulting cell pellet was resuspended in FACS buffer and transferred to FACS tubes.

2.5.2   Flow Cytometric Analysis

Following the staining process, cells were resuspended in 200µl of FACs/MACs buffer and transferred to FACS tube (Becton). BD LSR Fortessa and BD FACS Diva software was used. FlowJo (Treestar) was used for data analysis. Single colors were used to adjust voltages for the detection channels as well as the compensation for each fluorochrome. The gate for the desired population were set by using isotype controls or fluorescent minus one (FMO). For the majority of the samples, 1 million events were collected, unless the population was rare in which case events were collected until the sample was finished to improve the analysis.

2.5.3   Flow Cytometry Cell Sorting

For cell sorting experiments that required adoptive transfers into mice, tissue was disaggregated as described in Section 2.3.1. However, the process was done under sterile conditions. Prior to

sorting, the cells counted and depleted to decrease sorting time. Pre-depletion samples were taken to compare deletion accuracy. Following depletion, the cell suspension was stained for surface markers. As the sample was bigger than that used for flow cytometric analysis, staining volume remained consistent where 50µl of antibody was used to 5 million cells. Following the staining process, cells were washed and resuspended in RF10. Cells were then filtered through 30mm mesh membrane filter unit (Miltenyi Biotech) and transferred to a FACS tube and stored on ice. The sort was conducted using a FACS Aria Fusion (BD). The sorted populations were collected in 15ml Falcon tubes that contained 2ml of RF10. The falcon tube was then centrifuged and resuspended in 1ml RF10 to count and to also take a sample for purity check of the sorted population. The counted isolated cell population was then centrifuged and resuspended in PBS to be used for cell transfers.

2.6   Mouse Irradiations

Mice were irradiated to assess thymus recovery via SLI or the generation of bone marrow chimeras. Prior to irradiations, mice were placed on Baytril (Bayer; 0.16mg/ml) for 7 days and post irradiation mice were kept on Baytril for also 7 days. For SLI conditions, if the mice were on C57BL/6 background, they were given a single dose of 500 rad. If the mice were on BALB/c background, a single dose of 425 rad was given. For the generation of bone marrow chimeras, mice were given a lethal dose that was split on two days. The first dose was given at the start of the protocol, and the second dose was given the following morning. Following the second dose and in the afternoon of the same day, the mice were reconstituted with bone marrow.

2.6.1   Generation of Bone Marrow Chimeras

Bone marrow chimeras (BMC) were used to identify the kinetics of donor derived thymus recovery by using congenically marked bone marrow to distinguish between host and donor

cells. Hosts that were on the C57BL/6 background received two doses of 500 rad, while mice on the BALB/c background received two doses of 425 rad. The doses were split over two days.

2.6.1.1 Bone Marrow Preparation

Tibia and femur bones from donor mice were used to isolate bone marrow. In sterile conditions, all excess tissue was removed to fully expose the bone. The bones were separated by cutting above and below the knee joint to allow for access to flush the bone marrow using a needle. Sterile RF10 media was used to flush the bone marrow using a sterile needle (Terumo Agani). The flushed bone marrow was suspended in a sterile Petri dish (Sterilin). Using a pipette, the bone marrow was disaggregated to remove clumping. After disaggregation of the bone marrow, the suspension was transferred to a 50ml Falcon tube (Corning Centristar) using a sterile mesh membrane. The Petri dish was washed and transferred to a Falcon tube using RF10 media, and cells were then centrifuged for 10 minutes at 4°C at 1400 rpm. The supernatant was removed, and the resulting pellet was resuspended in RBC lysis buffer (Sigma-Aldrich) for 10 minutes at RT. An equivalent amount of RF10 was then added to neutralize the lysis action and cells were centrifuged. The resulting pellet was then resuspended in MACs buffer and counted. The bone marrow then required a depletion process to remove mature T cells within the suspension. A pre-depletion sample was taken to compare the accuracy of the depletion. Anti-CD3 antibody conjugated to PE was used to stain the bone marrow, and cells were then incubated in anti-PE beads (Miltenyi Biotech) and incubated for 20 minutes at 4°C. A QuadroMACS magnet was used to deplete the sample of $CD3^+$ cells. LS columns were place on the magnet and activated by 2ml of MACs, and then the sample was passed through the column. Once all of the sample passed through, the column was washed once using MACS buffer. The post depletion sample was then compared to the pre depletion sample to assess the efficacy of the removal of $CD3^+$ cells. Cells from the columns were counted and resuspended in sterile PBS without magnesium

or calcium (Sigma Aldrich). Each mouse received 5 million cells via intravenous injection under sterile conditions in a 200µl volume, and mice were then sacrificed at different timepoints to assess the kinetics of thymus recovery.

2.7 Adoptive Cell Transfer

Adoptive cell transfer experiments were utilized to assess T cells produced by the recovering thymus post BMT. Dual reporter (RAG2^{GFP}Foxp3^{RFP}) bone marrow (Table 2.1) was used to generate bone marrow chimeras as described in Section 2.8.1. After generation of bone marrow chimeras, the thymus was harvested 28 days post BMT alongside unmanipulated dual reporter controls. The BMT thymus and the control thymus were then mechanically digested as described in Section 2.3.1. The thymi were then counted and stained for cell surface markers. Following the staining process, the two samples were then high speed sorted as described in Section 2.5.3. The sorted populations were then checked for purity and counted. Following the sort, the two populations were resuspended in sterile PBS without calcium and magnesium. 1 million cells were then intravenously injected into nude host mice and were kept under surveillance.

2.8 Analysis of Autoimmunity

2.8.1 Detections of Autoantibodies

To examine signs of autoimmunity, the presence of autoantibodies was analysed. Prior to the sacrifice of mice, blood was collected via cardiac puncture under anesthesia (4% Isoflurane; May and Barker, Dagenham UK). Each mouse was placed in facemask with their chests upright. Blood was then drawn using a sterile needle (Terumo Agani), and then transferred to an Eppendorf. Directly after this process, the mice were then sacrificed via Schedule one. The

Eppendorf, containing the blood, was then centrifuged and the serum was collected, which was aliquoted into smaller quantities in Eppendorfs and stored at $^-20°C$ until needed for use.

To look for the presence of autoantibodies, composite tissue slides (INOVA Diagnostics) that contained rat liver, kidney, and stomach were used. Before the slides could be used, tissue sections were blocked with 10% Goat serum (Sigma-Aldrich) that was diluted in PBS. This was used to prevent non-specific binding of secondary antibodies. The sections were blocked for 10 minutes and the goat serum was removed from the slides by washing. The sample serum, serially diluted in PBS, was then added to each section and incubated in a dark humidified chamber for 30 minutes. After the incubation, the slides were placed in a PBS wash for 5 minutes. After the washing process, the tissue sections were stained with Goat F(ab')$_2$ anti-mouse IgG(H+L) FITC (Southern Biotech). The slides were then incubated in dark humidified chamber for 30 minutes and then were washed in the PBS for 5 minutes. The slides were then dipped in 4,6-diamidino-2-phenylindole (DAPI) for 10 seconds and then washed in PBS. The slides were then mounted with a coverslip and analyzed by microscope visualization.

2.8.2   Cellular Infiltrates

Cellular infiltrates were used as readout for autoimmunity. Tissue from sacrificed mice was harvested and placed in PBS. The tissue was then frozen in blocks containing Optimal Cutting Temperature compound (OCT) in liquid nitrogen. The tissue blocks were then stored at $^-80°C$. For analysis of cellular infiltrates, the tissue was removed from the $^-80°C$ freezer and placed on dry ice. The tissue was cut using a Cryostat at $^-30°C$. The tissue was cut at $7\mu m$ thickness and placed on slides (Hendley-Essex). The sections were cut approximately $35\mu m$ apart. Sections were then allowed to dry at RT before being fixed in acetone (Baker) for 10 minutes. After

fixation, the sections were left to dry at RT and then stored at $^-$20°C until use. For the identification of cellular infiltrates, the tissues were stained with Hematoxylin and Eosin (H&E). After the staining, the tissue was mounted using DPX Mountant (Sigma-Aldrich). The slides were then visualized on the slide scanner (Zeiss; Imaging Suit, University of Birmingham) to take whole tissue pictures for quantification of cellular infiltrates per cm^2.

2.9   Immunohistology

2.9.1   Freezing Tissue

Tissue was isolated from control or experimental mice. The tissue was cleaned to remove excess blood before freezing. Thymus lobes were carefully separated and placed in a foil casing and immediately frozen down on dry ice. The samples were then stored in $^-$80 degrees Celsius until use.

2.9.2   Preparation of Tissue Sections

Samples were removed from the $^-$80°C freezer and placed on dry ice. Thymus lobes were then mounted on OCT and placed on the microtome for preparation of cutting on cryostat that maintained $^-$30°C temperature. Tissue sections were then cut at 7µm depth and placed on glass slides. The slides were allowed to dry at RT and then fixed in acetone. After the fixation, the slides also were allowed to dry at RT before being stored at $^-$20°C until use.

2.9.3   Immunolabelling

For analysis of tissue sections, slides were removed from $^-$20°C and allowed to air dry for 30 minutes before they were rehydrated in a PBS bath for 10 minutes. After the rehydration process, the sections were then stained with antibodies (Table 2.7). All antibodies were diluted in 1% Bovine Serum Albumin (BSA) that was initially diluted in PBS. Stained sections were

incubated in dark humidified chamber for 30 minutes and then washed in a PBS bath for 5 minutes. If necessary, a secondary antibody was applied similarly and incubated for 30 minutes. Following the staining process, the slides were dipped in DAPI for 10 seconds and washed in PBS. The slides were then covered with a coverslip with the aid of Prolong Gold Antifade Mountant (Life Technologies) to prevent fading of the fluorochromes. The coverslip was sealed around the edges using nail varnish and allowed to dry. Slides were then imaged on the same day or the following day on the confocal microscope (Zeiss 880 Zen Microscope; Imaging Suit, University of Birmingham).

Table 2.7. Antibodies Used for Immunohistology

Antibody	Clone	Fluorochrome	Supplier
CD4	Rat/GK1.5	Alexa Fluor 647	Biolegend
CD8	Rat/ IgG2b 53-6.7	Biotin	ThermoFisher
ERTR5	Rat/IgM	N/A	ThermoFisher
CD205	205yekta	Biotin	ThermoFisher
Anti-Rat IgM	Goat/IgM	Alexa Fluor 488	ThermoFisher
Streptavidin	N/A	Alexa Fluor 555	ThermoFisher

2.10 Statistical Analysis

Analysis was done using GraphPad Prism 9 software. GraphPad Prism was also used to generate graphs from experimental data. Statistical analysis was completed using one-way ANOVA or student t-test in which symbols on graphs represent the level of significance where non-significant (ns), $p<.05$ (*), $p<.01$ (**), $p<.001$ (***), and $p<.0001$ (****). The type of test used is identified in the figure legend of each figure.

3   CHAPTER 3: INVESTIGATING KINETICS OF THYMUS RECOVERY POST SUB-LETHAL IRRADIATION

3.1 Introduction

As described in the previous chapters, the thymus is susceptible to stimuli that cause a decrease in thymus size as well as thymus function. This has an impact on the T cell development process that can cause severe effects on the function of the immune system. Studies have utilized different models to invoke thymus atrophy or damage and investigate the mechanism of thymus recovery. Sub-lethal irradiation (SLI) has been used as a model to examine thymus recovery post damage (Takada *et al.*, 1969; Zúñiga-Pflücker and Kruisbeek, 1990; Zubkova, Mostowski and Zaitseva, 2005; Xiao *et al.*, 2017). This model allows for examination of the mechanism of endogenous thymus recovery and identify differential elements that the thymus requires for the recovery and regeneration after damage.

The thymus contains different compartments that have unique roles during the T cell development process. In the initial process, progenitors colonize the thymus and are localized with in the cortical regions, and in contrast more developing thymocytes localize within the medullary regions before their egress into the periphery. Disruption of the compartmentalization can have severe consequences not only on developing thymocytes but also on the thymus microenvironment that is required for proper development. As a result, this chapter will focus on examining thymus recovery following damage using the SLI model.

In this model, we have utilized SLI as a type of ablative therapy to cause thymic damage and examine in detail the mechanism of thymus recovery. Furthermore, by using this model, we have posed the following questions:

1) What are the kinetics of endogenous thymus recovery following acute thymic damage?

2) Are there qualitative changes that occur following acute thymus damage that affect overall thymus function?

3.2 Results

3.2.1 Sub-Lethal Irradiation Is an Effective Model to Examine Acute Thymus Recovery

To investigate thymus recovery, SLI was used to cause thymic damage and investigate different parameters of thymus recovery. Adult mice were subjected to a single dose of total body irradiation (TBI), and tissue was harvested from different timepoints to examine thymus recovery (Figure 3.1). To analyse the recovery of the damaged thymus, unmanipulated thymus tissue was harvested and analysed to provide a comparative analysis between steady-state and damaged/regenerating thymus. Tissue was harvested and mechanically digested and then stained with antibodies to identify different developing thymocyte populations that included DN, DP, SP4, and SP8 (Figure 3.2 A). The SP4 population was then broken down into subsets that included T-conventional (Tconv) and Treg based on the differential expression of CD25 and Foxp3. Furthermore, the Tconv population was further broken down by the expression of the markers CD69 and CD62L to discriminate immature thymocytes ($CD69^+CD62L^-$) from mature thymocytes ($CD69^-CD62L^+$) (Figure 3.2 B). Quantification of the different populations in an unmanipulated thymus was then performed to effectively analyse and compare the damaged thymus (Figure 3.2 C).

Having identified and characterized the different populations in the unmanipulated thymus, mice were subjected to SLI and tissue was then harvested at different timepoints. Following thymus damage, it was observed that as early as day (d) 4 post SLI, thymus weight significantly decreased. An increase in thymus weight began at d7 post SLI, however it was found that a second drop in thymus weight occurred at d28 post SLI and reached normal weight at d35 post SLI (Figure 3.3 A). Interestingly, thymus cellularity followed a similar pattern, where at d4 post SLI, cellularity was at the lowest level. Total thymus cellularity began to increase at d7 post

damage; however, it was still significantly decreased compared to the control. At d14 post SLI, cellularity was observed to reach normal levels compared to the control, however a second decrease was recorded beyond d14 post SLI. Similar to the weight of the thymus, the cellularity was found to return to normal by d35 post damage (Figure 3.3 B). Gross appearance of the thymus was recorded and compared to control thymus and it is observed that there is a clear reduction in size by d4 post SLI (figure 3.3 C).
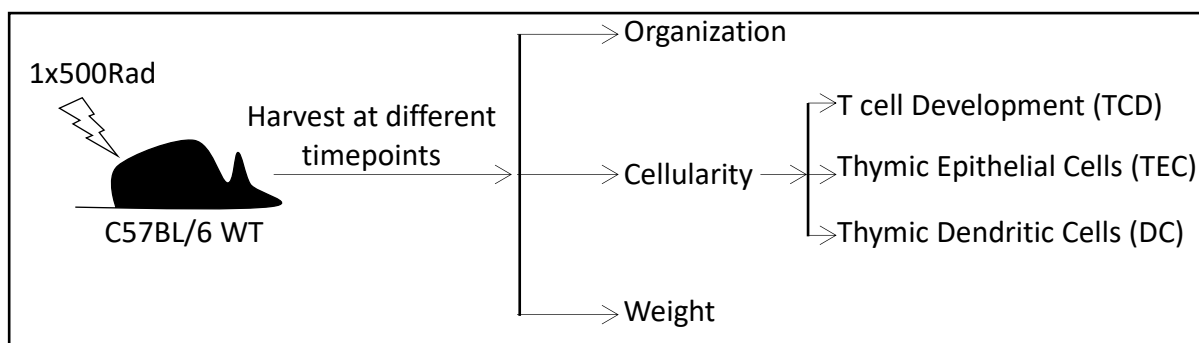
Figure 3.1. Analysis of Thymus Recovery Following Sub-Lethal Irradiation.

Female mice, at 6-8 weeks (wks.) of age, and placed on Baytril for 1 week prior to use, were subjected to one dose of SLI. Thymus tissue was harvested at different timepoints to analyse different parameters of thymus recovery.
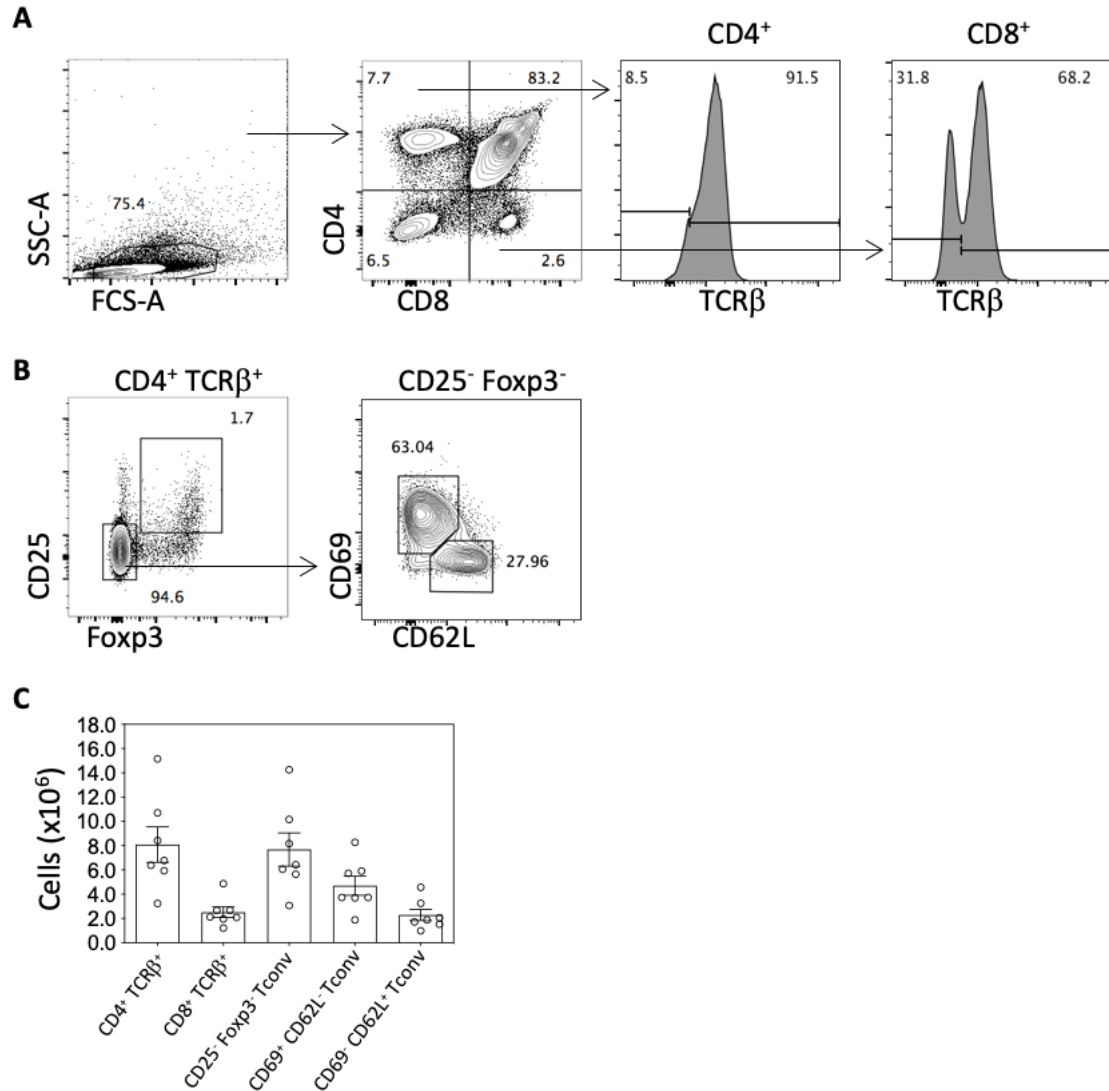
Figure 3.2. Identification of Mature CD4$^+$ and CD8$^+$ Thymocytes in WT Unmanipulated Adult Mice.

Female mice, age 6-8 weeks, were used as controls alongside experimental mice. Thymus tissue was harvested and mechanically digested for FACs analysis of unmanipulated non-irradiated T cell compartments. A. Gating strategy to identify CD4$^+$ and CD8$^+$ thymocytes in control thymus. B. Gating strategy to identify Tconv and Treg thymocytes in control thymus. Tconv are then broken into immature and mature by CD69 and CD62L expression. C. Numeral quantification of T cell compartments in control mice. Each dot represents one mouse where n=7. Error bars represent SEM.
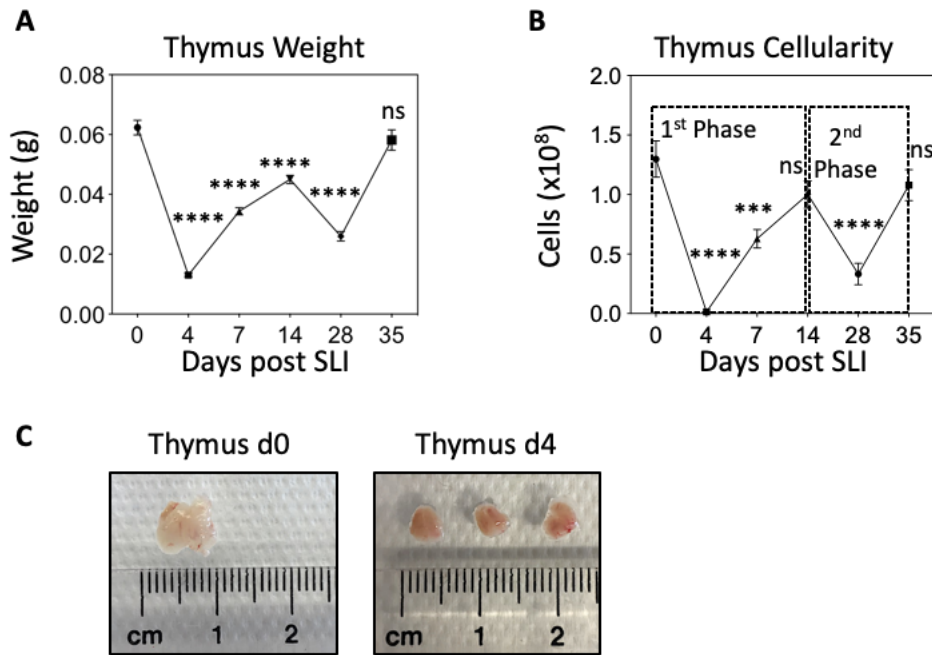
Figure 3.3. Thymus Recovery Following Damage is Biphasic.

A. Following SLI, thymus weight (g) was recorded at d0 (unmanipulated non-irradiated), d4, d7, d14, d28, and d35. B. Thymus cellularity was recorded following SLI at d0 (unmanipulated non-irradiated), d4, d7, d14, d28, and d35. Dotted line up to d14 shows initial and first recovery, while dotted line from d14 to d35 shows the second phase of thymus recovery. C. Thymus appearance at d0 (unmanipulated non-irradiated) and at d4 post damage shows reduction in thymus size highlighting the efficacy of SLI as a model to study thymus recovery post damage. For thymus weight n≥10 compiled from T cell development and TEC analysis. For thymus cellularity n=5 compiled from T cell development analysis where thymus was mechanically digested across two independent experiments. Error bars represent SEM. Ordinary One-way ANOVA was used for statistical analysis where each timepoint was compared to control. The level of significance is as follows where non-significant (ns), p<.05 (*), p<.01 (**), p<.001 (***), and p<.0001 (****).

3.2.2 Characterization of T cell Development Recovery Post Damage

Following acute thymus damage by means of SLI, thymus tissue was harvested, and mechanically digested and antibody staining was performed to characterize T cell development post damage. It was observed that following damage and specifically at d4 post SLI, there was a significant decrease and complete loss of the DP thymocyte ($CD4^+CD8^+$) population. Interestingly, at d14 post SLI, the DP thymocyte population began to reappear within the thymus and by d35 their proportion began to reach normal levels (Figure 3.4 A). Numerical quantification was analysed to compare DP thymocyte numbers after damage to the control (Figure 3.4 B) and after comparison it was observed that the complete loss of the DP thymocyte population was rapidly regained as early as d10 post SLI (Figure 3.4 C). However, extended analysis of the time course showed that after this rapid recovery there was a reduction in the DP thymocyte population that began at d14 post SLI and carried through until d28 post SLI. Interestingly, the extent of the reduction was lower in the second drop when compared to the initial decrease directly following SLI (Figure 3.4 C). To confirm the loss of this population, the organization of the thymus was analysed where thymus tissue was harvested and frozen and then cut for histology analysis. Following Hematoxylin and Eosin (H&E) staining, the loss of the DP thymocyte population can be seen at d4 post SLI as the H&E-stained section lacked distinctive dark areas that can be interpreted as the presence of DP thymocytes. However, sections from d7 and d14 following H&E staining show the presence of DP thymocytes (Figure 3.5 A), which is in line with previous flow cytometric analysis. To accurately confirm the loss of presence of the DP thymocyte population, sections were stained with antibodies to CD4 and CD8 for immunofluorescence analysis. A unmanipulated control thymus section was stained alongside as a comparison. Similarly, to the H&E staining, the immunofluorescence image revealed the loss of the DP thymocyte population at d4 post SLI by the loss of the CD4 and CD8 marker expression. At d7 and d14 post SLI, sections showed the presence of DP

thymocytes (Figure 3.5 B), confirming the flow cytometry data. Staining with the mTEC marker ERTR5, was also performed, which showed that the positioning of DP thymocytes did not occur within medullary regions (Figure 3.5 B).
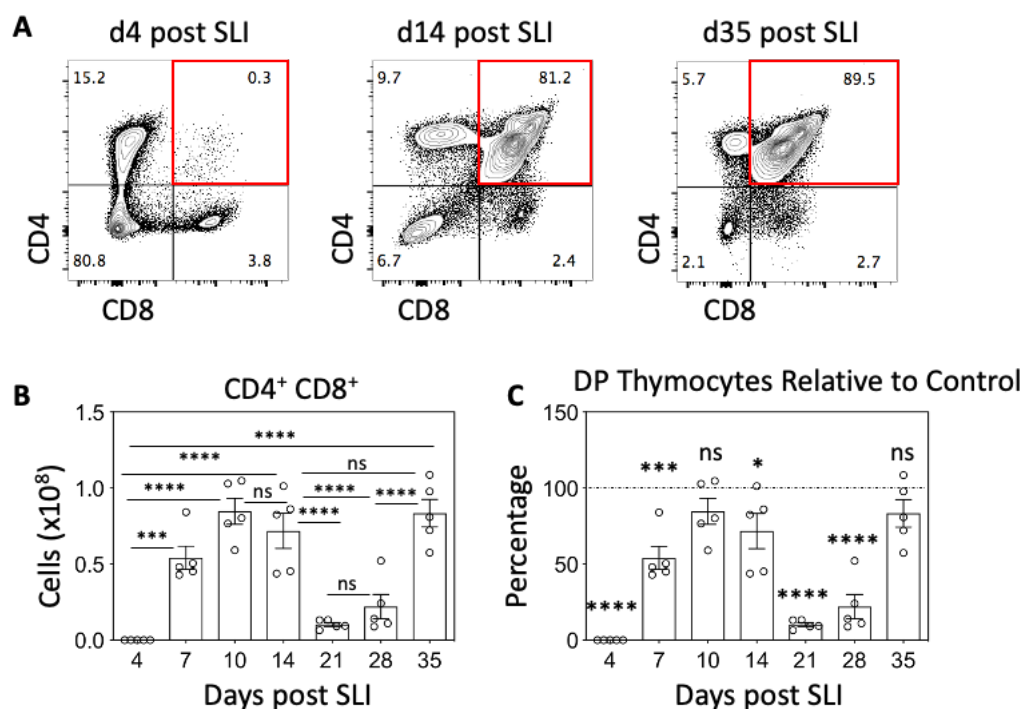
Figure 3.4. Rapid Restoration of CD4$^+$CD8$^+$ Thymocytes Post SLI.

Mice were subjected to SLI and thymus tissue was harvested and mechanically digested post damage for T cell development analysis A. Representative FACs plots of CD4 and CD8 staining in thymocytes, at d4, d14, d35 post SLI. B. Numerical quantification of CD4$^+$CD8$^+$ double positive (DP) compartment in experimental mice post SLI. C. Bar graph showing recovery of DP thymocyte compartment compared to control mice where dotted line represents the control. Each dot represents one mouse where n=5 for each time point across two independent experiments. Error bars represent SEM. Ordinary One-way ANOVA was used for statistical analysis where each timepoint was compared to control. The level of significance is as follows where non-significant (ns), p<.05 (*), p<.01 (**), p<.001 (***), and p<.0001 (****).
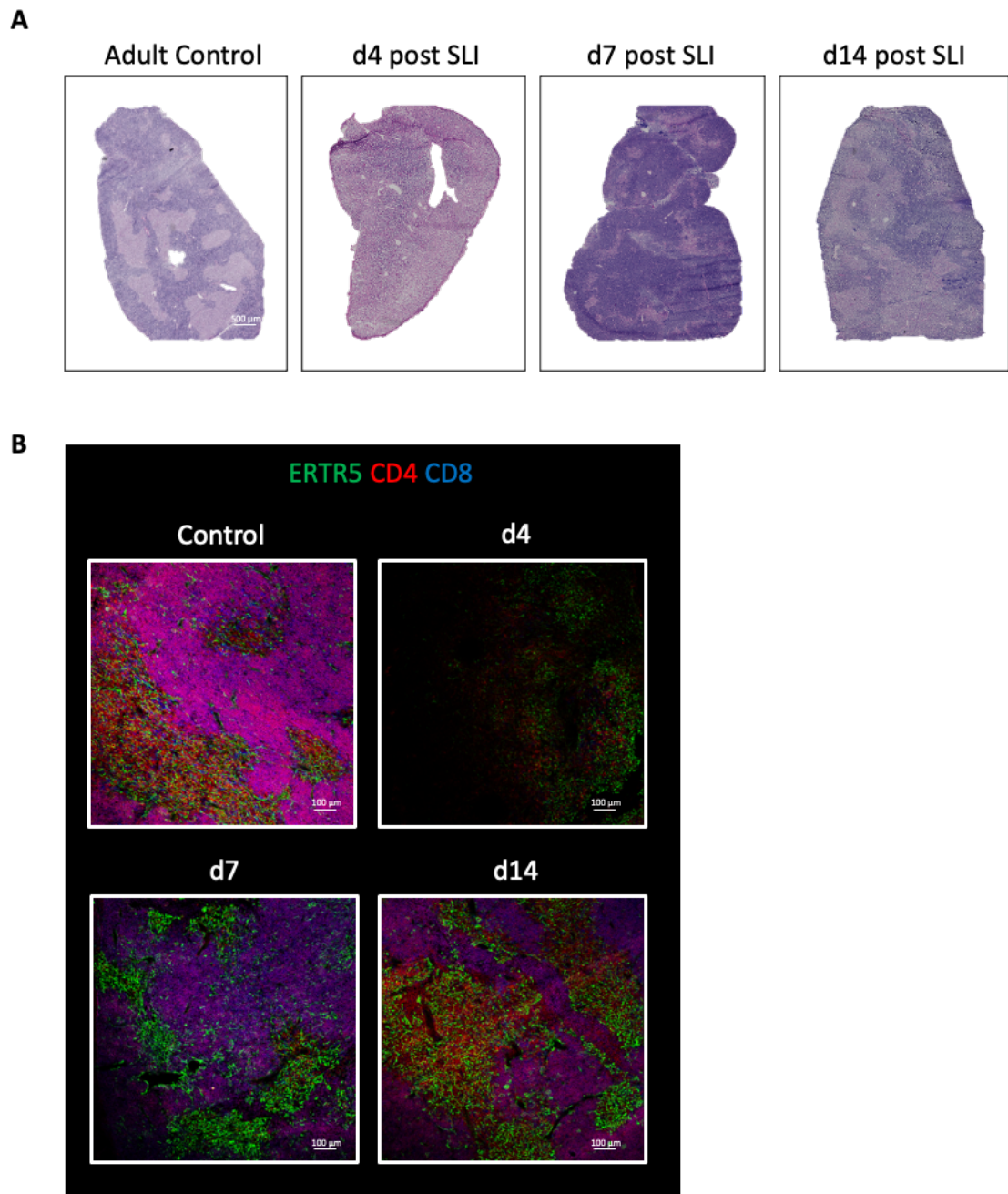
Figure 3.5. Organization of Thymus Post Damage.

Adult thymus tissue was harvested, frozen and then cut at 7μm thickness for histology analysis. A. Whole tissue imaging was performed post hematoxylin and eosin staining. Dark areas represent the cortical region while the lighter areas represent the medullary areas. B. Immunofluorescence image of thymus regions stained for CD4 (Red), CD8 (Blue), and ERTR5+ medulla areas (Green) post damage. All sections were stained and analysed alongside control sections. N=3 for each time point where thymus was harvested and frozen and then cut at 7μm thickness. Frozen sections were then stained, and pictures were taken using Zeiss 880 microscope.

The previous data shows that recovery of the DP thymocyte population occurs in two distinct phases (Figure 3.4 B). Because of this, the presence of the earliest thymic progenitors (ETP) was investigated. Thymus tissue from control mice were harvested and digested to analyse the presence of ETP under normal conditions (Figure 3.6 A). Further, mice were subjected to SLI and thymus tissue was harvested at different time points. Following analysis at d7, d10, and d14 post SLI, it was apparent that ETP were dramatically reduced at these timepoints compared to unmanipulated controls (Figure 3.6 B, C). To relate these differences in ETP and DP thymocytes to later stages of T cell development, we investigated the development of SP4 and SP8 thymocytes. Strikingly, at d4 post SLI a clear population of both SP4 and SP8 thymocytes remained after thymus damage. When the analysis was extended to d14 and 35, these populations persisted (Figure 3.7 A). When taking a closer look at the development of SP4 thymocytes in a time course experiment, it was observed that although at d4 post SLI there is a population present, the numbers were significantly decreased compared to the control. However, the numbers of SP4 thymocytes began to increase at d7 and d10 post SLI but did not reach normal levels (Figure 3.7 B). It was at d14 post SLI, numbers of SP4 thymocytes peaked and reached control numbers before beginning to decrease again at d21 and d 28 post SLI. In contrast to DP thymocytes at d35 (Figure 3.4 C), SP4 thymocytes did not recover to normal levels compared to the control at this timepoint (Figure 3.7 C). Similarly, when SP8 thymocyte analysis was performed, a similar pattern to the SP4 thymocytes was observed. Despite the presence of the SP8 thymocyte population at d4 post SLI, the numbers were dramatically decreased (Figure 3.7 D). Furthermore, numbers of SP8 thymocytes began to increase after d4 post SLI and reached a high peak at d14 post SLI before declining again (Figure 3.7 D). Analysis of SP8 thymocyte recovery at d35 post SLI remained significantly decreased when compared to the control (Figure 3.7 E).

By subdividing bulk SP4 thymocytes into CD25$^-$Foxp3$^-$ Tconv and CD25$^+$Foxp3$^+$ Treg (Figure 3.8 A), analysis revealed a significant decrease in both Tconv and Treg directly after damage and specifically at d4 and d7 post SLI (Figure 3.8 B and D). In the case of Tconv, numbers began to increase post d7 and reaching a peak at d14 post SLI, then began to decrease significantly (Figure 3.8 B). When comparing Tconv levels to the control, their numbers reached control levels by d14 before declining (Figure 3.8 C). In contrast, levels of Treg numbers did not reach control levels throughout the d35 time course (Figure 3.8 E).
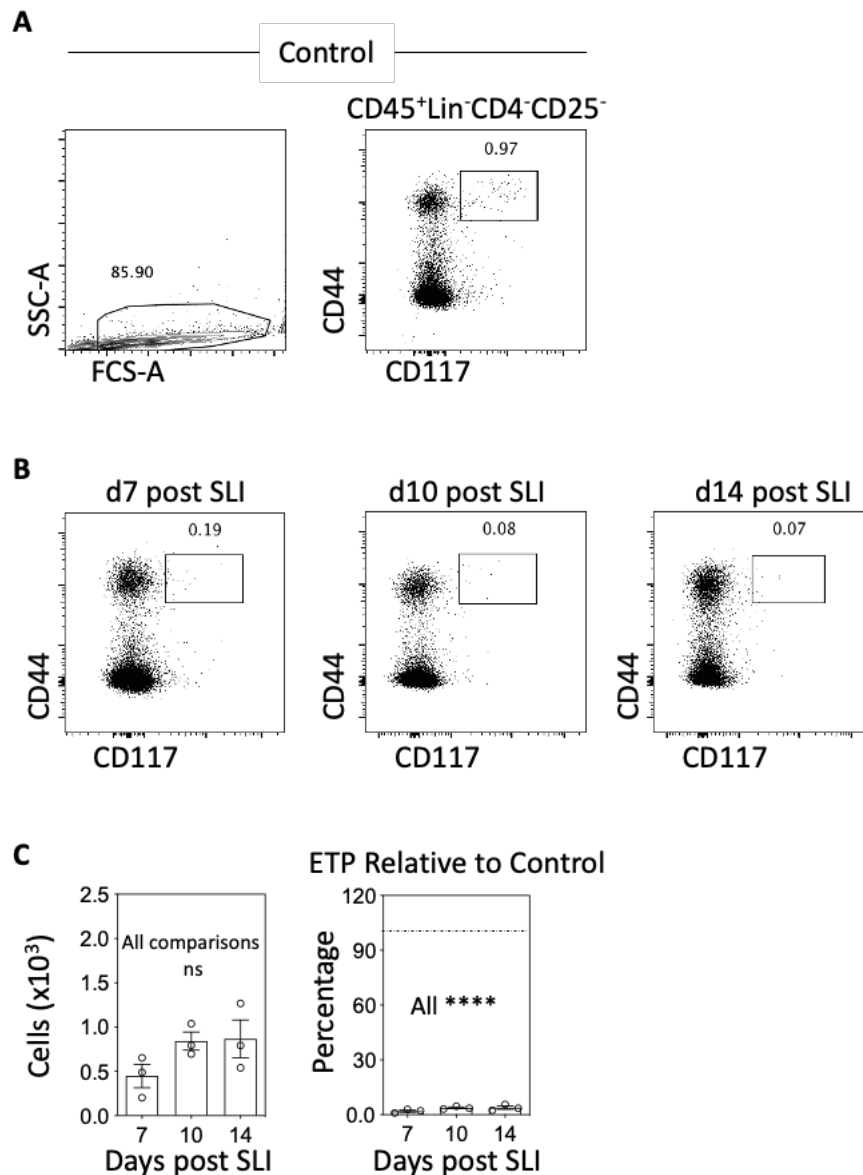
Figure 3.6. Thymus Colonization Does Not Supply Initial Recovery of T cell Development.

Mice were subjected to SLI and thymus tissue was harvested at d7, d10, and d14 post damage. A. Control phenotype of ETP where the Lin gate includes (CD3, TCRβ, TCRγδ, NK1.1, Ter119, Gr1, CD11c, CD11b, B220, CD8). Pre-gated on CD45$^+$Lin$^-$CD4$^-$CD25$^-$. B. FACs analysis of thymus tissue harvested following SLI. C. Numerical quantification of ETP number post SLI. Each dot represents one mouse where n=3 for each time point across one independent experiment. Dotted line represents control, which has combined the controls for each timepoint n=9 mice. Error bars represent SEM. Ordinary One-way ANOVA was used for statistical analysis where each timepoint was compared to control. The level of significance is as follows where non-significant (ns), p<.05 (*), p<.01 (**), p<.001 (***), and p<.0001 (****).
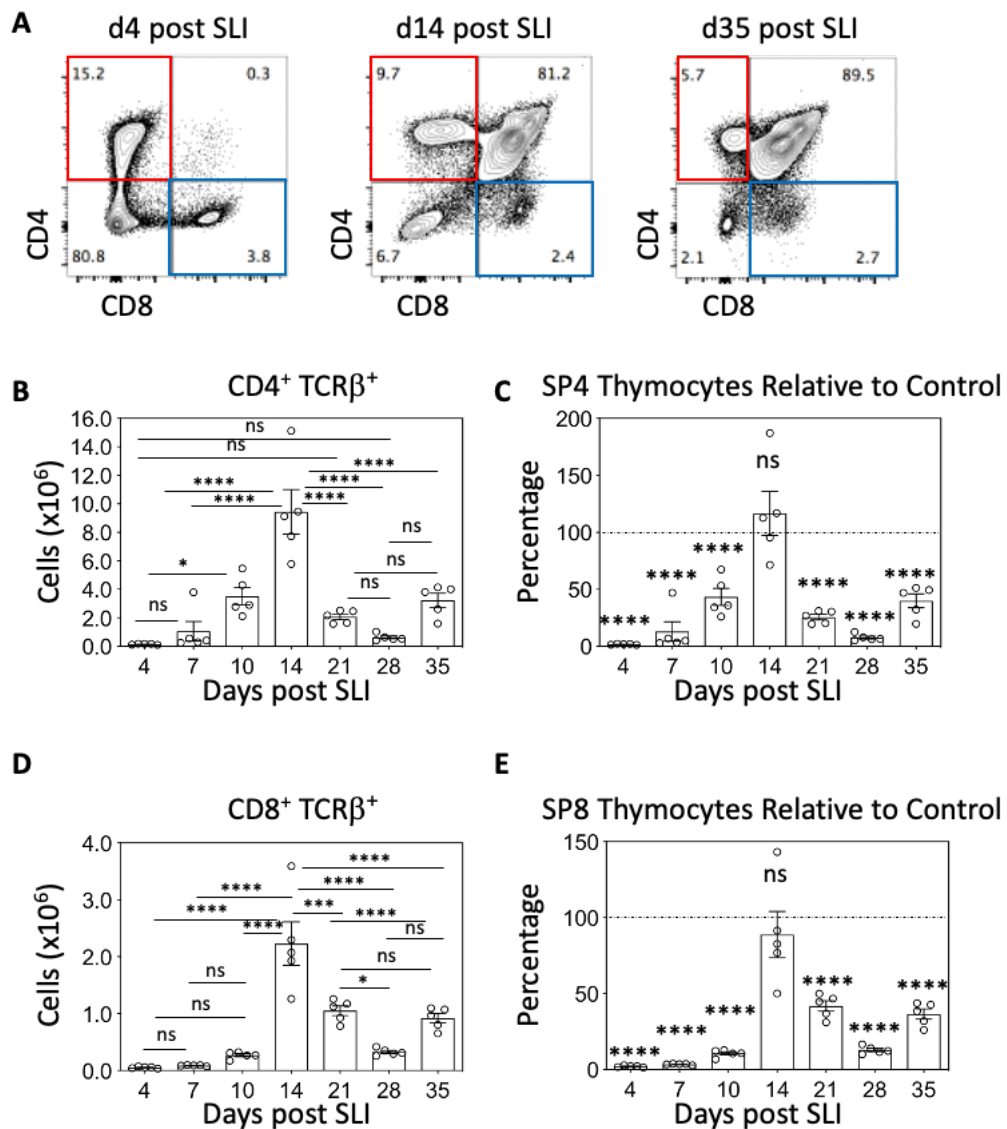
Figure 3.7. Reconstitution of CD4⁺ and CD8⁺ Thymocytes Post SLI Is Rapid and Transient.

Mice were subjected to SLI and thymus tissue was harvested and mechanically digested post damage for T cell development analysis A. Representative FACs plots of CD4 and CD8 staining in thymocytes, at d4, d14, d35 post SLI. B. Numerical quantification of CD4⁺TCRβ⁺ thymocytes (SP4; in red box) compartment in experimental mice post SLI. C. Numbers of SP4 were then compared to control where dotted line represents control mice. D. Numerical quantification of CD8⁺TCRβ⁺ thymocytes (SP8; in blue box) compartment in experimental mice post SLI. E. Numbers of SP8 were then compared to control where dotted line represents control mice. Each dot represents one mouse where n=5 for each time point across two independent experiments. Error bars represent SEM. Ordinary One-way ANOVA was used for statistical analysis where each timepoint was compared to control. The level of significance is as follows where non-significant (ns), $p<.05$ (*), $p<.01$ (**), $p<.001$ (***), and $p<.0001$ (****).
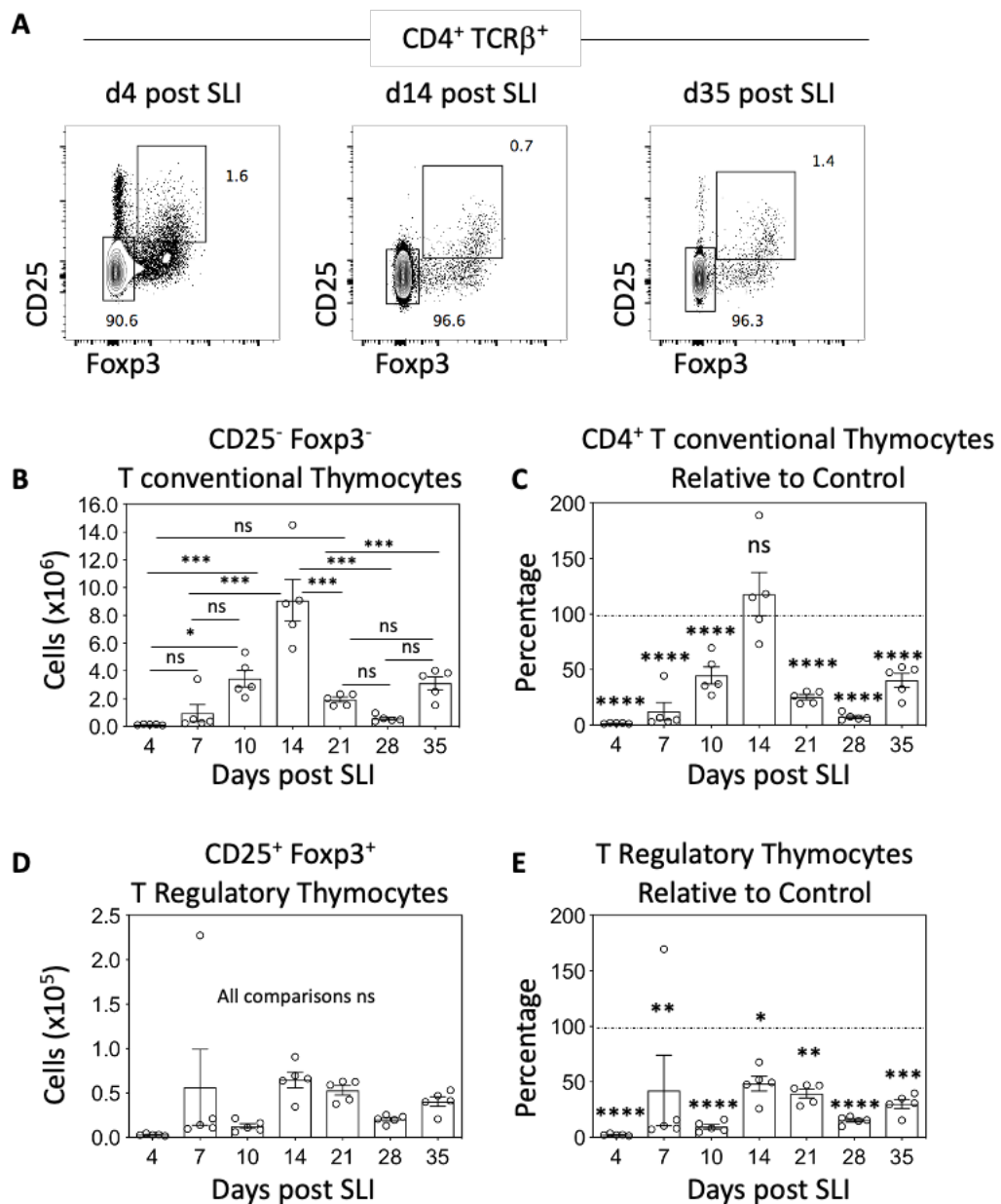
Figure 3.8. T Regulatory Thymocyte Recovery Is Slower Compared to T Conventional Thymocyte Recovery.

Mice were subjected to SLI and thymus tissue was harvested and mechanically digested post damage for T cell development analysis. A. Representative FACs plots of CD25 and Foxp3 staining in thymocytes, at d4, d14, d35 post SLI. Pre-gated on CD4+TCRβ+. B. Numerical quantification of C25‑Foxp3‑ T Conventional thymocyte compartment in experimental mice post SLI. C. Numbers of Tconv were then compared to control where dotted line represents control mice. D. Numerical quantification of CD25+ Foxp3+ T Regulatory thymocyte compartment in experimental mice post SLI. E. Numbers of Treg were then compared to control where dotted line represents control mice. Each dot represents one mouse where n=5 for each time point across two independent experiments. Error bars represent SEM. Ordinary One-way ANOVA was used for statistical analysis where each timepoint was compared to control. The level of significance is as follows where non-significant (ns), p<.05 (*), p<.01 (**), p<.001 (***), and p<.0001 (****).

3.2.3 Thymic Microenvironment Recovery Post Sub-Lethal Irradiation

Thymus tissue from unmanipulated control mice were harvested and enzymatically digested and then antibody stained to identify EpCAM1$^+$CD45$^-$ thymic epithelium (Figure 3.9 A). Furthermore, the overall thymic epithelial cell (TEC) population was broken down into cTEC and mTEC based on the expression of UEA-1 and Ly51 where cTEC displayed a UEA-1$^-$Ly51$^+$ phenotype and mTEC had a phenotype of UEA-1$^+$Ly51$^-$ (Figure 3.9 B). The mTEC population was then also broken down into two subsets based on the expression of MHCII and CD80 where mTEC^{lo} were identified as MHCII^{lo}CD80$^-$ and mTEC^{hi} were MHCII$^+$CD80$^+$ (Figure 3.9 C). Based on the characterization and identification of the TEC population in control mice, thymus tissue was then harvested from mice that received a single dose of SLI. Following thymus damage, the overall TEC population was significantly reduced (Figure 3.10 A, B). Furthermore, throughout the time course analysis, TEC numbers in SLI treated mice remained at approximately 30% of TEC numbers in control mice (Figure 3.10 C). This low recovery of TEC after SLI prompted investigation of the total TEC population in detail, which was split into cTEC and mTEC to compare their recovery after damage (Figure 3.11 A). Strikingly, when quantification analysis was performed it was shown that the cTEC population remained relatively constant throughout the d35 time course (Figure 3.11 B, C). In contrast, mTEC numbers did not follow the same pattern. Thus, mTEC numbers were at their highest level at d4 post SLI and then numbers began to decrease, where they were significantly reduced compared to control mice (Figure 3.11 D, E).
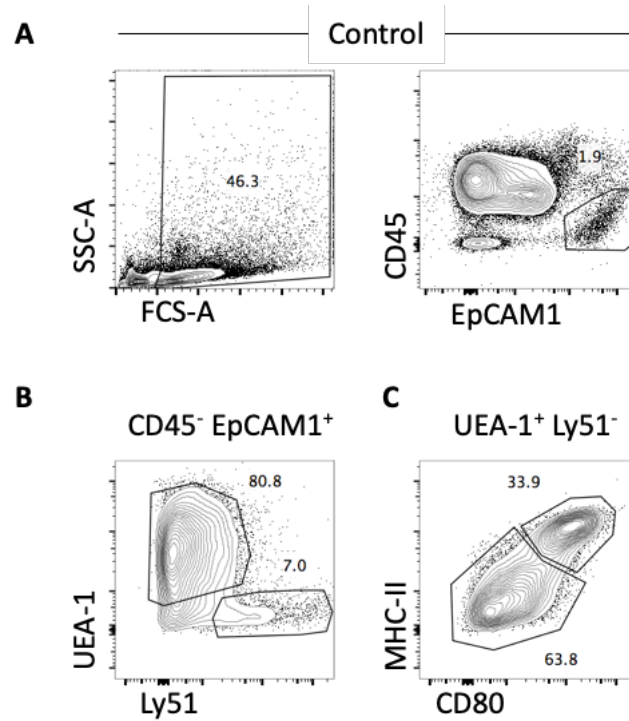
Figure 3.9. Identification of Thymic Epithelial Cells in Control Mice.

Female mice, age 6-8 weeks, were used as controls alongside experimental mice. Thymus tissue was harvested and enzymatically digested for FACs analysis of unmanipulated non-irradiated epithelial cell compartment. A. Gating strategy to identify the TEC population in control thymus as CD45$^-$ EpCAM1$^+$. B Gating strategy to identify the TEC subset population in control thymus; cTEC (Ly51$^+$ UEA-1$^-$) and mTEC (UEA-1$^+$ Ly51$^-$). C. Gating strategy to identify the mTEC subset population in control thymus; mTEC^{lo} (MHCII^{lo} CD80$^-$) and mTEC^{hi} (MHCII^{hi} CD80$^+$).
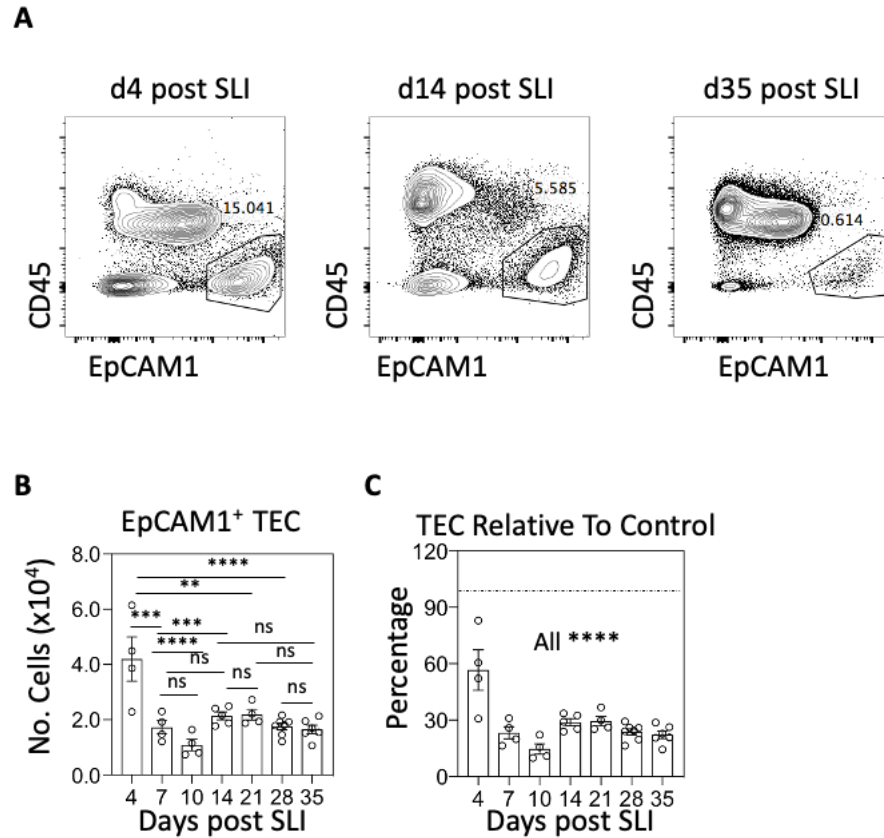
Figure 3.10. EpCAM1⁺ TEC Do Not Fully Recover Post SLI.

Mice were subjected to SLI and thymus tissue was harvested and enzymatically digested post damage for thymic epithelial cell analysis. A. Representative FACs plots of CD45 and EpCAM1 staining in thymic epithelial cells at d4, d14, d35 post SLI. B. Numerical quantification of EpCAM1$^+$ CD45$^-$ TEC compartment in experimental mice post SLI. C. Bar graph showing recovery of TEC compartment compared to control mice where dotted line represents the control. Each dot represents one mouse where n≥4 for each time point across two independent experiments. Error bars represent SEM. Ordinary One-way ANOVA was used for statistical analysis where each timepoint was compared to control. The level of significance is as follows where non-significant (ns), $p<.05$ (*), $p<.01$ (**), $p<.001$ (***), and $p<.0001$ (****).
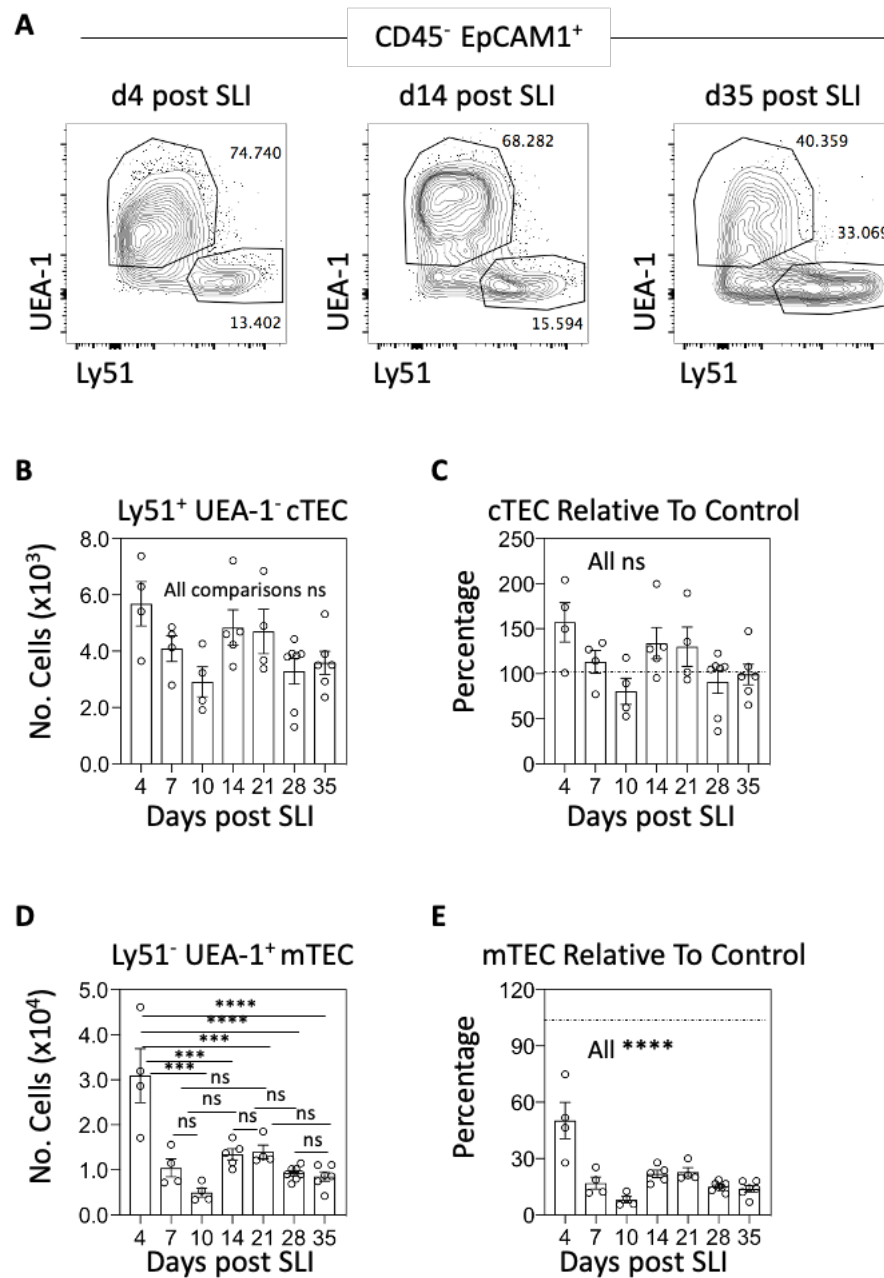
Figure 3.11. cTEC Have Improved Recovery Than mTEC Post SLI.

Mice were subjected to SLI and thymus tissue was harvested and enzymatically digested post damage for thymic epithelial cell analysis A. Representative FACs plots of UEA-1 and Ly51 staining in thymic epithelial cells at d4, d14, d35 post SLI. B. Numerical quantification of Ly51$^+$ UEA-1$^-$ cTEC compartment in experimental mice post SLI. C. Bar graph showing recovery of cTEC compartment compared to control mice where dotted line represents the control. D. Numerical quantification of Ly51$^-$ UEA-1$^+$ mTEC compartment in experimental mice post SLI. E. Bar graph showing recovery of mTEC compartment compared to control mice where dotted line represents the control. Each dot represents one mouse where n≥4 for each time point across two independent experiments. Error bars represent SEM. Ordinary One-way ANOVA was used for statistical analysis where each timepoint was compared to control. The level of significance is as follows where non-significant (ns), $p<.05$ (*), $p<.01$ (**), $p<.001$ (***), and $p<.0001$ (****).

As the cTEC populations were maintained post damage, we next tested the functionality of cTEC by measuring their ability to support positive selection. MHCI restricted T-cell receptor transgenic OT-I mice were used to assess positive selection, as these mice have a directed differentiation to the SP8 lineage which can be measured by expression of the TCRVα2 region. Thymus tissue from OT-I transgenic mice was harvested and mechanically digested and antibody stained to characterize under unmanipulated conditions. It was found that 75% of SP8 thymocytes express TCRVα2 (Figure 3.12 A). OT-I mice were then subjected to SLI and thymus tissue was harvested d10 post damage (Figure 3.12 B). Interestingly, the overall percentage of SP8 thymocytes between control and SLI mice were very similar with no statistical difference found (Figure 3.12 C). Furthermore, SP8 thymocytes from SLI mice were analysed for the expression of TCRVα2, and it was found that the proportion of cells expressing the transgenic TCRα chain was significantly higher (Figure 3.12 D), which overall suggests that following thymus damage, remaining cTEC can efficiently support the positive selection process.
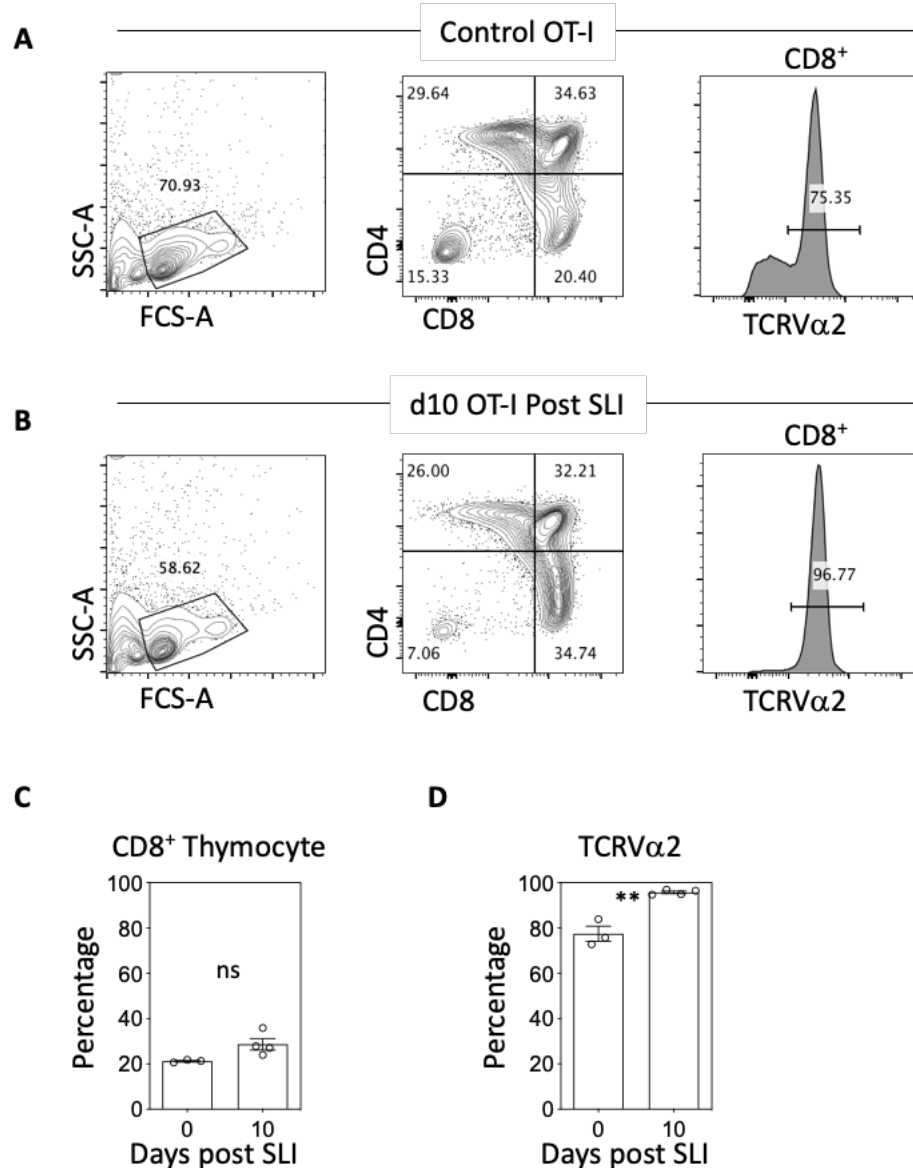
Figure 3.12. Positive Selection Is Functional Post SLI.

Transgenic OT-1 mice were subjected to SLI and thymus tissue was harvested at d10 post damage to assess positive selection. Adult unmanipulated non-irradiated OT-1 mice were used alongside as controls. A. FACs analysis showing staining for CD4, CD8, and TCRVα2 in control mice. B. FACs analysis showing staining for CD4, CD8, and TCRVα2 in experimental mice at d10 post SLI. C. Bar graph displaying comparison of CD8+ thymocyte percentage. D. Bar graph displaying TCRVα2 percentage. Each dot represents one mouse where n=4 for experimental mice and n=3 for control mice across one independent experiments. Error bars represent SEM. Unpaired student t test was used for statistical analysis where each timepoint was compared to control. The level of significance is as follows where non-significant (ns), p<.05 (*), p<.01 (**), p<.001 (***), and p<.0001 (****).

As bulk mTEC showed evidence of failed recovery following damage, analysis was extended to split them into mTEC^{lo} and mTEC^{hi} subsets. After damage, both mTEC populations were evident (Figure 3.13 A). However, both mTEC^{lo} and mTEC^{hi} showed significantly decreased numbers post damage, and this was maintained up to d35 post SLI with no increase in numbers (Figure 3.13 B and C). When compared to control mice, mTEC^{lo} had approximately 60% levels compared to the control at d4 post SLI but then significantly decreased to only 20% of control levels (Figure 3.13 D). However, mTEC^{hi} displayed a fluctuating pattern in which levels compared to the control were changed throughout the time course analysis. Thus, mTEC^{hi} were only at 30% of control levels at d4 post SLI and then decreased to the lowest levels at d10 post SLI. After this timepoint, mTEC^{hi} increased to approximately 50% compared to the control at d14 and d21 post SLI, before significantly declining at both d28 and d35 post damage (Figure 3.13 E). Thus, within the mTEC population, both mTEC^{lo} and mTEC^{hi} fail to fully recover from SLI damage during a 35d time course, and differing kinetics of recovery were seen for each population.

Figure 3.13. mTEC Subsets Do Not Recover Post SLI.

Mice were subjected to SLI and thymus tissue was harvested and enzymatically digested post damage for thymic epithelial cell analysis. A. Representative FACs plots of MHCII and CD80 staining in medullary thymic epithelial cells at d4, d14, d35 post SLI. B. Numerical quantification of mTEC^{lo} compartment in experimental mice post SLI. C. Numerical quantification of mTEC^{hi} compartment in experimental mice post SLI. D. Bar graph showing recovery of mTEC^{lo} compartment compared to control mice where dotted line represents the control. E. Bar graph showing recovery of mTEC^{hi} compartment compared to control mice where dotted line represents the control. Each dot represents one mouse where n≥4 for each time point across two independent experiments. Error bars represent SEM. Ordinary One-way ANOVA was used for statistical analysis where each timepoint was compared to control. The level of significance is as follows where non-significant (ns), $p<.05$ (*), $p<.01$ (**), $p<.001$ (***), and $p<.0001$ (****).

As mTEC have been shown to influence the intrathymic dendritic cell (DC) pool (Lei *et al.*, 2011; Cosway *et al.*, 2018), thymic DC were investigated. Freshly isolated thymus tissue from unmanipulated control mice was harvested and enzymatically digested and then antibody stained for the identification of thymic DC and their subsets, where pDC were $CD11c^{low}PDCA1^{+}$, conventional DC1 (cDC1) were $CDl1c^{+}Sirp\alpha^{-}$ and cDC2 were $CD11c^{+}Sirp\alpha^{+}$ (Figure 3.14 A, B). Following damage, thymus tissue from SLI mice was analysed in a similar manner (Figure 3.15 A). Following SLI, cDC numbers at d7 and d14 post SLI were significantly reduced at approximately 60% of control numbers (Figure 3.15 B and C). cDC were then broken down into cDC1 and cDC2 and shows significant reductions in both subsets (Figure 3.15 F and G). Interestingly, pDC displayed a different a recovery pattern compared to cDC, as their numbers and proportions were similar for the first three weeks post SLI at approximately 15% of control levels. Interestingly, while levels of pDC began to increase at d28 post SLI and d35 post SLI, they remained reduced, reaching only approximately 50% of the pDC in control mice (Figure 3.15 D and E).
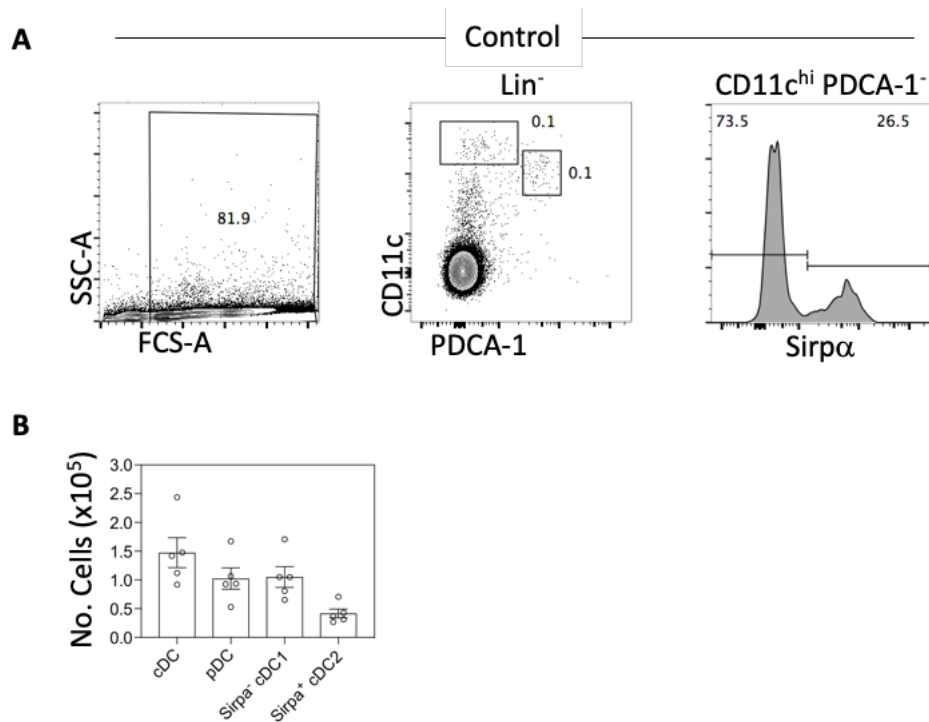
Figure 3.14. Identification of Thymic Dendritic Cells in Control Mice.

Female mice, age 6-8 weeks, were used as controls alongside experimental mice. Thymus tissue was harvested and enzymatically digested for FACs analysis of unmanipulated non-irradiated thymic dendritic cell compartment. A. Gating strategy to identify thymic dendritic cells and their subsets. B. Numeral quantification of thymic dendritic cells in control mice. Each dot in graph represents a mouse where n=5.
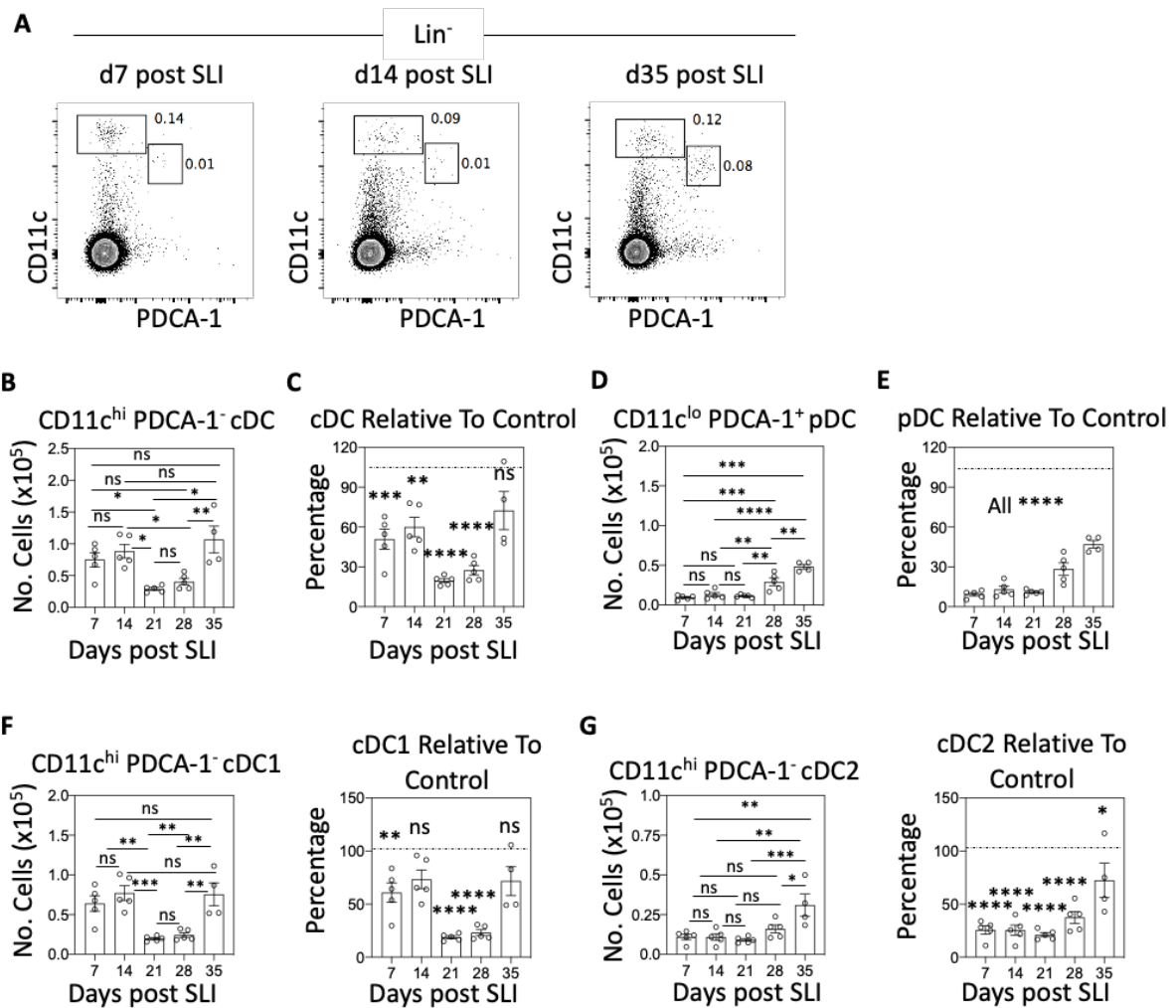
Figure 3.15. **Slow Recovery of Thymic Dendritic Cells Post SLI.**
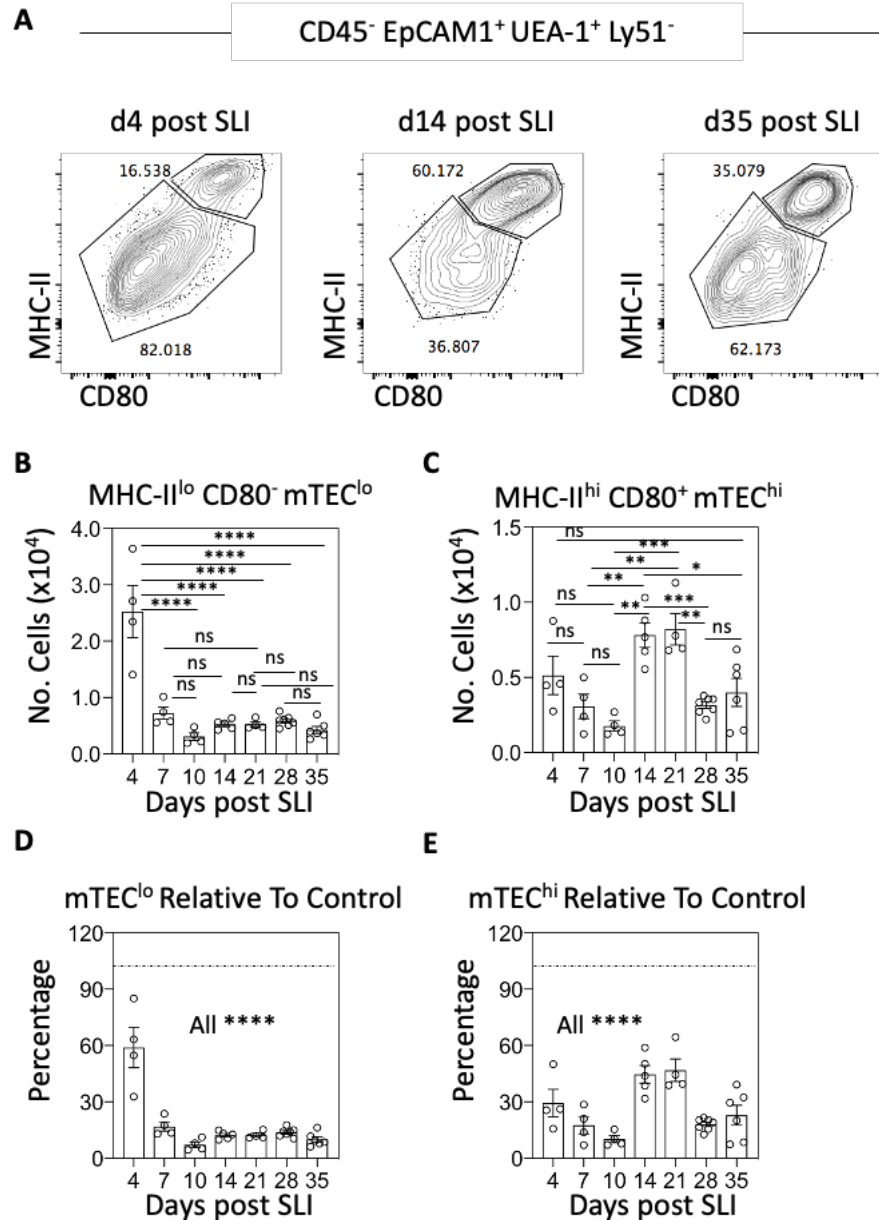
Mice were subjected to SLI and thymus tissue was harvested and enzymatically digested post damage for thymic dendritic cell analysis. A. Representative FACs plots of CD11c and PDCA-1 staining in thymic dendritic cells at d7, d14, d35 post SLI. B. Numerical quantification of cDC compartment in experimental mice post SLI. C. Bar graph showing recovery of cDC compartment compared to control mice where dotted line represents the control. D. Numerical quantification of pDC compartment in experimental mice post SLI. E. Bar graph showing recovery of pDC compartment compared to control mice where dotted line represents the control. F. Numerical quantification and bar graph showing recovery of cDC1. G. Numerical quantification and bar graph showing recovery of cDC2. Each dot represents one mouse where n=5 for d7, d14, d21, d28 and n=4 for d35 across two independent experiments. Error bars represent SEM. Ordinary One-way ANOVA was used for statistical analysis where each timepoint was compared to control. The level of significance is as follows where non-significant (ns), p<.05 (*), p<.01 (**), p<.001 (***), and p<.0001 (****).

3.2.4 Functional Assessment of Negative Selection Post Sub-Lethal Irradiation

As mTEC and DC are significantly reduced post SLI (Figure 3.10 and Figure 3.15), the functionality of negative selection was assessed. This was achieved by investigating the presence of thymocytes expressing TCRs with MMTV reactivity post SLI. BALB/c mice express the mouse mammary tumor virus (MMTV) genes MMTV 6, 8 and 9 that delete thymocytes expressing TCRs that contain Vβ3, 5 and 11 chains (Moore *et al.*, 1994). In contrast, C57BL/6 mice lack these MMTV genes and as a result SP thymocytes that express TCRVβ3, 5 and 11 chain escape negative selection and mature into peripheral T-cells. To demonstrate this, thymus tissue from unmanipulated BALB/c and C57BL/6 mice was mechanically disrupted, and antibody stained for the identification of TCRVβ thymocytes within the SP4 subset (Figure 3.16 A and B). As expected, in C57BL/6 mice that lack MMTV 6, 8 and 9, SP4 thymocytes expressing Vβ3, Vβ5 or Vβ11 were clearly identifiable (Figure 3.16 C). In contrast in BALB/c mice where MMTV 6, 8 and 9 are present, SP4 thymocytes expressing TCRVβ3, Vβ5 or Vβ11 are much reduced because of negative selection (Figure 3.16 D). Due to this ability to measure antigen-specific negative selection, BALB/c mice underwent SLI and were then analysed as above at d14 post SLI. Strikingly, when compared to untreated BALB/c mice, we saw a significant increase in the proportions of Vβ3$^+$, Vβ5$^+$ and Vβ11$^+$ SP4 thymocytes in SLI treated mice (Figure 3.17 A, B).
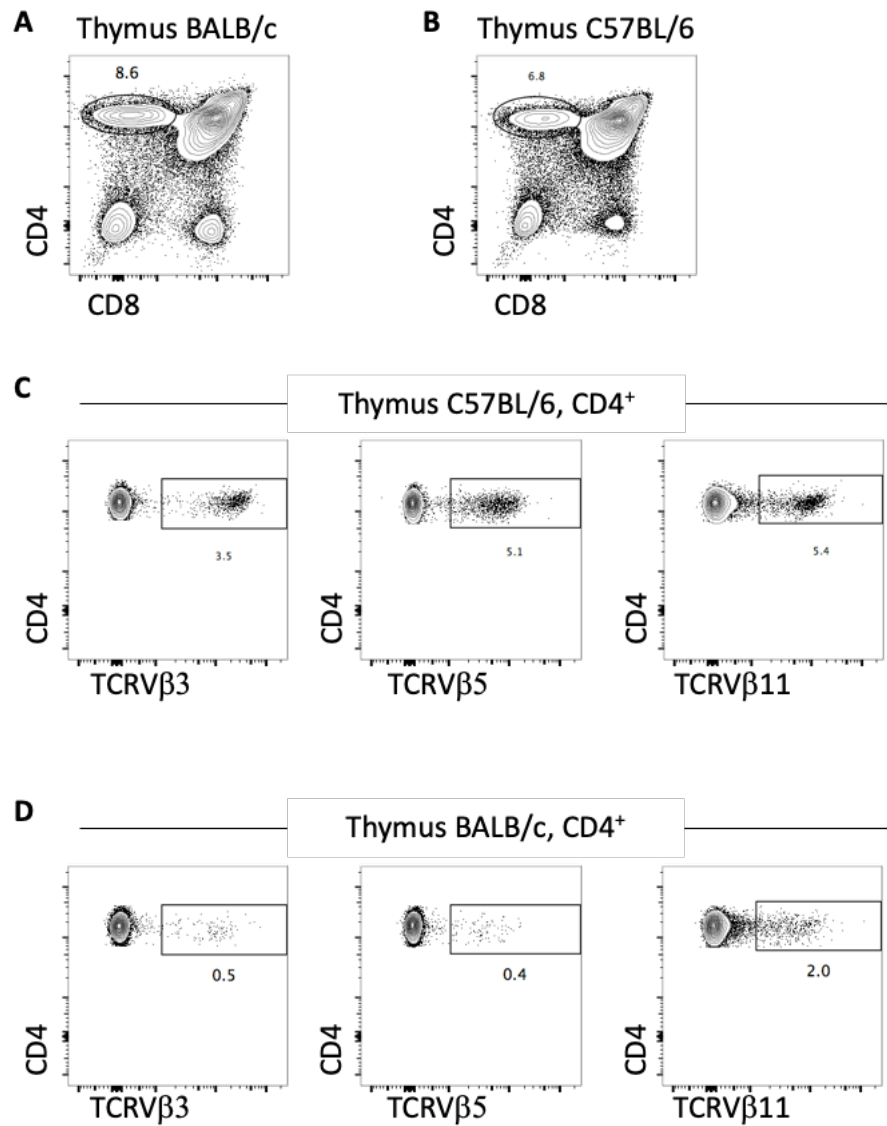
Figure 3.16. TCRVβ+ Thymocytes in Control Mice.

BALB/c and C57BL/6 thymus tissue were harvested and mechanically digested to identify the different thymocyte populations. Adult unmanipulated non-irradiated were used. A. FACs analysis showing staining for CD4, CD8, in control mice. B. FACs analysis showing staining for CD4, TCRVβ3, TCRVβ5 and TCRVβ11 in BALB/c control mice. C. FACs analysis showing staining for CD4, TCRVβ 3, TCRVβ5 and TCRVβ11 in C57BL/6 control mice.
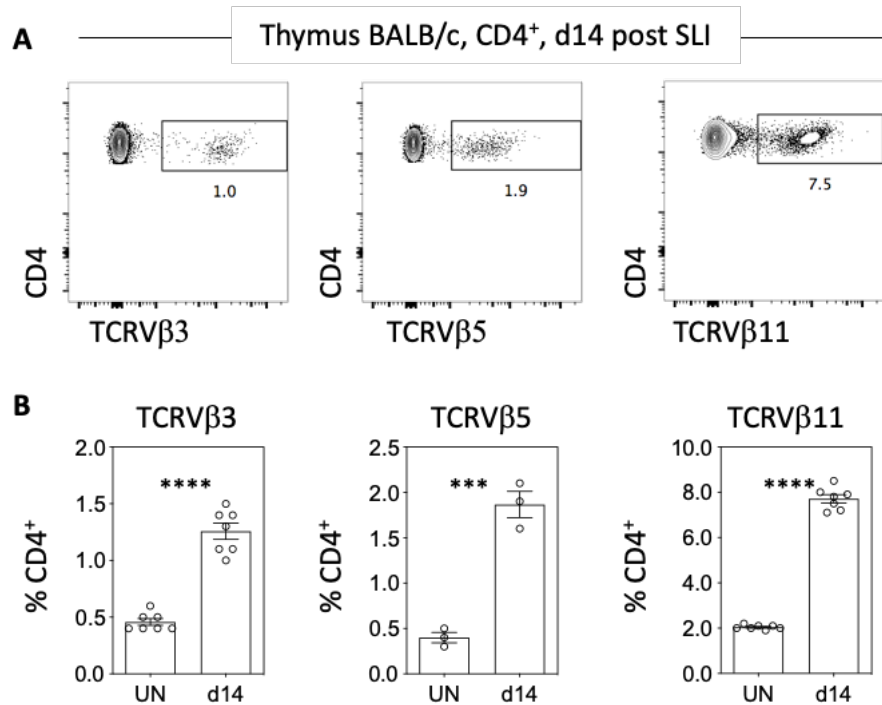
Figure 3.17. TCRVβ⁺ Thymocytes Do Not Get Deleted Post SLI.

BALB/c mice were subjected to SLI and thymus tissue was harvested at d14 post SLI and mechanically digested. A FACs analysis showing staining for CD4, TCRVβ3, TCRVβ5 and TCRVβ11 in BALB/c experimental mice. B. Bar graph displaying comparison of variable TCRVβ thymocyte percentages post SLI with unmanipulated controls (UN). Each dot represents one mouse where n=7 across two independent experiments for TCRVβ 3 and TCRVβ11 analysis and n=3 for TCRVβ5 analysis across one independent experiments. Error bars represent SEM. Unpaired student t test was used for statistical analysis where each timepoint was compared to control. The level of significance is as follows where non-significant (ns), $p<.05$ (*), $p<.01$ (**), $p<.001$ (***), and $p<.0001$ (****).

As the above findings suggest that SP thymocytes in SLI treated mice may be escaping negative selection, we investigated the presence of T-cells expressing 'forbidden' TCRVβ chains in the periphery of SLI treated BALB/c mice. Splenic tissue from BALB/c mice was harvested at d21 post SLI and TCRVβ3$^+$, Vβ5$^+$, Vβ11$^+$ CD4$^+$ bearing T cells were quantitated by flow cytometry. Strikingly, compared to untreated BALB/c mice Vβ11$^+$ CD4$^+$ T-cells were significantly increased post SLI, while Vβ3$^+$ and Vβ5$^+$ CD4$^+$ T-cells showed a trend towards an increase that was not statistically significant (Figure 3.18 A, B). Collectively these findings suggest that following SLI, intrathymic microenvironments that enable negative selection are impaired in their ability to delete self-reactive thymocytes, which results in their escape into the periphery as mature T-cells.
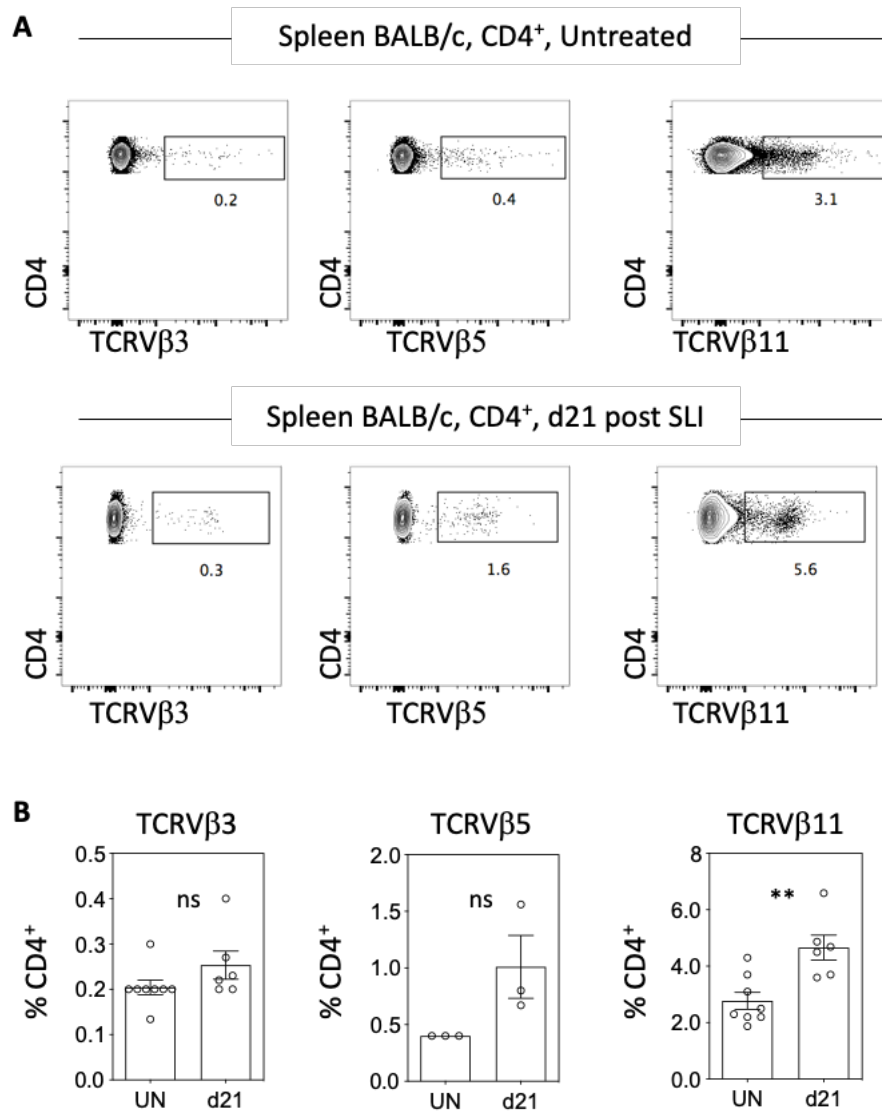
Figure 3.18. TCRVβ⁺ T cells Are Detected in The Periphery of BALB/c Mice Post SLI.

BALB/c mice were subjected to SLI and spleen tissue was harvested at d21 post SLI and mechanically digested. A. FACs analysis showing staining for CD4, TCRVβ3, TCRVβ5 and TCRVβ11 in BALB/c experimental mice. B. Bar graph displaying comparison of variable TCRVβ⁺ T cell percentages post SLI. Each dot represents one mouse where n=6 across two independent experiments for TCRVβ3 and TCRVβ11 analysis and n=3 for TCRVβ5 analysis across one independent experiment. For control analysis n=8 across two independent experiments for TCRVβ3 and TCRVβ11. Error bars represent SEM. Unpaired student t test was used for statistical analysis where each timepoint was compared to control. The level of significance is as follows where non-significant (ns), p<.05 (*), p<.01 (**), p<.001 (***), and p<.0001 (****).

3.2.5 Identifying Treatment Regimens to Boost Thymic Epithelium Recovery

Collectively, the findings above suggest that while the thymus is able to support new T-cell development post SLI, this process is compromised. Moreover, this reduction in thymus function correlates with changes in the mTEC compartment that is important in driving tolerance induction. Given these observations, we next performed experiments to try to boost the TEC compartment following SLI, in order to more effectively restore thymus function. Initially, as LTβR has been shown to be an important regulator of the mTEC compartment in the steady state (Cosway *et al.*, 2017), we examined the effects of injecting an agonistic antibody to LTβR after SLI treatment. Thus, mice were treated with either 100ug of anti-LTβR or an isotype control via intraperitoneal (Ip) injection one day prior SLI. Mice were then given three additional injections at 2d, 4d, and 6d post SLI, and thymus tissue was harvested at d7 and the TEC compartment analysed by flow cytometry (Figure 3.19). On day 7 post SLI, while the weight of the thymi between mice that received the isotype and the anti-LTβR treatment were comparable, the cellularity was decreased in mice receiving anti-LTβR compared to isotype treatment. Importantly when the TEC compartment was examined, we noted a slight decrease in TEC from mice receiving anti-LTβR compared to the isotype that was not statistically significant (Figure 3.20 A). Strikingly, when the TEC compartment was broken down into cTEC and mTEC, while there was no significant difference in the mTEC population, we saw a significant decrease in the cTEC population (Figure 3.20 B). Thus, stimulation of LTβR following SLI treatment does not result in enhancement of TEC recovery, but rather has a detrimental effect on cTEC frequency.

Figure 3.19. Analysis of Thymus Recovery Following Sub-Lethal Irradiation And anti-LTβR Treatment.

Female mice, at 6-8 weeks (wks.) of age, and placed on Baytril for 1 week prior to use, were subjected to one dose of SLI. Mice were treated with 100ug (5mg/ml) of anti-LTβR one day prior to SLI and then three different injections administered 2-, 4-, and 6-days post SLI. Thymus tissue was then harvested at d7 post SLI and the TEC compartment was analysed for improvement in recovery.
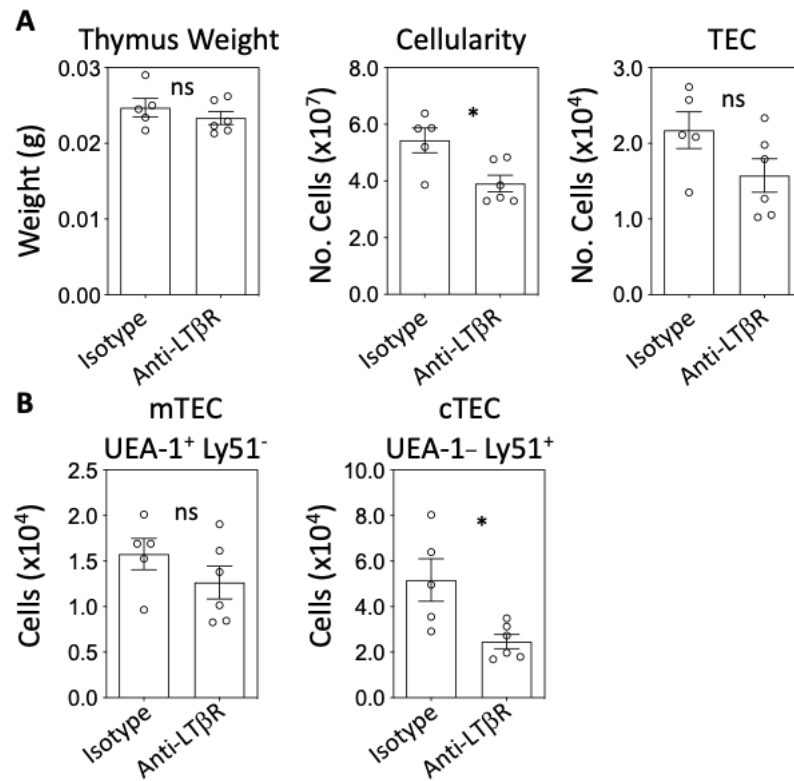
Figure 3.20. anti-LTβR Treatment Has No Positive Effect on TEC Compartment Post SLI.

Mice were treated with 100ug (5mg/ml) of anti-LTβR or Isotype one day prior to SLI and then three different injections administered 2-, 4-, and 6-days post SLI. Thymus tissue was then harvested at d7 post SLI and enzymatically digested for TEC compartment recovery improvement. A. Bar graph showing comparison of thymus weight, thymus cellularity and the thymic epithelial cell compartment post SLI and anti-LTβR treatment. B. Bar graph showing comparison of mTEC and cTEC post SLI and anti-LTβR or Isotype treatment. Each dot represents one mouse where n=6 across two independent experiments and n=5 across two independent experiments for Isotype mice. Error bars represent SEM. Unpaired student t test was used for statistical analysis where each timepoint was compared to control. The level of significance is as follows where non-significant (ns), p<.05 (*), p<.01 (**), p<.001 (***), and p<.0001 (****).

As an alternative approach to enhance thymus recovery post SLI, we reasoned that as SP thymocytes are known to control mTEC availability in the steady state through thymocyte-stromal crosstalk we explored the possibility that the intrathymic retention of SP thymocytes following SLI treatment may improve mTEC recovery by increasing crosstalk availability. Thus, mice were subjected to SLI, then split into two groups. One group received PBS, while the other was treated with the S1PR1 agonist FTY720 (Brinkmann *et al.*, 2002; Mandala *et al.*, 2002) which results in the blockade of thymus emigration and the intrathymic retention of SP thymocytes. Mice received PBS or 1mg/kg of FTY720 at d10 post SLI for 12 consecutive days. Thymus tissue was then harvested and analysed for both T cell development and the TEC compartment (Figure 3.21). As expected, and consistent with its ability to block thymic egress, mice receiving FTY720 showed a significant increase in the numbers and proportions of mature SP4 and SP8 thymocytes (Figure 3.22 A), To confirm the inhibition of thymocyte egress, splenic tissue was also harvested from treated mice and T-cells were quantitated. Consistent with a blockade in thymic emigration, CD4$^+$ and CD8$^+$ splenic T-cells were dramatically reduced in FTY720 treated mice (Figure 3.23). Interestingly, when we next compared the TEC compartment in SLI treated mice that received either PBS (Figure 3.24 A) or FTY720 (Figure 3.24 B), we saw a significant increase in both cTEC and mTEC in FTY720 treated mice (Figure 3.24 C, D). Thus, following SLI treatment, impairing the emigration of SP thymocytes from the thymus increases the intrathymic availability of cTEC and mTEC, suggesting that this may be an interesting approach to further investigate as a means to boost thymus recovery following damage.
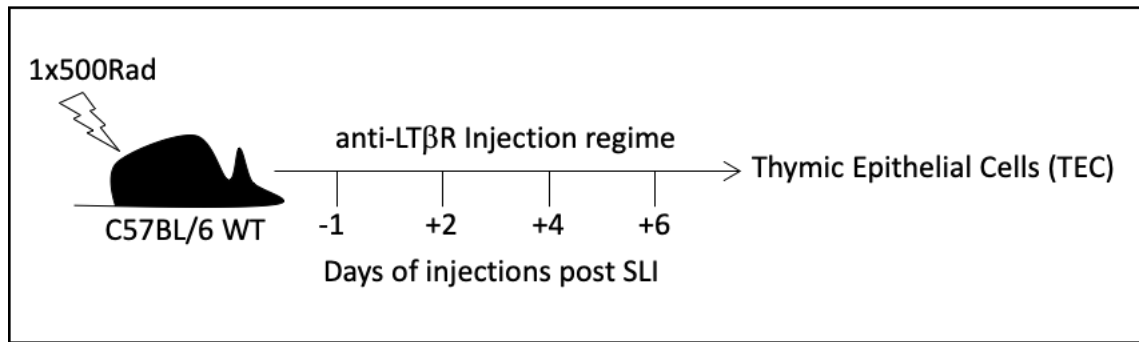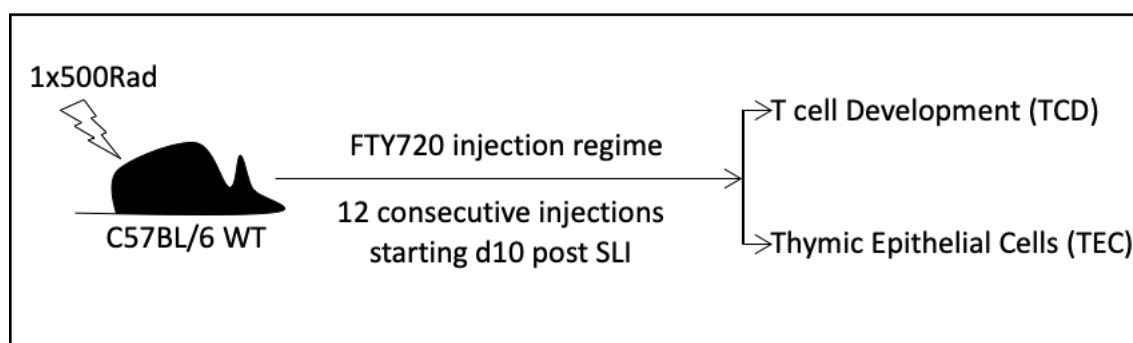
Figure 3.21. Analysis of Thymus Recovery Following Sub-Lethal Irradiation and FTY720 Treatment.

Female mice, at 6-8 weeks (wks.) of age, and placed on Baytril for 1 week prior to use, were subjected to one dose of SLI. Mice were treated with 1mg/kg of FTY720 after SLI starting at d10 and then twelve consecutive injections. Thymus and spleen tissue were then harvested at d22 post SLI and the TCD and TEC compartments were analysed. Control mice were used alongside that were also subjected to SLI, however they received PBS injections.
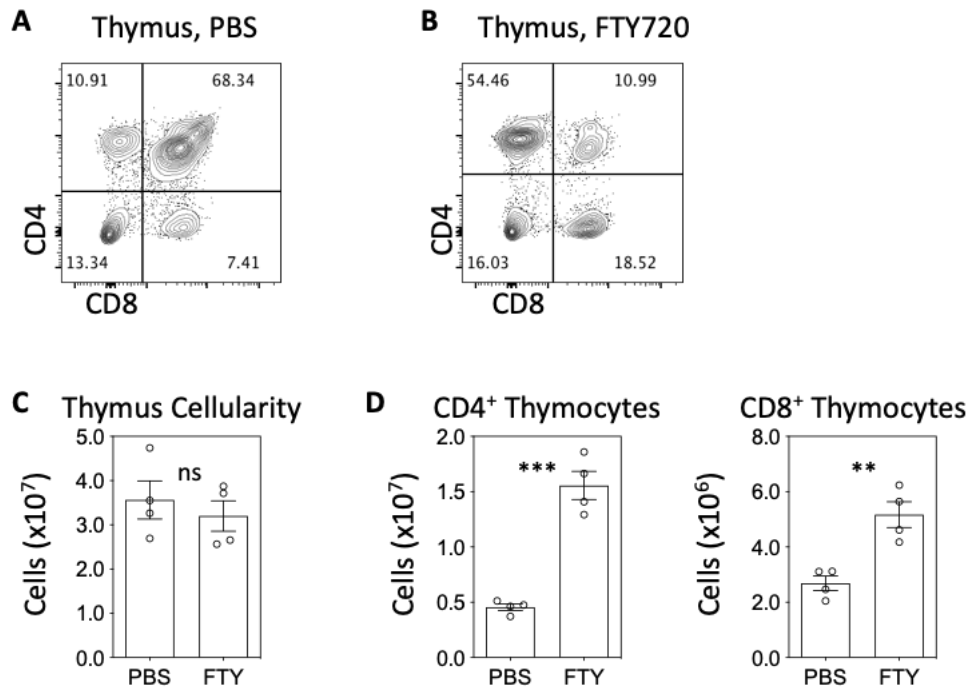
Figure 3.22. Block of Thymocyte Export Post SLI and FTY720 Treatment.

Mice were treated with 1mg/kg of FTY720 or PBS after SLI starting at d10 and then twelve consecutive injections. Thymus tissue was then harvested at d22 post SLI and mechanically digested for TCD compartment analysis. A. FACs analysis showing staining for CD4 and CD8 in mice receiving PBS post SLI. B. FACs analysis showing staining for CD4 and CD8 in mice receiving FTY720 post SLI. C. Bar graph showing comparison of thymus cellularity post SLI and FTY720 or Isotype treatment. D. Bar graph showing comparison of CD4^{+} and CD8^{+} thymocytes post SLI and FTY720 or Isotype treatment. Each dot represents one mouse where n=4 across one independent experiment. Error bars represent SEM. Unpaired student t test was used for statistical analysis where each timepoint was compared to control. The level of significance is as follows where non-significant (ns), $p<.05$ (*), $p<.01$ (**), $p<.001$ (***), and $p<.0001$ (****).
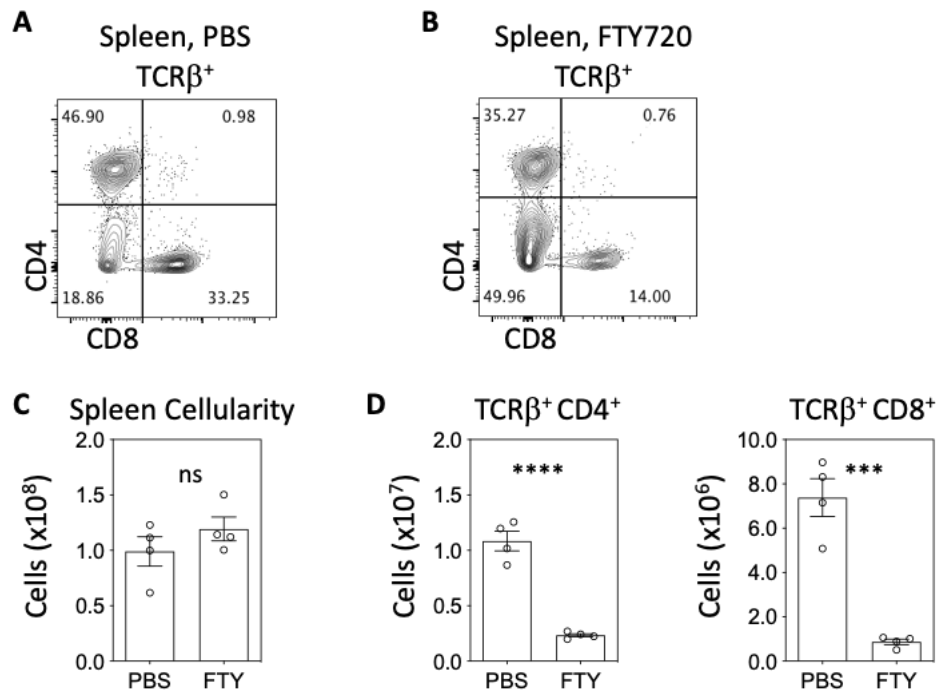
Figure 3.23. Reduced Peripheral T cells Post SLI and FTY720 Treatment.

Mice were treated with 1mg/kg of FTY720 or PBS after SLI starting at d10 and then twelve consecutive injections. Spleen tissue was then harvested at d22 post SLI and mechanically digested for TCD compartment analysis. A. FACs analysis showing staining for CD4 and CD8 in mice receiving PBS post SLI. B. FACs analysis showing staining for CD4 and CD8 in mice receiving FTY720 post SLI. C. Bar graph showing comparison of spleen cellularity post SLI and FTY720 or Isotype treatment. D. Bar graph showing comparison of CD4$^+$ and CD8$^+$ T cells post SLI and FTY720 or Isotype treatment. Each dot represents one mouse where n=4 across one independent experiment. Error bars represent SEM. Unpaired student t test was used for statistical analysis where each timepoint was compared to control. The level of significance is as follows where non-significant (ns), $p<.05$ (*), $p<.01$ (**), $p<.001$ (***), and $p<.0001$ (****).
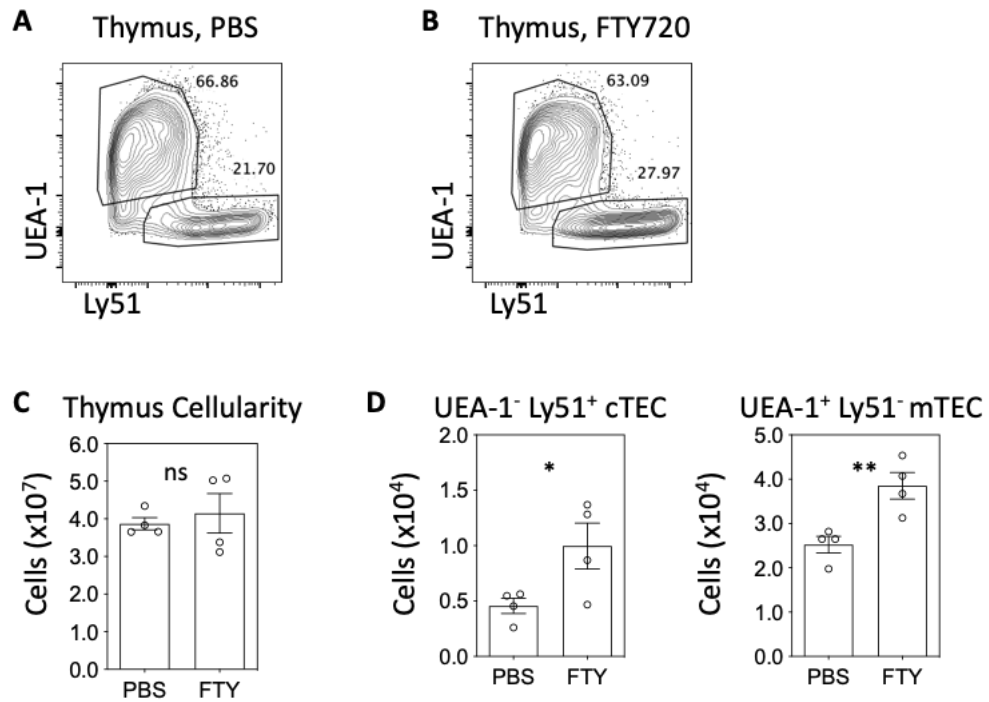
Figure 3.24. Increase in Thymic Epithelial Cell Compartment Post SLI and FTY720 Treatment.

Mice were treated with 1mg/kg of FTY720 or PBS after SLI starting at d10 and then twelve consecutive injections. Thymus tissue was then harvested at d22 post SLI and enzymatically digested for TEC compartment analysis. A. FACs analysis showing staining for UEA-1 and Ly51 in mice receiving PBS post SLI. B. FACs analysis showing staining for UEA-1 and Ly51 in mice receiving FTY720 post SLI. C. Bar graph showing comparison of thymus cellularity post SLI and FTY720 or Isotype treatment. D. Bar graph showing comparison of cTEC and mTEC post SLI and FTY720 or Isotype treatment. Each dot represents one mouse where n=4 across one independent experiment. Error bars represent SEM. Unpaired student t test was used for statistical analysis where each timepoint was compared to control. The level of significance is as follows where non-significant (ns), $p<.05$ (*), $p<.01$ (**), $p<.001$ (***), and $p<.0001$ (****).

3.3 Discussion

3.3.1 Initial Recovery of T Cell Development Post SLI Occurs Via Radioresistant Intrathymic Progenitors

Early studies have investigated thymus recovery post sublethal irradiation (SLI), and have suggested a biphasic mode that allows the thymus to recover in two distinct phases (Bourke, 1964; Takada *et al.*, 1969; Penit and Ezine, 1989). Following thymus injury, it is evident that thymocytes are rapidly depleted, which significantly affects thymus cellularity. Following SLI, we found the thymus recovers in a biphasic manner in which the first phase occurred at d4 after damage. This recovery was not maintained, and a second drop in thymus cellularity was observed at d14 post SLI. Furthermore, this drop in cellularity was seen in the recovery of different thymocyte subsets, which also recovered in two phases. Interestingly it was suggested that radioresistant CD4$^-$CD8$^-$ DN intrathymic progenitors facilitated the first phase of recovery by giving rise to all thymocyte subsets (Penit and Ezine, 1989). Our careful examination of ETP, that represent the earliest defined intrathymic T-cell progenitors, would agree with this scenario, as ETP were undetectable in the first phase of recovery. Further, we observed that a fraction of mature CD4$^+$ and CD8$^+$ thymocytes remained following SLI, suggesting that alongside radioresistant intrathymic progenitors, SP thymocytes also account for some of the thymocytes that are present in the first wave of thymus recovery. That such mature SP cells are present shortly after damage, and prior to the appearance of CD4$^+$CD8$^+$ thymocytes, suggests these cells are not a product of thymic selection post-damage, and their presence may have confused earlier studies looking at the timing of new SP thymocyte production.

3.3.2 Differential Recovery of Thymic Microenvironment Impacts Key Medulla Functions

The thymic microenvironment has a pivotal role in the education of newly developing thymocytes before their egress into the periphery. Different cell types reside within the thymic microenvironment and contribute to the process of thymocyte development. Lymphocyte regeneration is required through life to replace cellular losses from different stimuli. As such, the regeneration process occurs via an intrathymic mechanism. However, the thymus does not hold self-renewing progenitors and is dependent on progenitor colonization to produce new T-cells. cTEC play an important role in the progenitor colonization process as they express CCL25 and CXCL12 which have been both implicated in the recruitment as well as the positioning of recruited progenitors (Plotkin *et al.*, 2003; Scimone *et al.*, 2006). Furthermore, cTEC play an important role during the positive selection process (Murata *et al.*, 2007). Interestingly, while the TEC compartment was significantly affected post SLI, cTEC remained relatively consistent in numbers suggesting radioresistant properties of these cells. Furthermore, when we tested the functional capability of cTEC through the use of OT-1 transgenic mice, we saw no differences in the selection of CD8$^+$ thymocytes between irradiated and non-irradiated controls. The reason behind the maintenance of the cTEC compartment following damage and its functional capability is unclear at this moment and requires further experiments. One possibility is that mature cTEC represent long lived cells that are resistant to DNA damage caused by SLI. Here, cTEC would remain after damage to support early T-cell development and positive selection. Another possibility is that a pool of cTEC progenitors rapidly gives rise to new mature cTEC after damage. Given that cTEC numbers appear relatively normal shortly after damage, this second scenario is perhaps unlikely. Studies involving analysis of cTEC proliferation and apoptosis may help to reveal the underlying mechanism.

In contrast to cTEC, mTEC significantly decreased following thymus damage. This could have an immunologically important impact as mTEC are associated with TRA expression through Aire and Fezf2, which regulates the important process of negative selection for the deletion of self-reactive thymocytes (Takaba *et al.*, 2015). Further, mTEC are essential in Treg selection (Cowan *et al.*, 2013). In line with this, our data shows that the significant reduction in mTEC does indeed have a significant impact, Treg did not recover through the time course we analysed after damage. Interestingly a recent study has shown that negative selection and the process of tolerizing newly developing cells can occur despite a limited number of mTEC availability (Cosway *et al.*, 2017). Furthermore, DC also control the negative selection process (Anderson, Partington and Jenkinson, 1998). Interestingly, and related to the role of DC in negative selection, it was shown that Sirpα$^+$ DC have increased antigen processing capacities (Kroger, Wang and Tisch, 2016) which suggest their role in antigen presentation is essential for tolerance. Furthermore and related to DC contribution to antigen processing, Sirpα$^+$ DC localize in perivascular regions to capture antigens circulating in the blood through a CCR2 dependent manner as CCR2 deficient mice have reduced Sirpα$^+$ DC and thus decreased negative selection against blood borne antigens (Baba, Nakamoto and Mukaida, 2009). Interestingly shows a significant reduction in the thymic DC compartment following SLI, with both Sirpα$^-$ cDC1 and Sirpα$^+$ cDC2 being significantly decreased post thymus damage. Thus, alongside the reduction in mTEC, the negative selection process could be impaired. Indeed, our approach to test negative selection revealed that this process is impaired as different Vβ bearing thymocytes accumulated in thymus of BALB/c mice post damage and we were able to track these cells into the periphery suggesting an escape of self-reactive thymocytes post SLI.

3.3.3 Transient Block of Thymocyte Egress Improves Recovery of Thymic Epithelial Cell Compartments

The importance of S1PR1 in the egress mechanism was highlighted when Allende et al. deleted S1PR1 expression that resulted in the block of mature cells from exiting the thymus. This diminished T-cell numbers in peripheral tissues such as the spleen and lymph nodes (Allende *et al.*, 2004). FTY720, an agonist for the S1P receptor, has been shown to alter lymphocyte trafficking by binding to 4 of the 5 S1P receptors (Brinkmann *et al.*, 2002; Mandala *et al.*, 2002). In the thymus, FTY720 administration caused SP thymocyte accumulations with phenotypical changes in the expression of CD69 and CD62L as well as prohibited thymocyte egress into the periphery (Yagi *et al.*, 2000; Rosen *et al.*, 2003). Interestingly, it has been established that TEC-thymocyte interactions provide key signals for maturation of both cell types. Indeed, it has been shown that mTEC maturation can be altered through the interactions of RANKL and CD40L produced by positively selected thymocytes (Akiyama *et al.*, 2008; Hikosaka *et al.*, 2008; Irla *et al.*, 2008; Desanti *et al.*, 2012). Furthermore, and different from the previous mechanism, it was shown that positively selected thymocytes are required for the generation of post Aire cells. Using *Zap70*$^{-/-}$ mice, White et al. showed the presence of positively selected thymocytes are required for the maturation of terminally differentiated mTEC. Different to the requirements of RANKL or CD40L, these terminally differentiated involucrin$^+$ mTEC required the Ltα-LTβR axis for differentiation which highlights yet another important role thymocyte/epithelial cell cross talk (White *et al.*, 2010). To examine whether therapeutic manipulation of crosstalk may aid in thymus recovery after damage, we administered FTY720 post SLI. As expected, we saw a blockade of thymocyte egress. Importantly, we also saw an increase in mTEC numbers alongside the intrathymic accumulation of SP thymocytes. Thus, blockade of thymic egress may enhance mTEC development by sustaining the provision of crosstalk signals, suggesting the block of thymocyte exit as a

therapeutic approach to boost the TEC compartment post thymus damage. Further work is needed to examine the effects of FTY720 administration on the recovery of thymus function after damage. For example, it will be interesting to see whether defects in negative selection diminish, and intrathymic DC and Treg populations recover more effectively.

Overall work in this chapter provides a side-by-side analysis of the recovery of T-cell development and TEC microenvironments after low dose SLI as a model of thymus damage and regeneration. Collectively, the data suggests that shortly after damage, recovery of thymopoiesis is mediated by radio-resistant progenitors that continue their development in a thymus that is defective in medullary thymic areas. Initial experiments indicate this has a functional effect on recovery, including defective negative selection and Treg generation, which may mean that the first cohorts of T-cells to be produced during thymus regeneration are not fully tolerized. It will be important to continue to explore approaches to improve the recovery of mTEC, including blockade of thymus egress, to see whether defects in the thymus medulla and tolerance mechanisms can be improved.

4 <u>CHAPTER 4: INVESTIGATING THE KINETICS OF THYMUS RECOVERY POST BONE MARROW TRANSPLANTATION</u>

4.1 Introduction

Bone marrow transplant (BMT) is a widely used treatment technique for many immunological disorders. BMT is used in an approach to reconstitute the host hematopoietic system following ablative therapy. Murine models that incorporate the use of ablative therapy and BMT have been used to study the reconstitution of the damaged immune system as well as the limitations and complications of this treatment. Earlier studies conducted by Urso and Congdon have shown the importance of the infusion of cells following ablative therapy not only to achieve recovery, but also in determining the number of cells to be injected an important factor (Urso and Congdon, 1957).

BMT, as a mode of treatment, requires the niche availability to be able to engraft properly within the host system. Whether it is in clinical patients or in murine models, patients are subjected to ablative therapies to create space and allow for bone marrow (BM) engraftment. Indeed, it was shown by Mackall et al. that following intensive treatment there was a decrease in the T cell count, and the regeneration of this population was achieved following engraftment. Importantly, this study highlighted the role of the thymus during the engraftment process to regenerate the T cell compartment (Mackall *et al.*, 1995). Furthermore, a study by the same group has shown that following T cell depletion by ablative therapy in murine models, T cell recovery that was achieved through thymus-dependent mechanisms have decreased proliferation compared to recovery through homeostatic proliferation to fill the empty space (Mackall *et al.*, 1996). This difference can substantially impact the T cell receptor repertoire of the recovering immune system.

As previously mentioned in early chapters, the use of ablative therapy as a treatment for different disorders disrupts the size and function of the thymus. As a result, this chapter will

focus on thymus function following ablative therapy and BMT. We will determine the effect of BMT on immune system depletion and recovery and assess the kinetics of thymus recovery following BMT. Furthermore, this chapter will also focus on the impact of BMT in the balance and quality during the regeneration of the T cell cohorts.

4.2   Results

4.2.1   Assessment of Thymus Following Lethal Irradiation

To study the kinetics of thymus recovery following BMT, bone marrow chimeras (BMC) were generated. Adult mice were subjected to two doses of irradiation and reconstituted with congenically marked T cell depleted bone marrow. Adult C57BL/6 mice were used as hosts and expressed CD45.2. To allow for discrimination between host and donor cells, the bone marrow was harvested from BoyJ donor mice that expressed CD45.1. The bone marrow was then T cell depleted before transfer to the host mice. Following transfer, time course analysis was conducted to measure thymus regeneration by measuring different parameters. These parameters included the analysis of the T cell compartment, the thymic epithelial cell compartment, and also the thymic dendritic cell compartment (Figure 4.1).

Before analysing the thymus after BMT, it was critical to identify what was present in the thymus following lethal irradiation. Thus, adult host mice were subjected to two doses of TBI and were harvested four hours after the second dose without the transfer of the donor bone marrow. Thymus tissue was collected and mechanically digested and then antibody stained to identify different thymocyte populations (Figure 4.1 A). Interestingly, it was observed that following the two doses of irradiation there was a radioresistant population of both SP4 and SP8 thymocytes. The SP4 thymocyte population was then further characterized to identify Tconv and Treg and it was shown that both populations were present. Furthermore, invariant

natural killer T cells (iNKT) that are CD1d dependent and also express an invariant TCR have been identified by staining with the PBS57-CD1d tetramer in the thymus following lethal irradiation (Figure 4.2 A). Numerical quantification was then performed, and it was observed that most populations analyzed were present following lethal irradiation at approximately 20% compared to the control. However, intrathymic Treg was the only population that displayed approximately 40% compared to the control after irradiation suggesting their radio resistance capability (Figure 4.2 B).
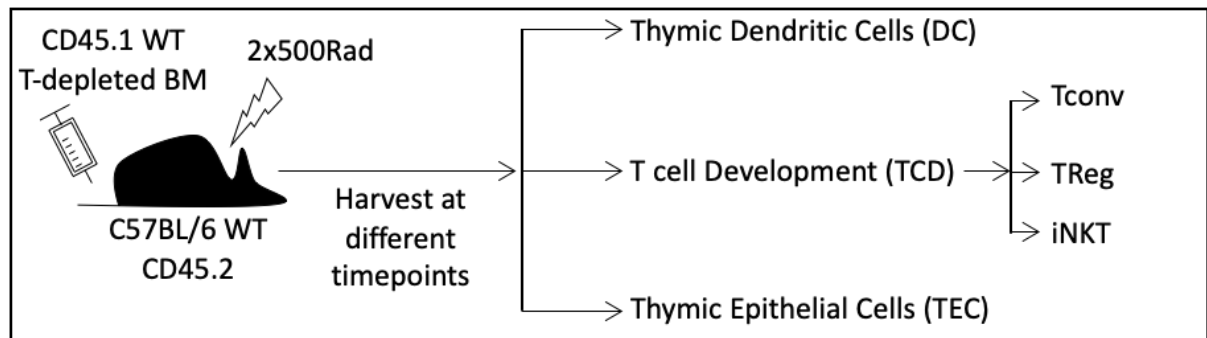
Figure 4.1. Analysis of Thymus Recovery Following Bone Marrow Transplantation (BMT).

Female mice (CD45.2), at 6-8 weeks of age, and placed on Baytril for 1 week prior to use, were subjected to two dose of total body irradiation (TBI). Bone marrow, congenically marked (CD45.1), was used for immune reconstitution. Thymus and spleen tissue were harvested at different timepoints to analyse different parameters of thymus recovery.

A

Thymus

CD4⁺ TCRβ⁺

B Composition Relative To Control
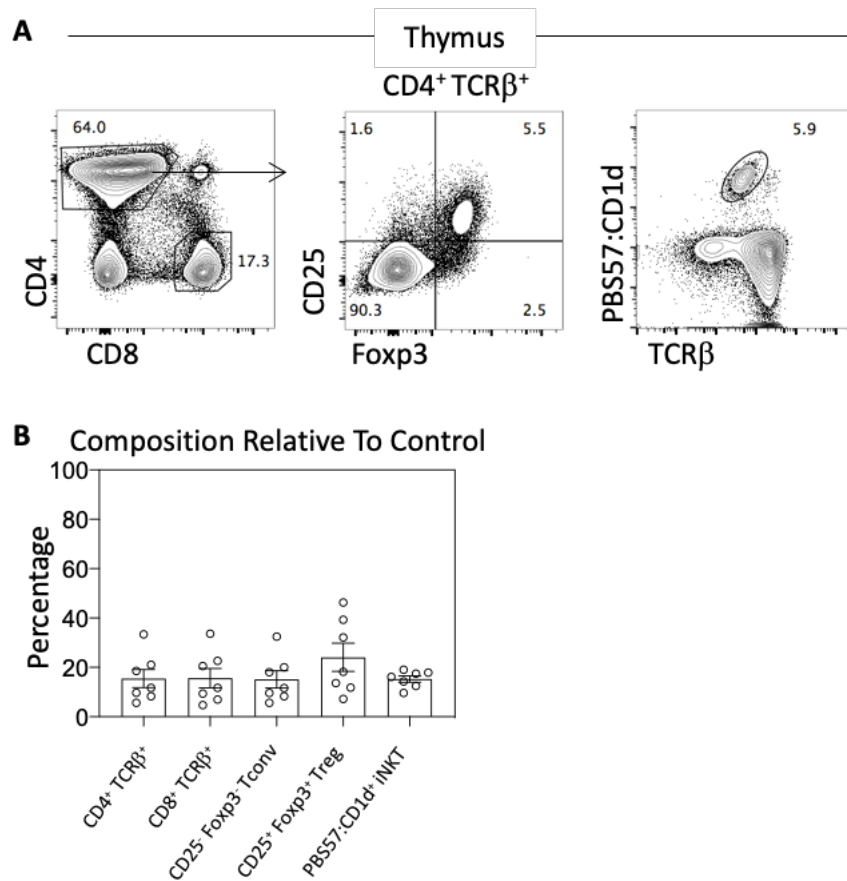
Figure 4.2. Thymus Composition Post TBI.

Mice were subjected to two doses of TBI and thymus tissue was harvested without bone marrow reconstitution. The doses were split over two days and tissue was harvested 4 hours post the second dose. A. FACs analysis showing staining for CD4, CD8, CD25, Foxp3, and the PBS57:CD1d tetramer for iNKT identification. B. Bar graph showing composition of thymocyte subsets post lethal irradiation and compared to control. Each dot represents one mouse where n=7 across two independent experiments. Error bars represent SEM.

Following thymus analysis, similar analysis was performed in the periphery. Spleen tissue was harvested from mice that had received two doses of TBI. Tissue was mechanically digested and then antibody stained for T cell compartment analysis. Similarly, it was found that after TBI, $CD4^+$ and $CD8^+$ T cells were identifiable in the periphery. $CD4^+$ T cells were then broken down into Tconv and Treg and both populations were observed to be present. iNKT cells were also analysed, and a very clear population in the periphery could be visualized (Figure 4.3 A). However, when quantification analysis was performed and compared to the control it was observed that $CD4^+$ T cells were found to be at a significantly reduced level. Interestingly, $CD8^+$ T cells did not follow the same pattern observed in the thymus. Peripheral $CD8^+$ T cells were shown to be significantly affected as their presence following TBI were less than 5%. Tconv and Treg numbers were to a similar degree in the spleen. Strikingly, iNKT numbers compared to the control suggest that peripheral iNKT are more radioresistant because there was approximately 40% iNKT present in the periphery post TBI.
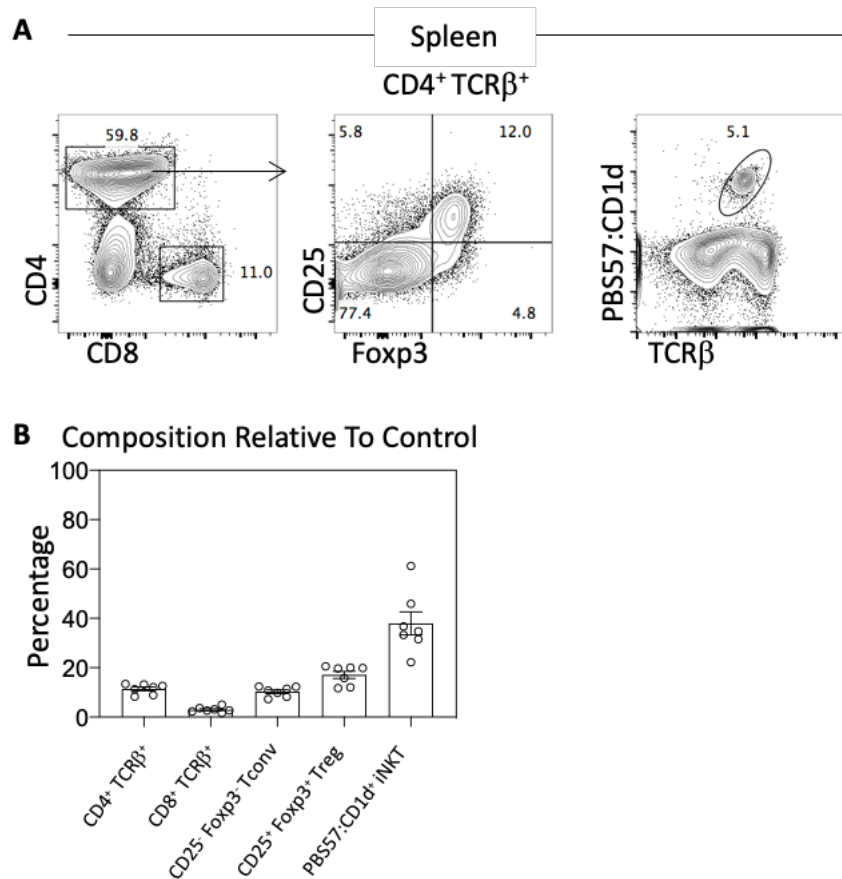
Figure 4.3. Spleen Composition Post TBI.

Mice were subjected to two doses of TBI and spleen tissue was harvested without bone marrow reconstitution. The doses were split over two days and tissue was harvested 4 hours post the second dose. A. FACs analysis showing staining for CD4, CD8, CD25, Foxp3, and the PBS57:CD1d tetramer for iNKT identification. B. Bar graph showing composition of thymocyte subsets post lethal irradiation and compared to control. Each dot represents one mouse where n=7 across two independent experiments. Error bars represent SEM.

4.2.2 Investigation of Thymus Recovery Following Bone Marrow Transplantation (BMT)

Having visualized what was present following TBI and in the absence of bone marrow transfer, it was important to analyse the kinetics of thymus recovery following irradiation and BMT. BMC were generated using C57BL/6 and BoyJ mice to distinguish host and donor cells. Host C57BL/6 mice received two doses of TBI split over two days and following the second dose, bone marrow was harvested and T cell depleted from BoyJ mice and transferred. Time course analysis was then performed to study the kinetics of donor derived thymocyte development post BMT.

Following TBI and BMT, thymus tissue was harvested and mechanically digested and then antibody stained to study the donor thymocyte compartment. It was observed that by day 14 post BMT, there was a clear DP thymocyte population. However, this time point lacked the presence of SP4 and SP8 thymocytes. FACs staining at day 28 post BMT revealed clear populations of both SP4 and SP8 thymocyte populations. Furthermore, staining at day 56 post BMT also showed clear populations of the three populations previously described (Figure 4.4 A). Numerical analysis was performed, and it was shown that the DP thymocyte population displayed similar numbers at day 14 and day 21 post BMT. Following that timepoint and specifically at day 28, numbers of the DP thymocyte population increased. Interestingly, at day 56 post BMT, numbers decreased again (Figure 4.4 B). This pattern was not followed when SP4 and SP8 thymocytes were analysed. For SP4 and SP8 thymocyte development, it was observed that numbers were significantly reduced at day 14 post BMT. Strikingly, for both populations the numbers increased and maintained similar numbers for the remaining timepoints (Figure 4.4 B).

Numbers of the analysed thymocyte populations were compared to the control to measure the relative recovery status. At day 14 and day 21 post BMT, the DP thymocyte population was significantly reduced compared to the control. However, after their increase at day 28 post BMT this population was comparable to the control. Although there was a slight decrease in numbers of DP thymocytes at day 56 post BMT, it was not statistically significant when compared to the control (Figure 4.4 C). For SP4 thymocyte relative recovery, it was observed that at day 14 post BMT there was a significant reduction where percentage was approximately 10% relative to the control. However, numbers of SP4 thymocytes were significantly increased post day 14 and it was observed that at the remaining time points the SP4 thymocytes population was comparable to the control. This pattern was followed for the SP8 thymocyte population, in which the population was merely absent at day 14 post BMT when compared to the control and for the remaining timepoints the numbers of the SP8 thymocyte population was comparable to the control (Figure 4.4 C).
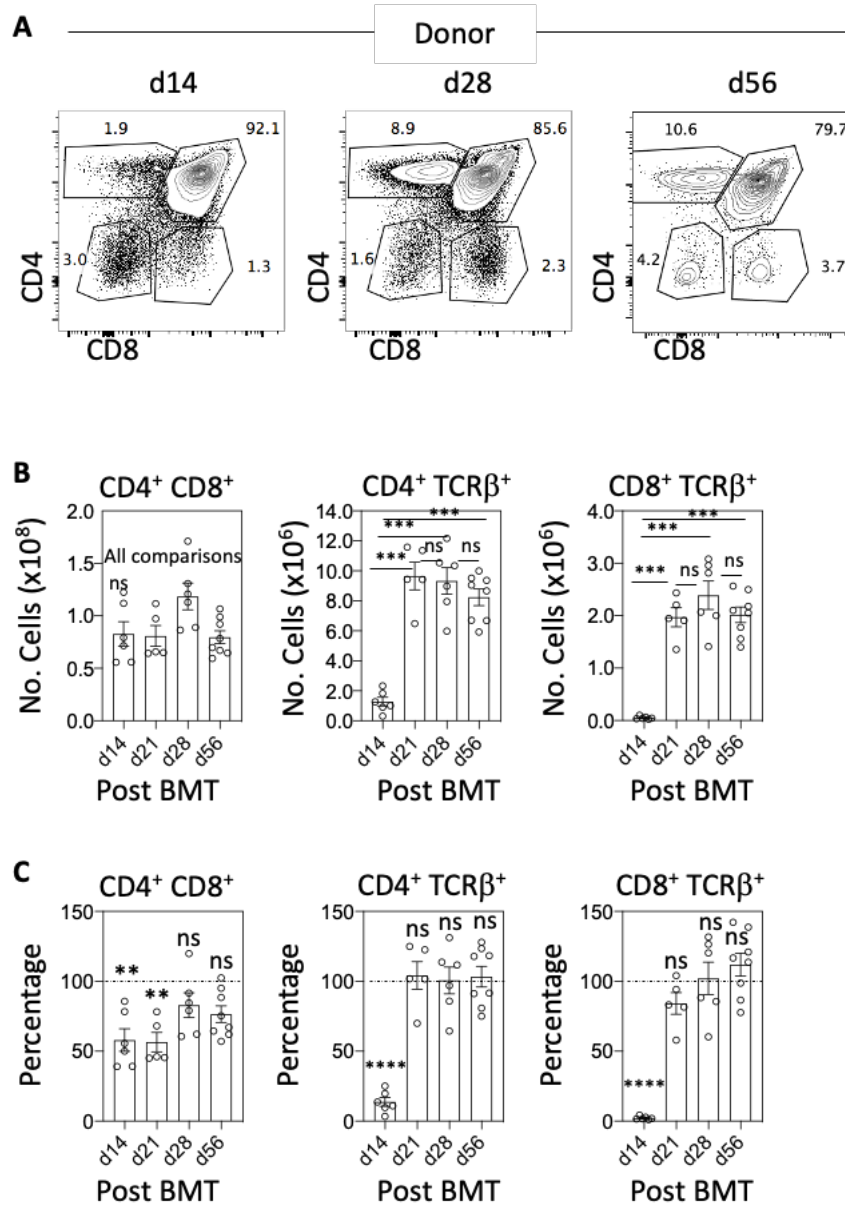
Figure 4.4. Rapid Reconstitution of Donor Derived T cell Development Post BMT.

Mice were subjected to two doses of TBI and reconstituted with T cell depleted bone marrow. Thymus tissue was harvested and mechanically digested for FACs analysis. A. Representative FACs plots of CD4 and CD8 staining in donor thymocytes at d14, d28, and d56 post BMT. B. Numerical quantification of donor thymocytes in experimental mice post BMT. C. Bar graph showing recovery of donor thymocytes compared to control mice where dotted line represents the control. Each dot represents one mouse where n≥5 for each time point across two independent experiments. For d56 n=8 across three independent experiments. Error bars represent SEM. Ordinary One-way ANOVA was used for statistical analysis where each timepoint was compared to control. The level of significance is as follows where non-significant (ns), $p<.05$ (*), $p<.01$ (**), $p<.001$ (***), and $p<.0001$ (****).

To complement the previous FACs data of donor derived thymocyte recovery, thymus tissue was harvested at different time points after BMT and frozen to be sectioned for immunofluorescence imaging. Frozen thymus tissue was cut at 7μm thickness and labelled with CD4, CD8, and ERTR5 to identify medullary areas. Control sections were stained and imaged alongside all time points. It was visualized that at day 7 post BMT, the thymus lacked SP4 and SP8 thymocytes as ERTR5 stained regions were almost empty of these cell types. Furthermore, cortical regions, identified by lack of ERTR5 staining, did not reveal the presence of cells co-expressing CD4 and CD8 markers. However, at day 14 post BMT, and in agreement with the previous FACs data, cortical regions began to fill with DP thymocytes. Medullary region analysis also showed CD4 expression marking the presence of the SP4 thymocytes population. Day 21 post BMT images maintain the DP thymocyte population staining and visual appearance looks similar to the control. Single expression of both CD4 and CD8 markers could also be visualized at this time point which correlates with their presence seen in the FACs data (Figure 4.5 A).
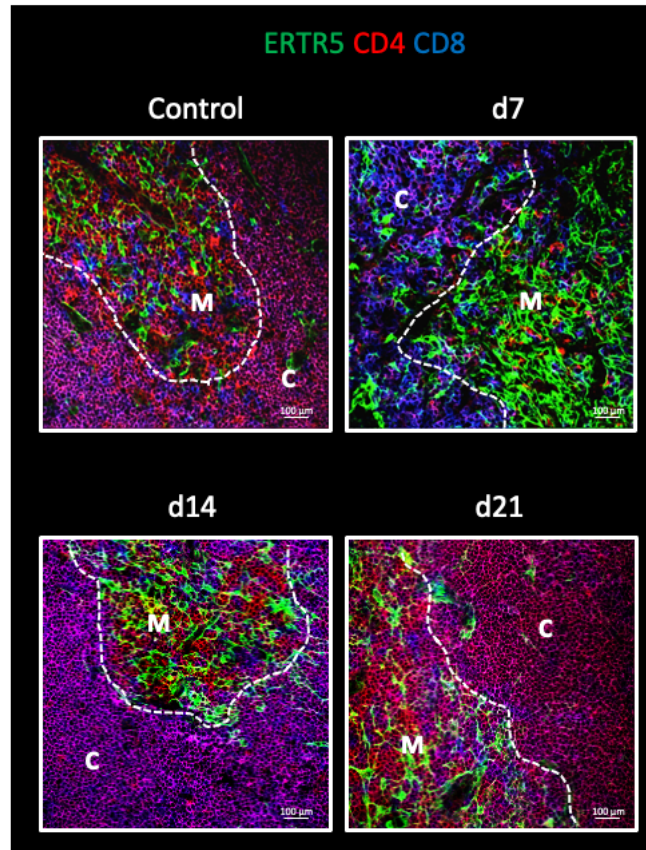
Figure 4.5. Organization of Thymus Post BMT.

Mice were subjected to two doses of TBI and then reconstituted with T cell depleted bone marrow. Thymus tissue was harvested at different timepoints, frozen and then cut at 7μm thickness for histology analysis. Each section was approximately 35μm apart. A. Immunofluorescence image of thymus regions stained for CD4 (Red), CD8 (Blue), and ERTR5$^+$ medulla areas (Green) post damage. All sections were stained and analysed alongside control sections. Dotted line defines cortical (C) and medullary (M) regions. N=3 for each time point where thymus was harvested and frozen and then cut at 7μm thickness.

Following analysis of SP4 thymocyte development (Figure 4.4), this population was further explored to characterize the individual recovery of Tconv and Treg post BMT. Thymus tissue was harvested and mechanically digested and antibody stained at different timepoints post BMT. FACs staining analysis for CD25 and Foxp3 was conducted to segregate the Tconv population from Treg. At day 14 post BMT, it was observed that Tconv population could be clearly identified while the Treg population was absent. Furthermore, at day 28 post BMT both populations can be visualized, and this was similar at day 56 post BMT (Figure 4.6 A). Numerical quantification was performed, which showed that Tconv are present in very small numbers. However, at day 21 post BMT, their numbers increased and remained constant for the remaining timepoints. In contrast, Treg were absent at day 14 post BMT and this population began increasing at day 21 post BMT. Different from Tconv, Treg numbers slowly increased at day 28 and day 56 post BMT (Figure 4.6 B). Tconv, when compared to the control, displayed a significant reduction at day 14 post BMT. Interestingly though, this population significantly increased at day 21 post BMT to levels that were comparable to the control. These levels were maintained for the remaining time points of the time course analysis. Treg, on the other hand, did not follow the same pattern, and at day 14 post BMT, they were absent. Although their numbers began to increase at day 21 post BMT, the Treg population was significantly reduced compared to the control, and this persisted until day 28. By day 56 post BMT, Treg had increased to levels comparable to control mice (Figure 4.6 C).

Interestingly, iNKT cells differed markedly in their kinetics of recovery compared to conventional thymocytes post BMT. iNKT cells were identified by reactivity with the PBS57-CD1d tetramer. Thymus tissue that was harvested and mechanically digested and antibody stained for iNKT cells showed a loss of this population at day 28 post BMT. FACs analysis of

iNKT cells shows a very small proportion at day 28 post BMT with a slight increase at day 56 post BMT (Figure 4.7 A). Numerical quantification was performed, and it was observed that numbers of iNKT cells at day 28 were reduced, however extended analysis at day 56 post BMT showed a numerical increase (Figure 4.7 B). Numbers of iNKT cells post BMT were then compared to the control and strikingly, they were significantly reduced at day 28 post BMT. Although the number of iNKT cells were increased at day 56 post BMT, levels remained significantly decreased when compared to the control (Figure 4.7 C) which was the opposite of conventional thymocyte recovery.
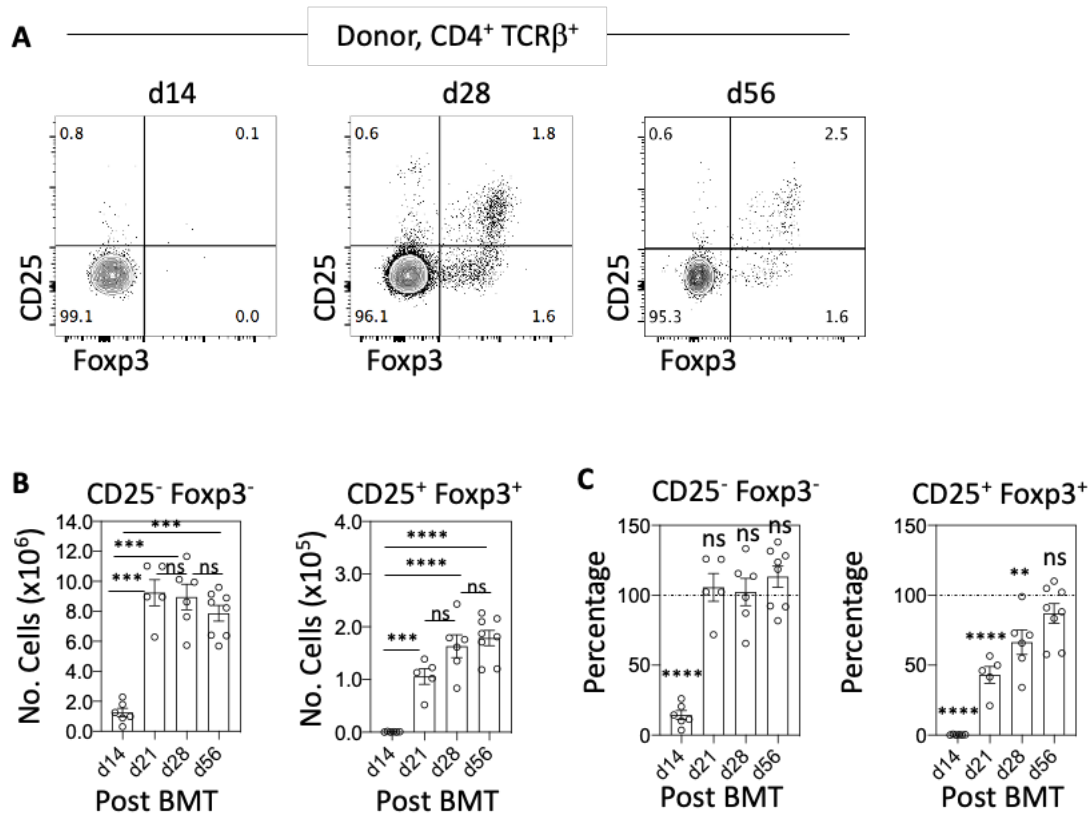
Figure 4.6. Slow Intrathymic T Regulatory Recovery Post BMT Compared to T Conventional Recovery.

Mice were subjected to two doses of TBI and reconstituted with T cell depleted bone marrow. Thymus tissue was harvested and mechanically digested for FACs analysis. A. Representative FACs plots of CD25 and Foxp3 staining in donor thymocytes, at d14, d28, d56 post BMT. Plots pre-gated on CD4+ TCRβ+. B. Numerical quantification of donor Tconv and Treg in experimental mice post BMT. C. Bar graph showing recovery of donor Tconv and Treg compared to control mice where dotted line represents the control. Each dot represents one mouse where n≥5 for each time point across two independent experiments. For d56 n=8 across three independent experiments. Error bars represent SEM. Ordinary One-way ANOVA was used for statistical analysis where each timepoint was compared to control. The level of significance is as follows where non-significant (ns), p<.05 (*), p<.01 (**), p<.001 (***), and p<.0001 (****).
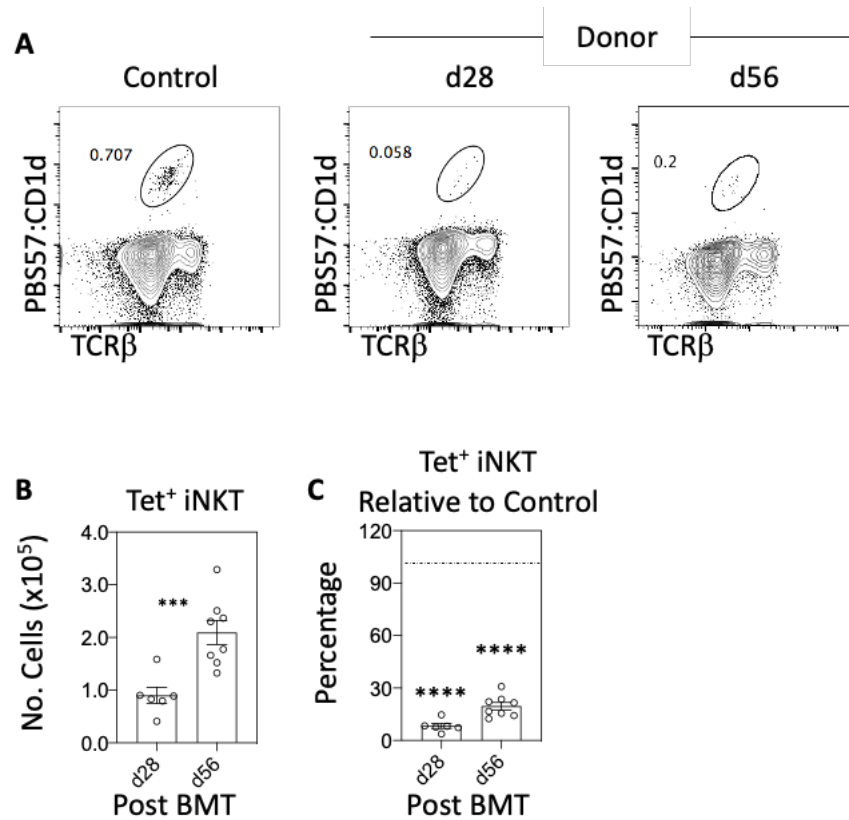
Figure 4.7. Intrathymic iNKT Cells Do Not Recover Post BMT.

Mice were subjected to two doses of TBI and reconstituted with T cell depleted bone marrow. Thymus tissue was harvested and mechanically digested for FACs analysis. A. Representative FACs plots of TCRβ and the PBS57:CD1d tetramer for iNKT identification at d28 and d56 post BMT. B. Numerical quantification of donor iNKT in experimental mice post BMT. C. Bar graph showing recovery of donor iNKT compared to control mice where dotted line represents the control. Each dot represents one mouse where n=6 for d28 across two independent experiments and n=8 for d56 across three independent experiments. Error bars represent SEM. Ordinary One-way ANOVA was used for statistical analysis where each host was compared to control. The level of significance is as follows where non-significant (ns), p<.05 (*), p<.01 (**), p<.001 (***), and p<.0001 (****).

To further identify the reason behind the very slow recovery of the iNKT population, iNKT precursors (NKTp) identified by the expression of CCR7 were investigated (Wang and Hogquist, 2018). FACs analysis revealed a high proportion of CCR7$^+$ iNKTp in the thymus at day 28 post BMT. Extended analysis at day 56 post BMT also shows a clear population but to a lesser extent (Figure 4.8 A). Control mice had approximately 2-3% of NKTp that give rise to different lineages of iNKT. However, after thymus damage and BMT the percentage increased to approximately 28-30% at day 28 post BMT. The increase in NKTp percentage was transient because the NKTp population decreased to 10% at day 56 post BMT (Figure 4.8 B). Numerical quantification analysis was also performed and displayed high numbers of NKTp at day 28 and a lower number at day 56 post BMT (Figure 4.8 C). When the numbers were compared to the control, it was apparent that at day 28 post BMT there was double the number of NKTp present. Although percentages of the NKTp population at day 56 post BMT were higher than the control, when the numbers were compared to the control the levels were very comparable (Figure 4.8 D).
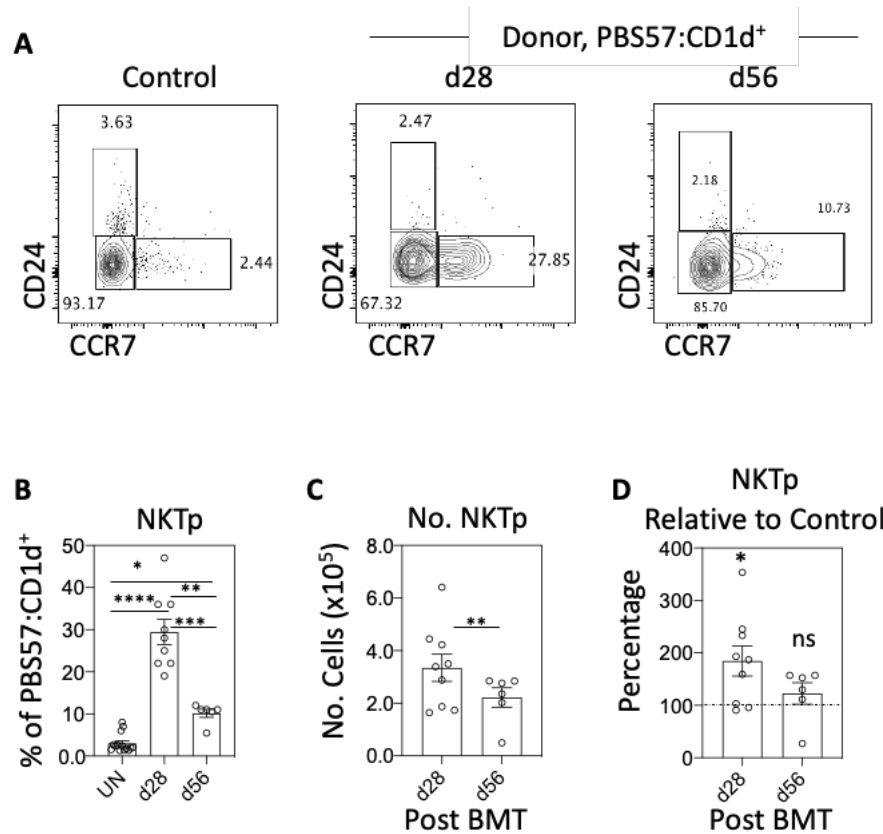
Figure 4.8. Transient Block of iNKT Development at Precursor Stage Post BMT.

Mice were subjected to two doses of TBI and reconstituted with T cell depleted bone marrow. Thymus tissue was harvested and mechanically digested for FACs analysis. A. Representative FACs plots of CD24 and CCR7 at d28 and d56 post BMT. B. Bar graph showing percentage of iNKT precursors (NKTp) in experimental mice post BMT. Pre-gated on PBS57:CD1d. C. Numerical quantification of donor NKTp in experimental mice post BMT. D. Bar graph showing recovery of donor NKTp compared to control mice where dotted line represents the control. Each dot represents one mouse where n=9 for d28 across three independent experiments and n=6 for d56 across two independent experiments. Untreated (UN) represents the unmanipulated non-irradiated control. Error bars represent SEM. Ordinary One-way ANOVA was used for statistical analysis where each host was compared to control. The level of significance is as follows where non-significant (ns), $p<.05$ (*), $p<.01$ (**), $p<.001$ (***), and $p<.0001$ (****).

4.2.3 Investigation of The Peripheral T Cell Compartment Post BMT

Following thymus recovery analysis post BMT, the next step was to investigate the recovery of the peripheral T cell pool. This was analysed using the same model of BMC generation. Spleen tissue was harvested at different timepoints following BMT and mechanically digested and then antibody stained for peripheral T cell compartment. Following FACs analysis, it was apparent that post BMT, peripheral recovery of CD4$^+$ and CD8$^+$ T cells was not evident at day 14 post BMT, and T cells began to appear at day 28 post BMT (Figure 4.9 A). When extended analysis was performed up to day 56 post BMT, proportions of CD4$^+$ and CD8$^+$ T cells had increased and formed very clear populations (Figure 4.9 A). Numerical quantification analysis was performed on peripheral T cells to accurately measure the recovery of this compartment in the periphery post BMT. In agreement with the above, donor CD4$^+$ T cells at day 14 post BMT were absent. However, their numbers began to increase at day 21 post BMT which could be the timepoint that marks the first cohort of thymus dependent donor T cells. Interestingly at day 28 post BMT, numbers highly increased and continued to increase up to day 56 post BMT (Figure 4.9 B). Numbers of CD4$^+$ T cells were then compared to the control and it was observed that at day 14 post BMT the levels of CD4$^+$ T cells was nearly 0% which correlated with the FACs data. At day 21 post BMT, T cell levels began to rise to reach 30% of control levels and then interestingly levels rose to 60% of control levels. Despite all previous rises in levels of CD4$^+$ T cells, the levels were significantly decreased. It was at day 56 post BMT that levels of donor derived CD4$^+$ T cells reached comparable numbers to the control (Figure 4.9 C). Recovery of donor derived peripheral CD8$^+$ T cells followed in a similar pattern in which numbers were recorded at low level at day 14 post BMT. Increased CD8$^+$ T cell numbers was observed at day 21 post BMT and they continued to increase up to day 56 post BMT (Figure 4.9 D). Overall numbers of CD8$^+$ T cells were lower than CD4$^+$ T cells and this was also visualized by the FACs data as proportion of CD4$^+$ T cells were higher.

Figure 4.9. Slow Reconstitution of Peripheral T cell Compartment Post BMT.

Mice were subjected to two doses of TBI and reconstituted with T cell depleted bone marrow. Spleen tissue was harvested and mechanically digested for FACs analysis. A. Representative FACs plots of CD4 and CD8 staining in donor T cells at d14, d28, d56 post BMT. Plots pre-gated on TCRβ+. B. Numerical quantification of donor CD4+ T cells in experimental mice post BMT. C. Bar graph showing recovery of donor CD4+ T cells compared to control mice where dotted line represents the control. D. Numerical quantification of donor CD8+ T cells in experimental mice post BMT. E. Bar graph showing recovery of donor CD8+ T cells compared to control mice where dotted line represents the control. Each dot represents one mouse where n≥5 for each time point across two independent experiments. For d56 n=9 across three independent experiments. Error bars represent SEM. Ordinary One-way ANOVA was used for statistical analysis where each timepoint was compared to control. The level of significance is as follows where non-significant (ns), p<.05 (*), p<.01 (**), p<.001 (***), and p<.0001 (****).

To further examine the recovery of peripheral CD4$^+$ T cells, they were split into different subsets and analysed post BMT. CD4$^+$ T cells were split based on the expression of CD25 and Foxp3 to identify peripheral Tconv and Treg and measure their recovery. At day 14 post BMT, donor derived Tconv and Treg were visualized by FACs analysis, however the populations were not similar to controls. At day 28 post BMT, it was observed that populations of Tconv and Treg began to form and at day 56 post BMT these populations were clearly identifiable (Figure 4.10 A). Numbers of Treg were then quantified in WT hosts post BMT, showing that Treg were absent at day 14 post BMT. Numbers began to rise slightly at day 21 and day 28 post BMT and strikingly there was a big increase of Treg numbers at day 56 post BMT (Figure 4.10 B). The numbers of Treg were then compared to the control to measure the relative recovery of this population. It was observed at day 14 Treg were absent, however levels began to rise to approximately 15% at day 21 post BMT. At day 28 post BMT, levels of Treg rose slightly but remained significantly decreased. Interestingly, the spike in numbers of Treg at day 56 post BMT were comparable to control levels (Figure 4.10 C).

Having seen the significant increase in Treg numbers in WT hosts at day 56 post BMT and having observed low levels of Treg at day 28 post BMT, proliferation analysis was performed to dissect the reason behind this significant increase. Spleen tissue harvested from control mice and BMC at day 28 post BMT was mechanically digested and antibody stained for the proliferation marker Ki67. It was visualized by FACs analysis that approximately 15% of Treg in control mice were Ki67$^+$. In contrast, this increased following BMT such that approximately 35% of Treg compartment expressed Ki67 (Figure 4.11 A, B). This finding suggests that the marked increase in Treg numbers at day 56 post BMT may be due to increased proliferation rather than thymus output.
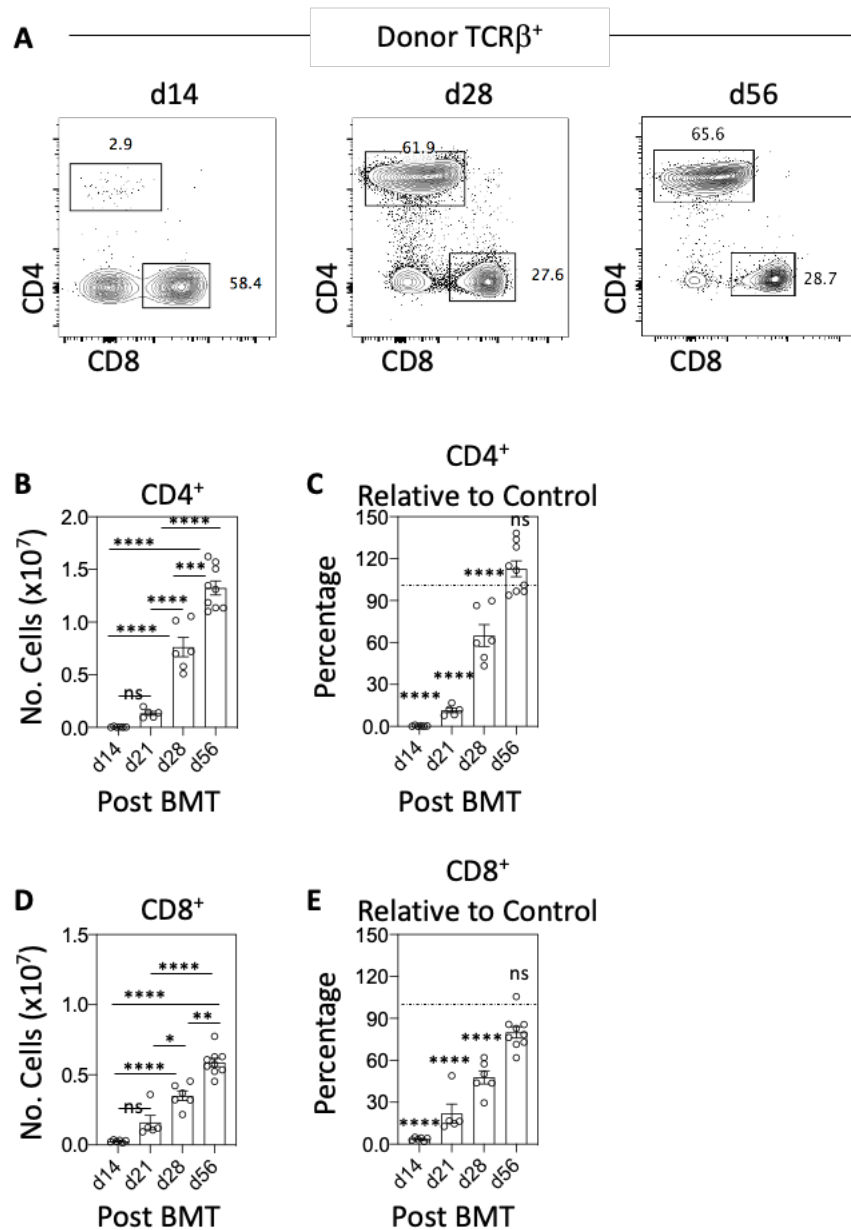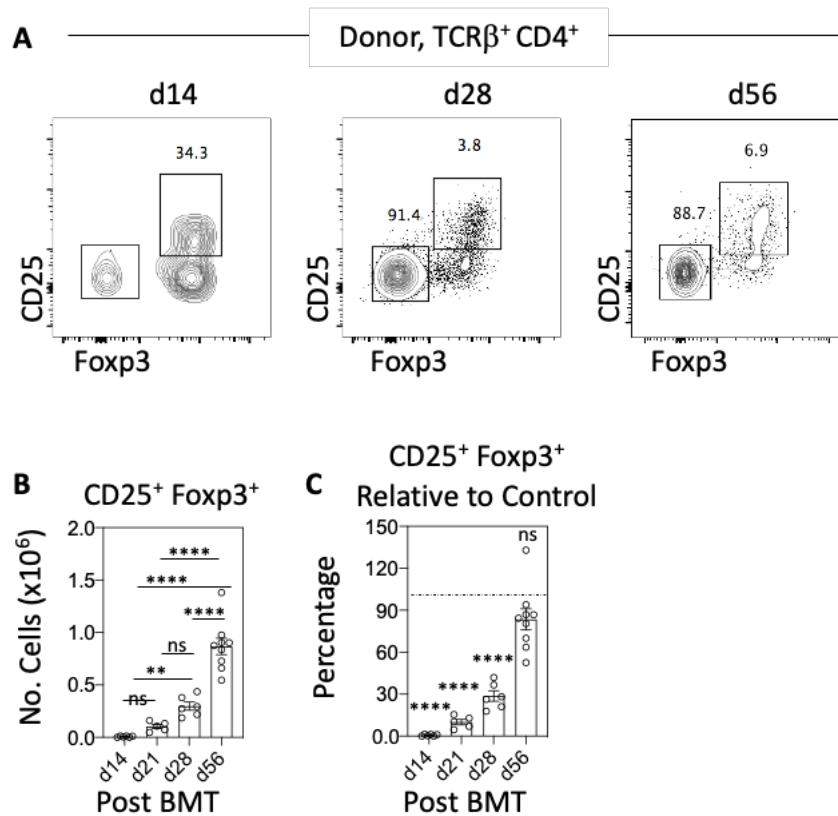
Figure 4.10. Slow Reconstitution of Peripheral T Regulatory Compartment Post BMT.

Mice were subjected to two doses of TBI and reconstituted with T cell depleted bone marrow. Spleen tissue was harvested and mechanically digested for FACs analysis. A. Representative FACs plots of CD25 and Foxp3 staining in donor T cells at d14, d28, d56 post BMT. Plots pre-gated on TCRβ+ CD4+. B. Numerical quantification of donor Treg in experimental mice post BMT. C. Bar graph showing recovery of donor Treg compared to control mice where dotted line represents the control. Each dot represents one mouse where n≥5 for each time point across two independent experiments. For d56 n=9 across three independent experiments. Error bars represent SEM. Ordinary One-way ANOVA was used for statistical analysis where each timepoint was compared to control. The level of significance is as follows where non-significant (ns), p<.05 (*), p<.01 (**), p<.001 (***), and p<.0001 (****).

A

Control
TCRβ⁺ CD4⁺ CD25⁻ Foxp3⁺

d28
TCRβ⁺ CD4⁺ CD25⁻ Foxp3⁺

14.5

36.3

CD4

Ki67

CD4

Ki67

B CD25⁺ Foxp3⁺

% Ki67
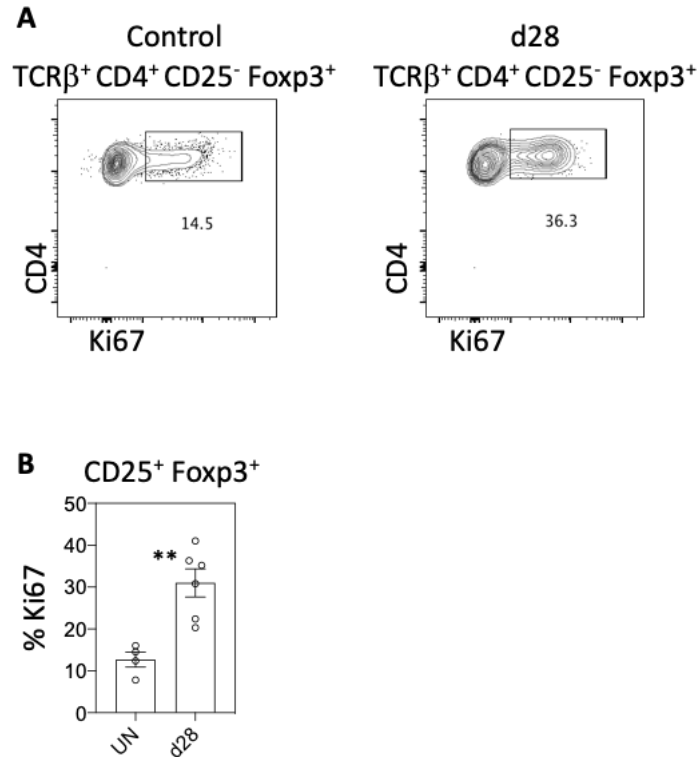
Figure 4.11. Increased Proliferation in Peripheral T Regulatory Cells Post BMT.

Mice were subjected to two doses of TBI and reconstituted with T cell depleted bone marrow. Spleen tissue was harvested and mechanically digested for FACs analysis. A. Representative FACs plots of CD4 and Ki67, an indicator of proliferation, staining in control mice and donor Treg at d28 post BMT. Plots pre-gated on TCRβ⁺ CD4⁺ CD25⁻ Foxp3⁺. B. Bar graph showing percentage of Ki67 in Treg. Each dot represents one mouse where n=4 for untreated (UN) and n=6 for d28 across two independent experiments. Error bars represent SEM. Unpaired student t test was used for statistical analysis where d28 was compared to control. The level of significance is as follows where non-significant (ns), $p<.05$ (*), $p<.01$ (**), $p<.001$ (***), and $p<.0001$ (****).

Intrathymic development of iNKT cells was compromised post BMT, thus it was essential to characterize the iNKT compartment in the periphery post BMT. Spleen tissue was harvested at day 28 and day 56 and mechanically digested and then antibody stained for peripheral iNKT cells in which they were identified by co-staining with PBS57:CD1d and anti-TCRβ. FACs analysis showed that in control mice iNKT cells were clearly identified with a proportion of 0.9%. However, at day 28 post BMT the peripheral iNKT compartment was significantly reduced. Extended analysis at day 56 post BMT, showed a slight improvement, as the proportion of iNKT cells rose from 0.1 to 0.3% from day 28 to day 56 post BMT (Figure 4.12 A). Numerical analysis performed post BMT showed that at day 28 post BMT, iNKT numbers were very low, which then increased at day 56 post BMT (Figure 4.12 B). Numbers were then compared to the control and it was observed that at day 28 post BMT the iNKT compartment was only at 20% compared to the control. Following the increase in numbers at day 56 post BMT, the relative recovery also increased to approximately 50% however that level remained significantly decreased (Figure 4.12 C).

Further analysis was conducted to characterize the recovery of the peripheral iNKT compartment by analysing non-lymphoid tissues. Liver and lung tissue were harvested at day 28 post BMT to investigate the recovery of the iNKT compartment within these tissues. For liver analysis, it was visualized that control mice had a very clear population that could be identified by expression of the PBS57:CD1d tetramer. At day 28 post BMT, this population was still present but to a much lower extent (Figure 4.13 A). Percentages of the iNKT compartment were compared between control and d28 BMC and it was observed that the proportions had decreased from approximately 15% to less than 5%. In turn, iNKT numbers were significantly decreased in liver tissues at day 28 post BMT (Figure 4.13 B). Unfortunately,

iNKT cells were less clear in digested lung tissue and there was minimal tetramer-stained population in the control. Nevertheless, post BMT the iNKT population was also reduced as visualized by FACs analysis (Figure 4.13 C). Although proportions of iNKT cells were low in control mice, the proportion after BMT was even lower and subsequently numbers were significantly affected (Figure 4.13 D).

Figure 4.12. Defective Recovery of Peripheral iNKT Compartment Post BMT.

Mice were subjected to two doses of TBI and reconstituted with T cell depleted bone marrow. Spleen tissue was harvested and mechanically digested for FACs analysis. A. Representative FACs plots of TCRβ and the PBS57:CD1d tetramer for iNKT identification at d28 and d56 post BMT. B. Numerical quantification of donor iNKT in experimental mice post BMT. C. Bar graph showing recovery of donor iNKT compared to control mice where dotted line represents the control. Each dot represents one mouse where n=6 for d28 across two independent experiments and n=9 for d56 across three independent experiments. Error bars represent SEM. Ordinary One-way ANOVA was used for statistical analysis where each host was compared to control. The level of significance is as follows where non-significant (ns), p<.05 (*), p<.01 (**), p<.001 (***), and p<.0001 (****).

Figure 4.13. Defective Recovery of Peripheral iNKT In Non-Lymphoid Tissues Post BMT.

Mice were subjected to two doses of TBI and reconstituted with T cell depleted bone marrow. Liver and Lung tissue was harvested and enzymatically digested for FACs analysis. A. Representative FACs plots of TCRβ and the PBS57:CD1d tetramer for iNKT identification in control and at d28 post BMT in the liver. B. Graph displaying total percentage of iNKT cells as well as numerical quantification of donor iNKT in experimental mice post BMT in the liver. C. Representative FACs plots of TCRβ and the PBS57:CD1d tetramer for iNKT identification in control and at d28 post BMT in the lung. D. Graph displaying total percentage of iNKT cells as well as numerical quantification of donor iNKT in experimental mice post BMT in the lung. Each dot represents one mouse where n=6 across two independent experiments. Error bars represent SEM. Unpaired student t test was used for statistical analysis where d28 was compared to untreated (UN). The level of significance is as follows where non-significant (ns), p<.05 (*), p<.01 (**), p<.001 (***), and p<.0001 (****).

4.2.4 Investigation of Thymic Microenvironment Post BMT

To analyse thymic epithelial cell (TEC) compartment, BMC were generated, and thymus tissue was harvested at different timepoints for time course analysis. Tissue was enzymatically digested, and antibody stained for TEC compartment analysis. Following BMT, it was observed that the EpCAM1$^+$ TEC were reduced in numbers at day 7. This reduction remained constant for day 14 and day 21 post BMT and was followed by a slight increase in numbers at day 28 post BMT. However, at day 56 post BMT it was observed that there was again a reduction in numbers of overall TEC (Figure 4.14 A). Numbers of TEC were then compared to the control for relative recovery analysis, and it was shown that for the first three timepoints of analysis, TEC were present at reduced levels up to 40% of the control. Following that, specifically at day 28 post BMT, levels of TEC slightly increased to approximately 60% of control levels. However, the increase in levels was followed by another decrease that remained at 40% of control levels (Figure 4.14 B). The TEC compartment was then broken down into cTEC and mTEC subset populations. Strikingly, numbers of cTEC remained relatively constant post BMT and throughout the time course analysis (Figure 4.14 C). The relative recovery of cTEC was then measured and it was shown that cTEC seemed to be affected post BMT, as levels remained comparable to the control (Figure 4.14 D). Interestingly numbers of mTEC were constant for day 7 and 14 post BMT, and then increased at day 21 and 28 post BMT which was followed by a decrease in their numbers at day 56 post BMT (Figure 4.14 E). mTEC relative recovery was significantly reduced compared to the control as mTEC levels did not increase above 40% recovery throughout the time course analysis (Figure 4.14 F).

To complement the FACs analysis of the TEC compartment, immunofluorescence images of frozen thymus sections were taken. Thymus tissue was harvested at different timepoints post BMT and frozen for tissue sections. Frozen tissue was then cut at 7μm thickness and labelled

for TEC markers that included DEC205 for cTEC analysis and ERTR5 to identify mTEC. Interestingly, at all timepoints analysed, discrete cortex and medulla areas were detected (Figure 4.15 A), suggesting that the changes in T-cell development that occur during BMT are not simply due to the loss of thymic organization.
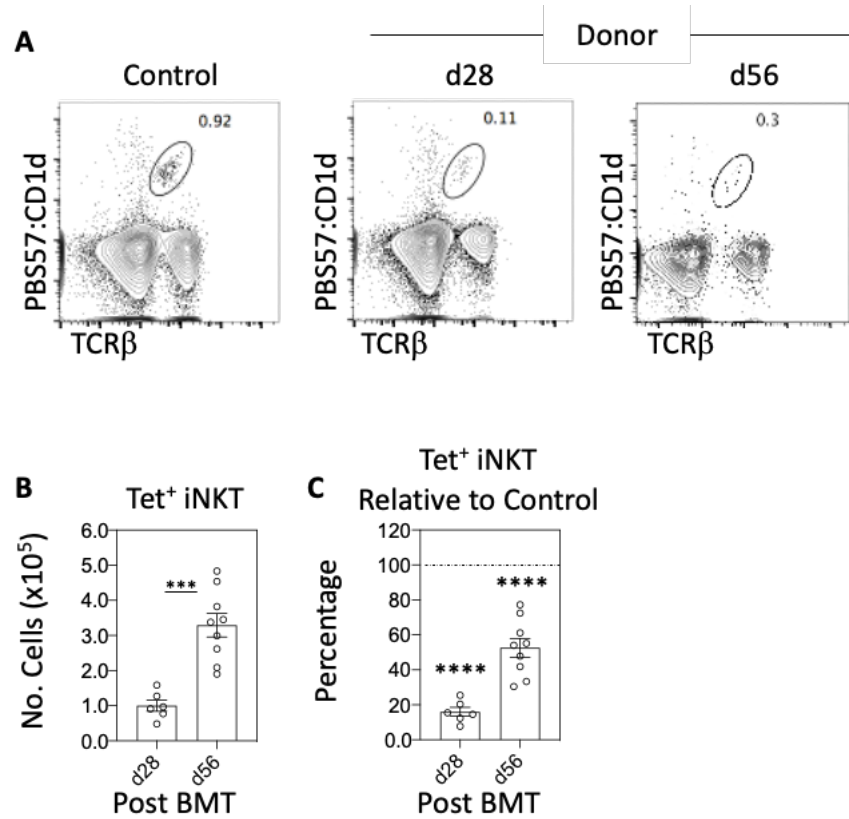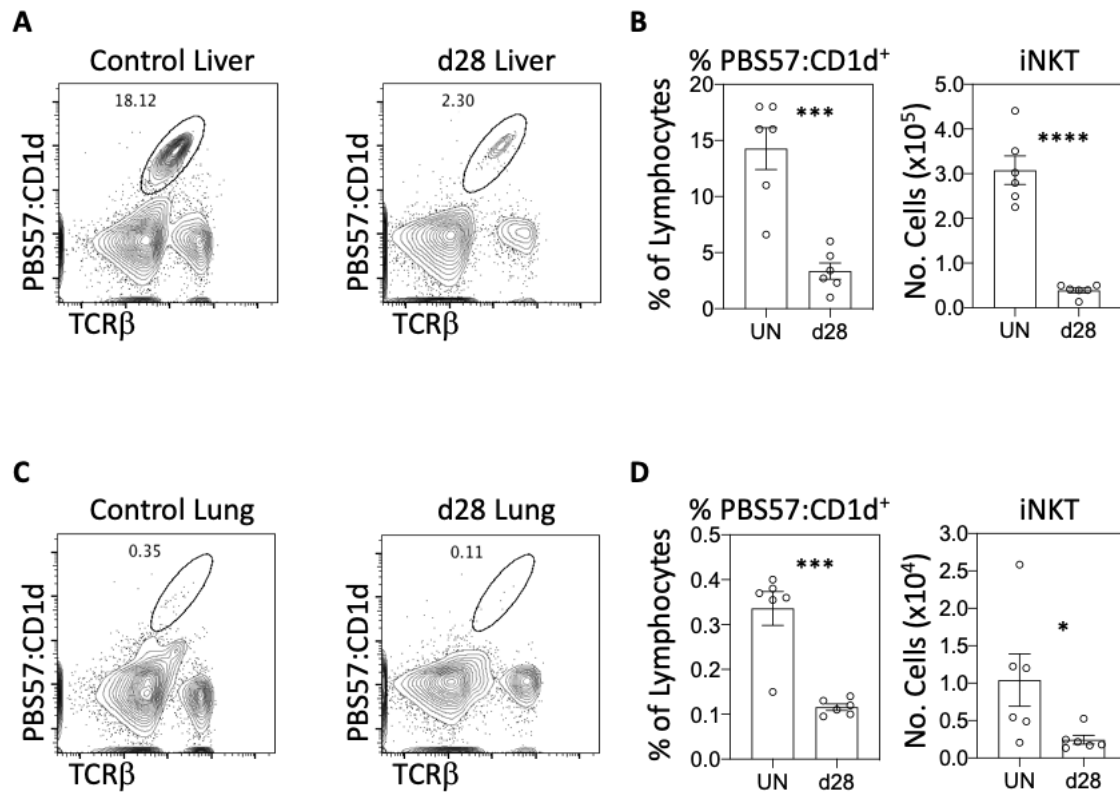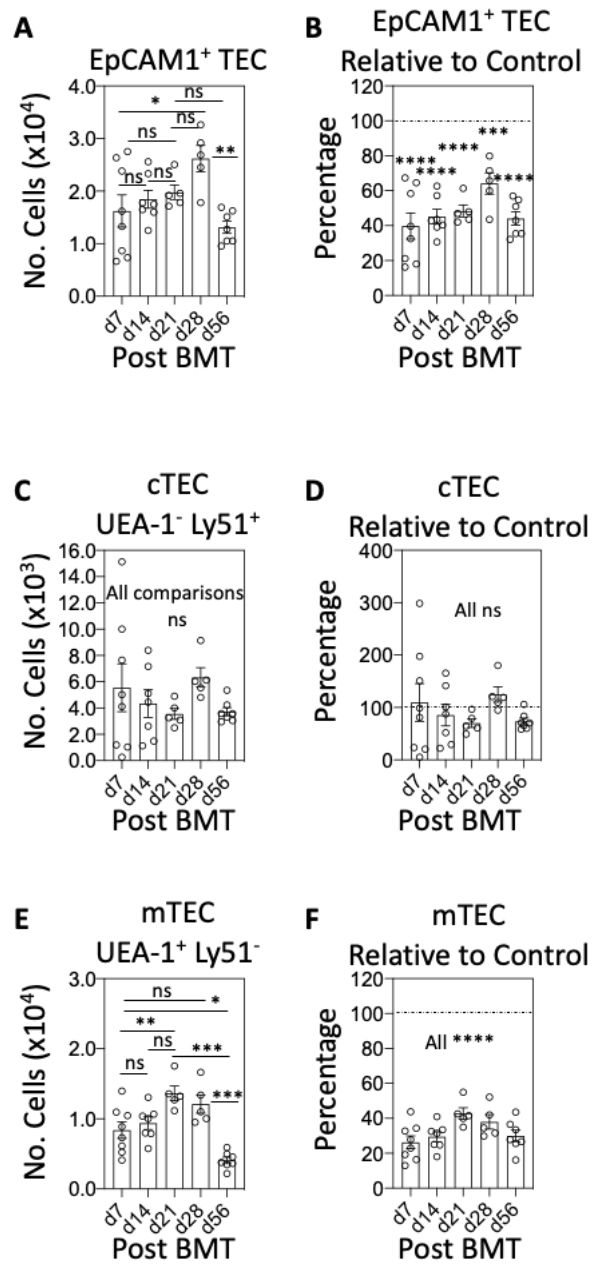
Figure 4.14. Defective Recovery of Thymic Epithelial Cells Post BMT.

Mice were subjected to two doses of TBI and reconstituted with T cell depleted bone marrow. Thymus tissue was harvested and enzymatically digested for FACs analysis. A. Numerical quantification of total EpCAM1$^+$ thymic epithelial cells (TEC). B. Bar graph displaying recovery of TEC compared to the control where the dotted line represents the control. C. Numerical quantification UEA-1$^-$ Ly51$^+$ cortical thymic epithelial cells (cTEC). D. Bar graph displaying recovery of cTEC compared to the control where the dotted line represents the control. E. Numerical quantification of UEA-1$^+$ Ly51$^-$ medullary thymic epithelial cells (mTEC). F. Bar graph displaying recovery of mTEC compared to the control where the dotted line represents the control. Each dot represents one mouse where n≥7 across three independent experiments for d7 and d14 post BMT. For d21 and d28 n=5 across two independent experiments. For d56 n=7 across three independent experiments. Error bars represent SEM. Ordinary One-way ANOVA was used for statistical analysis where each host was compared to control. The level of significance is as follows where non-significant (ns), $p<.05$ (*), $p<.01$ (**), $p<.001$ (***), and $p<.0001$ (****).
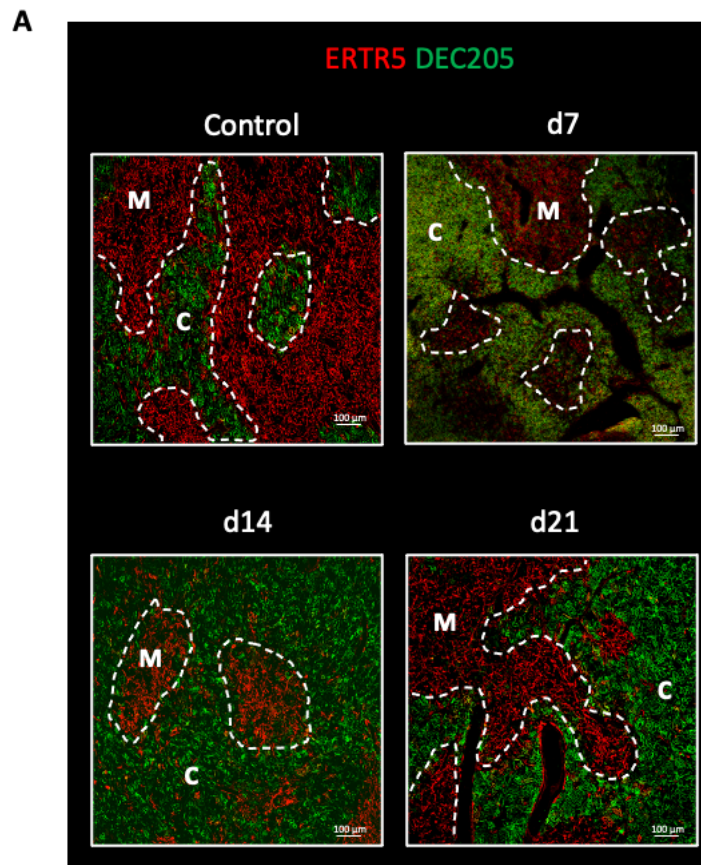
Figure 4.15. Organization of Thymic Epithelial Cell Compartment Post BMT.

Mice were subjected to two doses of TBI and then reconstituted with T cell depleted bone marrow. Thymus tissue was harvested at different timepoints, frozen and then cut at 7μm thickness for histology analysis. Each section was approximately 35μm apart. A. Immunofluorescence image of thymus regions stained for ERTR5 (Red) to identify medullary regions and DEC205 (Green) to identify cortical regions post damage. All sections were stained and analysed alongside control sections. Dotted line defines cortical (C) and medullary (M) regions. N=3 for each time point where thymus was harvested and frozen and then cut at 7μm thickness.

Having seen irregularities in thymocytes development post BMT, it was important to investigate the recovery of the additional accessory cells within the thymic microenvironment that aid in the proper development of thymocytes. As a result, BMC were generated using the previous methods described and thymus tissue was harvested at different timepoints for time course analysis. First, tissue was enzymatically digested and then antibody stained to detect the thymic DC compartment. It was observed that overall conventional dendritic cells (cDC) were absent from the thymus at day 7 post BMT. However, this was followed by an increase in numbers that remained constant for day 14 and day 21 post BMT. Following day 21, the cDC compartment had an increase in numbers (Figure 4.16 A). Further analysis was conducted to split the cDC compartment into subsets based on the expression of Sirpα. cDC1 were identified by lack of Sirpα expression, while cDC2 were identified by positive expression of Sirpα Following BMT, cDC1 had an identical recovery pattern as overall cDC, where they were undetectable at day 7 post BMT. Furthermore, there was an increase in numbers at day 14 post BMT that remained constant up to day 21 post BMT. It was at day 28 post BMT that numbers of cDC1 increased again. In contrast, we saw differences in the recovery of cDC2. Again, at day 7 this population was also absent followed by a slight increase in numbers at day 14 post BMT. The slight increase in numbers carried through day 21 and day 28 post BMT (Figure 4.16 B). Numbers of cDC was then compared to the control to measure the relative recovery. It was observed that the overall cDC compartment did not manage to recover at all timepoints, there was a significant reduction in the population (Figure 4.16 C). Interestingly, breaking down the cDC compartment into cDC1 and cDC2, it was observed that both populations did not fully recover during the time course analysed (Figure 4.16 D). Another population present in the DC compartment can be identified as plasmacytoid dendritic cells (pDC). Strikingly this population had a different recovery pattern as cDC in which numbers of pDC were absent at day 7 post

BMT but numbers increased and remained constant for the remaining timepoints (Figure 4.16 E). When the number of pDC were compared to the control, it was apparent that this population had approximately recovered only 50% of the population post BMT (Figure 4.16 F). The lack of recovery in the donor DC compartment was significant, thus the host DC compartment was investigated. It was visualized by FACs analysis that the host DC compartment was absent throughout the time course analysis (Figure 4.17 A).

Figure 4.16. Defective Recovery of Intrathymic Dendritic Cells Post BMT.

Mice were subjected to two doses of TBI and reconstituted with T cell depleted bone marrow. Spleen tissue was harvested and enzymatically digested for FACs analysis. A. Numerical quantification of CD11c^{hi} PDCA-1$^-$ conventional dendritic cells (cDC). B. Numerical quantification of cDC subsets; Sirpα$^-$ cDC1 and Sirpα$^+$ cDC2. C. Bar graph displaying recovery of cDC compared to the control where the dotted line represents the control. D. Bar graph displaying recovery of cDC1 and cDC2 compared to the control where the dotted line represents the control. E. Numerical quantification of CD11c^{lo} PDCA-1$^+$ plasmacytoid dendritic cells (pDC). F. Bar graph displaying recovery of pDC compared to the control where the dotted line represents the control. Each dot represents one mouse where n=6 across two independent experiments. For d28 n=7 across two independent experiments. Error bars represent SEM. Ordinary One-way ANOVA was used for statistical analysis where each host was compared to control. The level of significance is as follows where non-significant (ns), $p<.05$ (*), $p<.01$ (**), $p<.001$ (***), and $p<.0001$ (****).

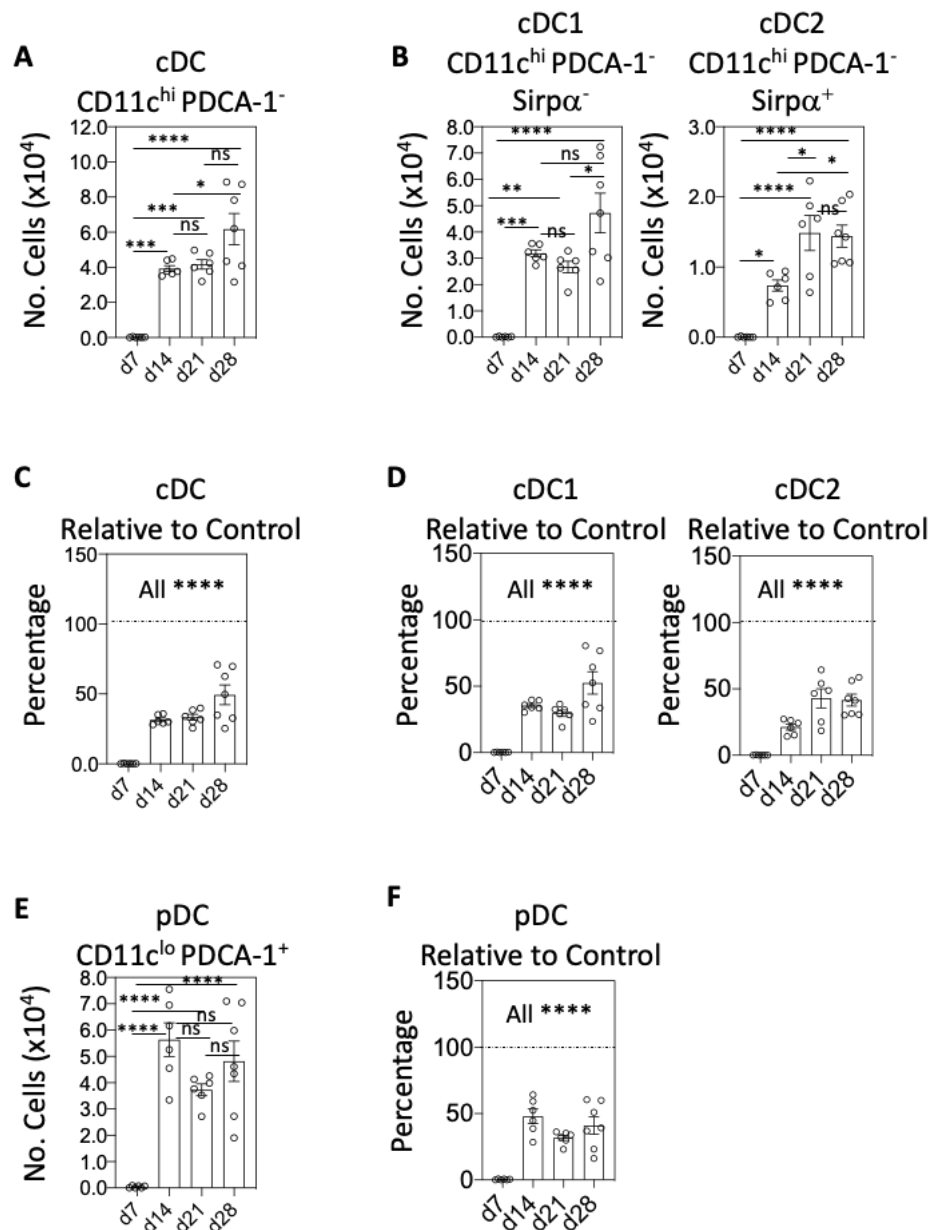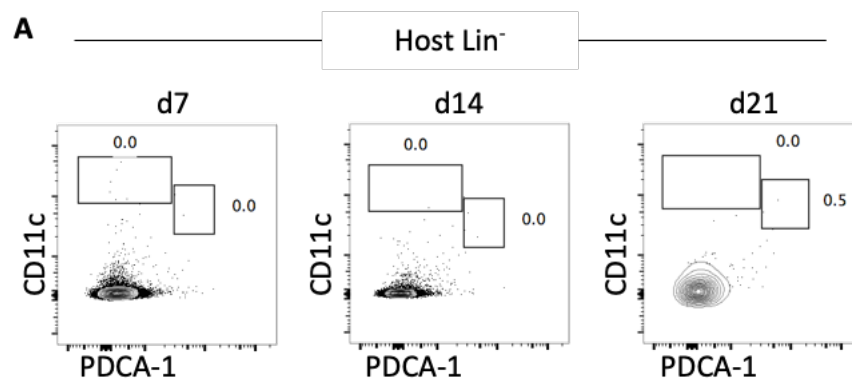**Figure 4.17. Absence of Host Dendritic Cells Post BMT.**

Mice were subjected to two doses of TBI and reconstituted with T cell depleted bone marrow. Spleen tissue was harvested and enzymatically digested for FACs analysis. A. Representative FACs plots of CD11c and PDCA-1 in the host dendritic cell compartment at d7, d14, and d21 post BMT. N=6 across two independent experiments.

4.3 Discussion

4.3.1 Rapid Restoration of T Cell Development Is Skewed Towards T Conventional Recovery

Thymus regeneration post ablative therapy and BMT is critical in re-establishing the peripheral T cell compartment. Studies have identified that following lethal irradiation, the thymus begins the regeneration process from an intrathymic source derived of host origins (Kadish and Basch, 1975; Ceredig and Macdonald, 1982; Bosco *et al.*, 2010). Indeed, our data has shown that donor colonization of the thymus is observed at d14 post BMT and immunofluorescence analysis provides evidence of the presence of DP thymocytes in cortical regions following BMT, which correlates with the previous studies. However, in depth analysis of the thymus donor compartment shows bias towards Tconv recovery. Foxp3$^+$ Treg development has been shown to be dependent on the presence of an intact medulla through the production of Treg precursors (Cowan *et al.*, 2013). Furthermore, more evidence emerged to support the role of the medulla in Treg development, as it has been shown that combined depletion of mTEC and thymic CD8α^+ DCs caused peripheral autoimmunity (Herbin *et al.*, 2016). Selective depletion of either mTEC or CD8α^+ DC showed only decreased Treg selection when mTEC were depleted suggesting that CD8α^+ DC are not essential for Treg selection (Herbin *et al.*, 2016). Thus, when analyzing Treg selection post BMT, we observed slower kinetics of recovery compared to Tconv. This could be in relation to the reduction in mTEC that was observed during thymus regeneration post BMT. Interestingly, immunofluorescence analysis following BMT shows distinctive medullary areas, however this was not sufficient for initial Treg recovery, perhaps suggesting additional mTEC availability and/or mTEC functions are required for Treg development. This needs to be investigated further. In contrast, a previous study has shown that DC can also be implicated in the Treg selection. Sirpα^+ cDC were cocultured with CD4$^+$ thymocytes that contained Treg precursors, and it was evident that Sirpα^+ cDC were efficient

at selecting Foxp3$^+$ Treg (Proietto *et al.*, 2008). Furthermore, DC and their role in Treg generation has also been shown by the investigation of *Ccr7*$^{-/-}$ thymus in which the loss of CCR7 on Sirpα$^-$ DC allowed for expansion of the Sirpα$^+$ DC that resulted in the increased Treg generation (Hu *et al.*, 2017). Additionally, the localization of DC in medullary areas has been shown to be dependent on mTEC expression of the chemokine XCL1 (Lei *et al.*, 2011). mTEC mediated DC localization has been shown to be important for Treg generation as XCL1 deficient mice has reduced Treg (Lei *et al.*, 2011). Nevertheless, our data shows reductions in both the mTEC and DC compartment may be important factors that are causing the decreased Treg selection. However, further examination is required to determine whether XCL1 expression post BMT is affected and whether localization of DC to medullary regions is impaired. Furthermore, the reduction in thymic Treg selection has also impacted the peripheral Treg compartment with significant reductions in numbers. However, it was observed that at d56 post BMT, Treg numbers were relatively similar to control levels even though thymic selection was reduced. In depth analysis of Treg identified that post BMT, Treg show increased proliferation status as shown by Ki67 expression. This increase in proliferation could explain the increase in peripheral Tregs as thymic output of Tregs was still reduced.

4.3.2   Impaired Recovery of Thymic Microenvironments Post BMT

The thymus is organized into distinctive cortical and medullary regions to compose the thymic microenvironment. Functional cortical and medullary regions provide essential requirements for the development of T cell progenitors. Furthermore, it is apparent that the thymus is also the site of development for other cell types of which include the CD1d restricted iNKT cells. The cortical region of the thymus fosters DP thymocytes which are required for the selection of iNKT cells (Bendelac, 1995; Gapin *et al.*, 2001). Following iNKT selection in cortical

regions, studies have shown that iNKT cells require the medulla for further maturation (Cowan *et al.*, 2014; White *et al.*, 2014). Furthermore and in relation to the previous studies, a more recent study identified the importance for the diversity in the mTEC^{lo} compartment in shaping the iNKT population and also how LTβR expression by the TEC compartment can have a direct effect on peripheral iNKT populations (Lucas *et al.*, 2020). Following BMT, our data shows that the cTEC compartment is relatively maintained and is able to support DP thymocyte development. In contrast, the mTEC compartment is significantly reduced throughout the time course analysis. Subsequently, analysis of iNKT shows a significant reduction that could be related to missing factors required for further maturation as a result of the decrease in the mTEC compartment. Interestingly, a recent study has classified iNKT cell precursors as CCR7^{+} that give rise to the different iNKT subsets (Wang and Hogquist, 2018). In depth analysis of iNKT precursors shows that following BMT there is a significant increase in the precursors stage, however the lack of mTEC could be compromising the latter stages of development. Consequently, the block in iNKT development following BMT resulted in the decrease of the peripheral iNKT compartment as splenic, liver, and lung tissue analysis following BMT shows a significant reduction in iNKT cells.

Following lethal irradiation, the thymus is dependent on donor progenitor colonization to restore the T cell immunity. However, the data shown provides evidence that T cell development is occurring in a thymus microenvironment that recovers differentially. While cTEC were found to be maintained post BMT, mTEC and DC sustained a significant reduction throughout the time course analysis. This differential recovery can impact the quality of T cells produced.

5 CHAPTER 5: INVESTIGATING THE FUNCTIONAL CONSEQUENCE OF FAILED NEGATIVE SELECTION POST BMT

5.1 Introduction

Following ablative therapies for the treatment of hematological cancers, host immune cells are depleted and thus there is an important need for immune reconstitution including repopulation of the T cell compartment. Failure to do so can cause severe consequences that could mount to immune deficiency. The use of ablative therapies also includes drug administration to help ensure successful engraftment. Indeed, early studies have analysed the use of Cyclosporin A (CsA) as an effective immunosuppressant that can aid successful engraftment (Klaus, 1981). Furthermore, it was shown in a murine model that the use of such immunosuppressants interfered with the ability of the thymus to generate new T cells that could suppress cells with self-reactive capabilities (Sakaguchi and Sakaguchi, 1988). In this study, it was shown that thymus lobes that were treated with CsA and engrafted onto nude mice initiated autoimmune disease. Furthermore, it was also shown that autoimmune disease could be prevented by the inoculation of thymocytes following the lobe engraftment. However, it was also shown that the prevention of autoimmunity was achieved if thymocytes used for transfer were from CsA treated mice (Sakaguchi and Sakaguchi, 1988). Such findings are in line with later studies demonstrating that use of lethal irradiation and CsA led to the initiation of autoimmune disease (Beijleveld, Damoiseaux and Van Breda Vriesman, 1995). Indeed, it was observed that the use of CsA had a negative effect on the medulla as medulla involution was observed. Interestingly, the use of the CsA and irradiation had a differential impact on the different regions of the thymus. It was shown that while cortical and medullary regions could be distinguished, the recovery of the medulla was inhibited (Beijleveld, Damoiseaux and Van Breda Vriesman, 1995). In the thymus, negative selection is mediated by the presence of antigen presenting cells that present self-antigens through MHC. Indeed, it was shown through a chimeric model of BMT that mice lacking MHCII on thymic APCs developed autoimmune disease (Teshima *et al.*, 2003). Further, it was shown in the same study that when CD4^{+} T cells from MHCII

deficient chimeras were transferred to irradiated mice, GVHD was initiated (Teshima *et al.*, 2003). These data highlight the importance of self-antigen presentation and the process of negative selection to avoid initiation of autoimmune disease. In the previous chapter it was shown that medullary thymic microenvironments and the APC they contain are significantly reduced post BMT. As such, this chapter will focus on the functional consequences of the loss of thymus medulla and ask whether the thymus is able to functionally impose T-cell tolerance during immune reconstitution.

5.2 Results

5.2.1 Accumulation of Mature T conventional (Tconv) Thymocytes Post BMT

Having completed characterization of intrathymic T cell development post BMT, it was evident that mature Tconv identified by CD69$^-$ CD62L$^+$ phenotype had accumulated post BMT. Early FACs analysis revealed donor mature Tconv were absent at d14 post BMT, however the proportion increased significantly at d28 post BMT, surpassing the untreated control proportion. Strikingly, at d56 post BMT Tconv proportions continued to increase and were recorded at double the proportion of untreated controls (Figure 5.1 A). Having seen the increased proportions in mice post BMT by FACs analysis, thymocyte numbers were analysed to compare to the untreated control. As seen by the FACs analysis, it was also confirmed by analysing the numbers at d14 post BMT where mature Tconv were absent. Also, numbers began to increase at d21 post BMT and was maintained through the d56 time course. Interestingly, the increase in numbers, when it was compared with control, was found to be statistically significantly higher than the control levels (Figure 5.1 B) revealing that mature Tconv accumulate in the thymus post BMT.
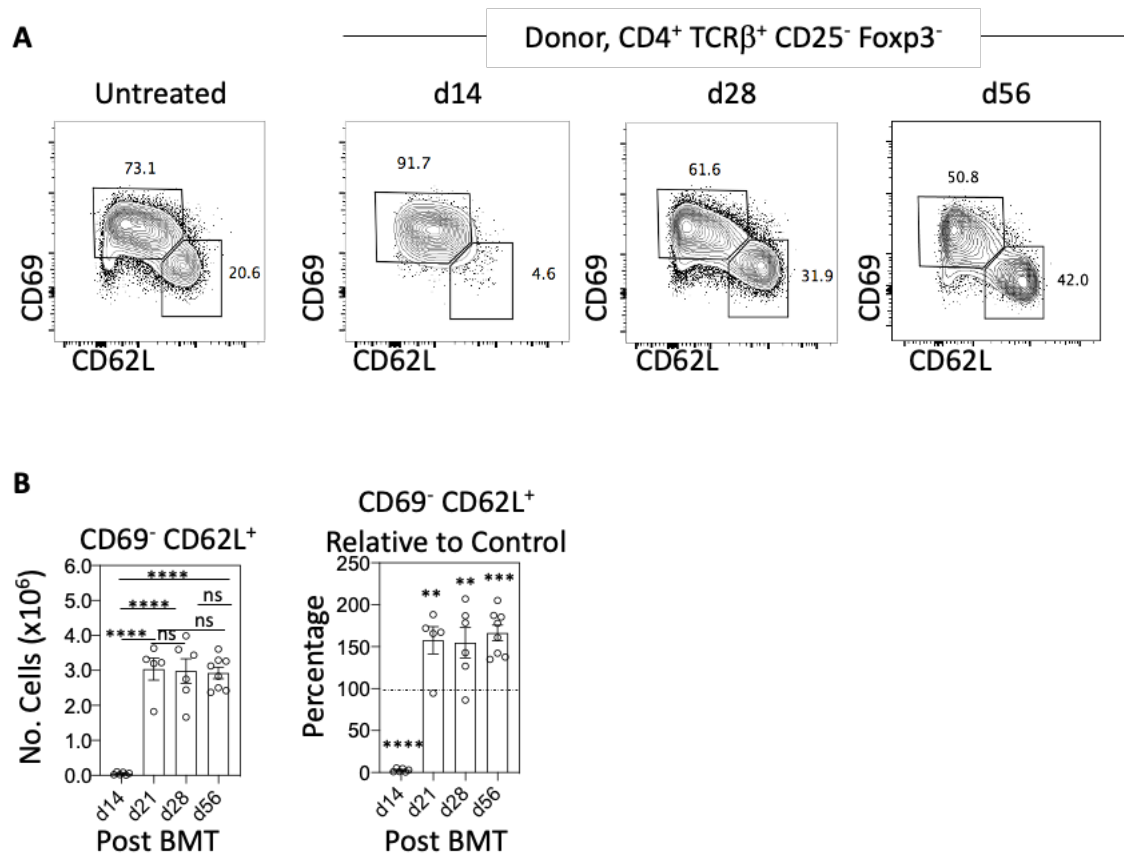
Figure 5.1. Accumulation of Mature T Conventional Cells in The Thymus Post BMT.

Mice were subjected to two doses of TBI and reconstituted with T cell depleted bone marrow. Thymus tissue was harvested and mechanically digested for FACs analysis. A. Representative FACs plots of CD69 and CD62L staining in donor thymocytes at d14, d28, and d56 post BMT. B. Numerical quantification of donor mature T conventional (Tconv) in experimental mice post BMT. C. Bar graph showing recovery of donor mature Tconv compared to control mice where dotted line represents the control. Each dot represents one mouse where n≥5 for each time point across two independent experiments. For d56 n=8 across three independent experiments. Error bars represent SEM. Ordinary One-way ANOVA was used for statistical analysis where each timepoint was compared to control. The level of significance is as follows where non-significant (ns), $p<.05$ (*), $p<.01$ (**), $p<.001$ (***), and $p<.0001$ (****).

The accumulation of Tconv was a striking observation and thus prompted further experiments to examine this accumulation post BMT. Rag2^{GFP}Foxp3^{RFP} dual reporter (DR) mice were used as BM donors into WT hosts. BM from DR mice that was used to reconstitute WT hosts also exhibited an accumulation phenotype (Figure 5.2 A, B). Furthermore, a possible explanation of Tconv accumulation post BMT was that excessive proliferation was taking place in mature thymocytes post BMT. To test this hypothesis, thymus tissue was harvested at d28 post BMT and antibody stained for the proliferation marker Ki67. Having identified the Tconv population by FACS, Tconv were then assessed for Ki67 expression to measure their proliferation post BMT. Interestingly, control and BMC were very similar and Ki67$^+$ cells were similar between control and BMT mice (Figure 5.3 A, B), suggesting the accumulation of mature Tconv post BMT was not due to increased proliferation.

Another possibility as to why mature Tconv accumulated intrathymically post BMT could be an increased time in the thymus. As such, DR mice were then used as BM donors into WT hosts. This allowed for GFP to act as a molecular timer to study newly developed thymocytes. Thymus tissue from the BMC that received DR BM was harvested at d28 post BMT to measure the GFP levels of mature Tconv post BMT. Interestingly it was observed that GFP levels in CD4$^+$ T-conv, as shown by histogram analysis between control and d28 BMC, were overlapping. Furthermore, fluorescence intensity of GFP levels were compared in the BMC to the control and it was shown that levels were similar with no significant difference (Figure 5.3 C, D). Collectively, these findings suggest that the accumulation of mature Tconv post BMT is not due to increased proliferation or increased dwell time post BMT.
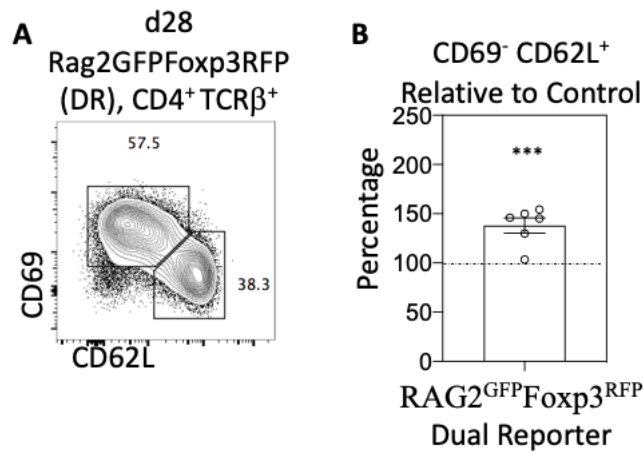
Figure 5.2. Intrathymic Accumulation of Mature Conventional αβT Cells Is Present in Different Bone Marrow Chimera Models Post BMT.

Mice were subjected to two doses of TBI and reconstituted with T cell depleted bone marrow. Thymus tissue was harvested and mechanically digested for FACs analysis. A. Representative FACs plots of CD69 and CD62L staining in mature T conventional (Tconv) at d28 post BMT in RAG2^{GFP} x Foxp3^{RFP} Dual Reporter (DR) B. Bar graph showing recovery of donor mature Tconv compared to control mice where dotted line represents the control. Each dot represents one mouse where n=6 for each time point across two independent experiments for DR hosts. Error bars represent SEM. Unpaired student t test was used for statistical analysis where d28 was compared to control. The level of significance is as follows where non-significant (ns), p<.05 (*), p<.01 (**), p<.001 (***), and p<.0001 (****).
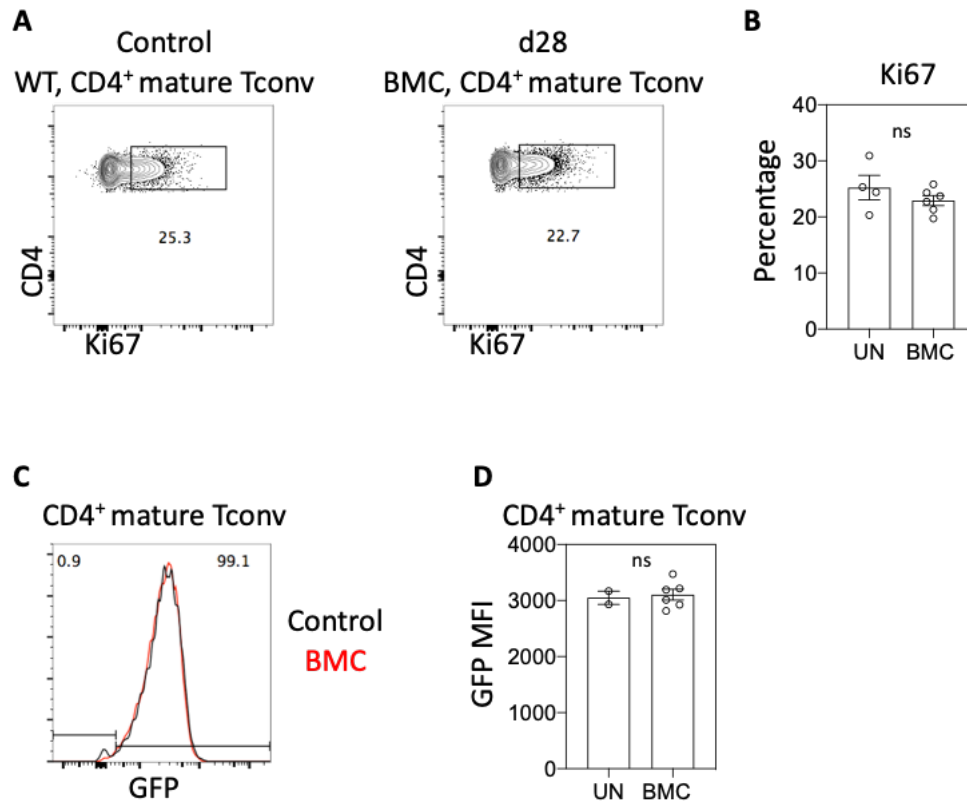
Figure 5.3. Accumulation of Mature T Conventional Post BMT Is Not Due to Proliferation or Increased Dwell Time.

Mice were subjected to two doses of TBI and reconstituted with T cell depleted bone marrow. Thymus tissue was harvested and mechanically digested for FACs analysis. A. Representative FACs plots of CD4 and Ki67 staining in mature T conventional (Tconv) at d28 post BMT and in control mice showing indicator of proliferation. B. Bar graph showing percentage of Ki67 expression in control untreated (UN) and d28 bone marrow chimera (BMC). C. Histogram of GFP levels in control dual reporter mice (DR) and d28 BMC. D. Bar graph showing level of expression of GFP between DR and BMC mice. Each dot represents one mouse. For Ki67 analysis n=6 for BMC and n=4 for control across two independent experiments. For GFP level of expression analysis n=6 for BMC and n=2 for control across two independent experiments. Error bars represent SEM. Unpaired student t test was used for statistical analysis where d28 was compared to control. The level of significance is as follows where non-significant (ns), $p<.05$ (*), $p<.01$ (**), $p<.001$ (***), and $p<.0001$ (****).

5.2.2 Negative Selection Failure Post BMT

In the previous chapter it was found that mTEC and DC were significantly reduced through the time course analysis. Furthermore, it was also found that mature Tconv accumulation was not because of proliferation or increased dwell time in thymus. Thus, it was important to test the functionality of negative selection to determine whether this may be contributing to the increase in accumulation of mature Tconv in the thymus. Thymocytes that express TCRs with MMTV reactivity are usually deleted in the BALB/c mouse as this mouse strain expressed the particular MMTV genes to achieve this. Thus MMTV-6 deletes thymocytes bearing the Vβ3 chain, while MMTV-8/9 delete thymocytes that express the Vβ5/11 chain (Moore *et al.*, 1994; Barnett *et al.*, 1999). BMC were generated to identify if the thymocytes bearing the relative Vβ chains were deleted. Here, as the hosts used were BALB/c mice, we used BALB/c Kaede mice as BM donors, therefore expression of the green fluorescent protein Kaede could be used to specifically identify donor derived thymocytes. By gating in Kaede[+] donor-derived thymocytes, FACs analysis at d28 post BMT clearly identified the presence of Vβ3, Vβ5, and Vβ11 bearing thymocytes, and proportions of the different Vβ thymocytes were all recorded as significantly higher than the untreated control (Figure 5.4 A, B). Thus, this data suggests that following BMT, thymocytes expressing TCRs that recognize self-antigens are readily detectable, suggesting their appearance could be due to defective negative selection.
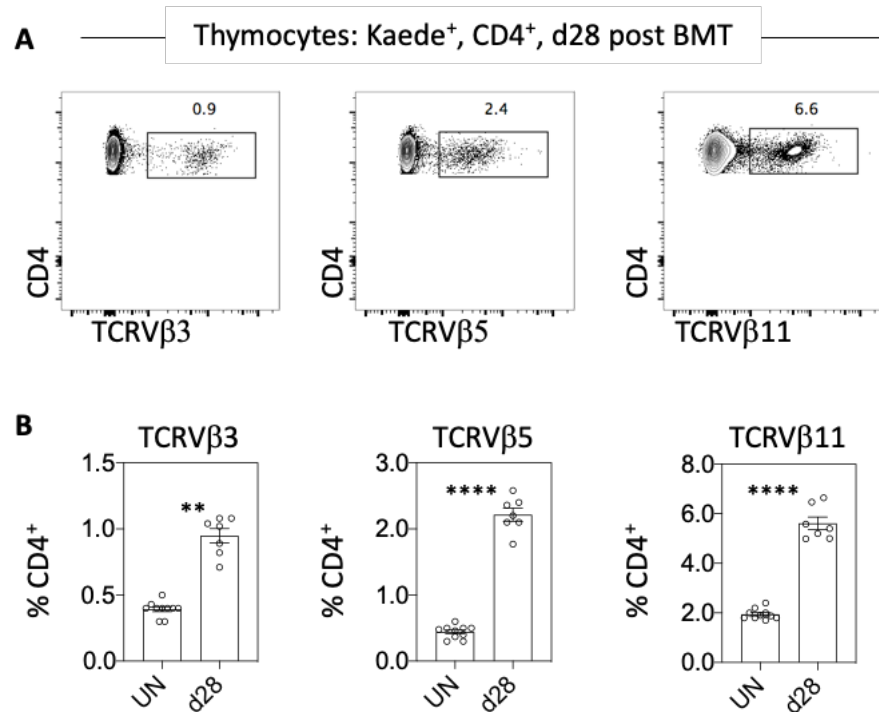
Figure 5.4. Failure in MMTV-mediated Deletion Of TCRVβ Thymocytes Occurs Post BMT.

BALB/c were subjected to two doses of TBI and reconstituted with Kaede⁺ T cell depleted bone marrow. Thymus tissue was then harvested and mechanically digested. A. FACs analysis showing staining for CD4, TCRVβ3, TCRVβ5 and TCRVβ11 in Kaede⁺ BALB/c experimental mice. B. Bar graph displaying comparison of variable TCRVβ thymocyte percentages post BMT. Each dot represents one mouse where n=7 for TCRVβ3, TCRVβ5, and TCRVβ 11 across two independent experiments. For untreated (UN) n=10 complied from previous time points across three independent experiments. Error bars represent SEM. Unpaired student t test was used for statistical analysis where each timepoint was compared to control. The level of significance is as follows where non-significant (ns), $p<.05$ (*), $p<.01$ (**), $p<.001$ (***), and $p<.0001$ (****).

To examine this further, active Caspase-3 staining was used to identify thymocytes undergoing programmed cell death. Earlier studies have used this method to identify thymocytes undergoing apoptosis through negative selection as Caspase-3 is involved in the apoptosis pathway. Signaled cells to undergo selection were identified by the expression of CD5 and TCRβ. Following that, the expression of active Caspase-3 was able to identify thymocytes that are undergoing clonal deletion (Breed, Watanabe and Hogquist, 2019). Mouse chimeras were generated as previous, and thymus tissue was harvested and mechanically digested and antibody stained for clonal deletion analysis at d28 post BMT. Active Caspase-3 expression was then analysed to identify the proportion of thymocytes undergoing negative selection. It was apparent, that untreated WT mice, the expression of active Caspase-3 was approximately 0.6% of signaled thymocytes. Interestingly, the proportion of active Caspase-3[+] signaled thymocytes post BMT was slightly lower and has been identified as statistically significantly lower (Figure 5.5 A, B), suggesting that post BMT there are reduced active Caspase-3^{+} cells which are undergoing clonal deletion.
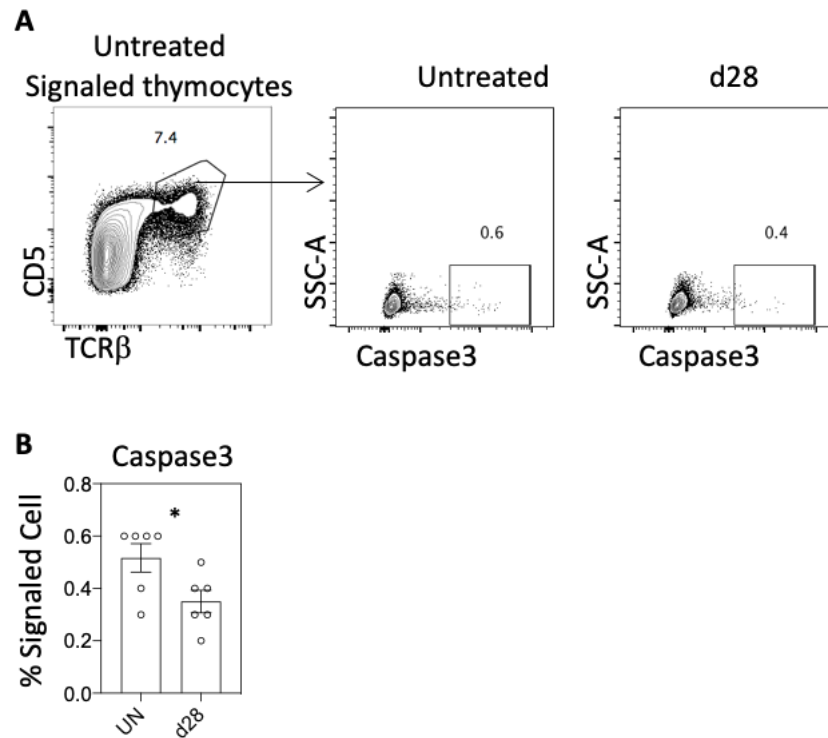
Figure 5.5. Decreased Frequency of Caspase3 Expressing Thymocytes Post BMT.

Mice were subjected to two doses of TBI and reconstituted with T cell depleted bone marrow. Thymus tissue was harvested and mechanically digested for FACs analysis. A. Representative FACs plots of CD5, TCRβ, and Caspase3 staining in signaled thymocytes at d28 post BMT. B. Bar graph showing percentage of Caspase3 in signaled thymocytes. Each dot represents one mouse where n=6 across two independent experiments. Error bars represent SEM. Unpaired student t test was used for statistical analysis where d28 was compared to control. The level of significance is as follows where non-significant (ns), p<.05 (*), p<.01 (**), p<.001 (***), and p<.0001 (****).

To examine whether thymocytes that escape negative selection following BMT are detectable in the periphery, mouse chimeras were generated, and splenic tissue was harvested at d28 post BMT to identify peripheral T cells bearing the different Vβ TCRs that react with MMTV. Importantly, T cells bearing Vβ3, Vβ5, and Vβ11 were clearly visible in the spleens of BMC mice (Figure 5.6 A). Moreover, analysis of Vβ proportions showed a significant increase (Figure 5.6 B). Cumulatively, these data identify that post BMT, the thymus is capable of generating new T cells, however important educational steps are compromised during the regeneration process.
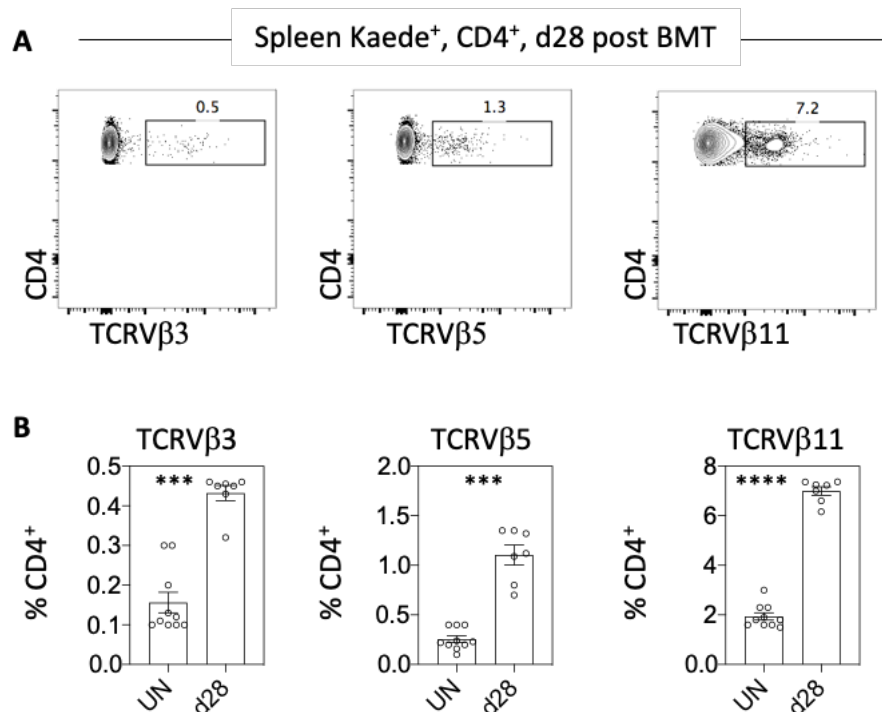
Figure 5.6. TCRVβ Thymocytes Escape Deletion and Exit to The Periphery Post BMT.

BALB/c were subjected to two doses of TBI and reconstituted with Kaede⁺ T cell depleted bone marrow. Spleen tissue was then harvested and mechanically digested. A. FACs analysis showing staining for CD4, TCRVβ3, TCRVβ5 and TCRVβ11 in Kaede⁺ BALB/c experimental mice. B. Bar graph displaying comparison of variable TCRVβ T cells percentages post BMT. Each dot represents one mouse where n=7 for TCRVβ3, TCRVβ5, and TCRVβ11 across two independent experiments. For untreated (UN) n=10 complied from previous time point across three independent experiments. Error bars represent SEM. Unpaired student t test was used for statistical analysis where each timepoint was compared to control. The level of significance is as follows where non-significant (ns), p<.05 (*), p<.01 (**), p<.001 (***), and p<.0001 (****).

5.2.3 Impaired Negative Selection Leads to Signs of Autoimmunity Post BMT

As shown by the previous data, it was apparent that post BMT, the accumulation of mature conventional thymocytes in the thymus was not due to proliferation or loss of egress ability. In fact, it was shown that negative selection post BMT was affected and as a result thymocytes that should have been deleted were found present. Furthermore, it was apparent that the should be deleted cells were clearly identified in the periphery. Caspase-3 analysis identified the lack of thymus ability to efficiently induce negative selection as Caspase-3$^+$ proportion has been significantly reduced. As a result, the functional capability of negative selection has been tested by the set-up of adoptive transfer experiments. Rag2^{GFP}Foxp3^{RFP}(DR) mice were used as either donors of BM or mature Tconv thymocytes. DR BM was used to reconstitute irradiated hosts. At d28 post BMT, thymus tissue was harvested and mechanically digested for high-speed sorting of mature T conv thymocytes. Alongside, untreated DR thymus was high speed sorted for mature T conv and used as control cells for the adoptive transfers. Sorted cells were then injected into nude host mice and monitored for autoimmunity (Figure 5.7 A). High purity was achieved after cell sorting (Figure 5.7 B).

Splenic tissue from nude mice was harvested at 4 weeks post transfer from both mice that either received control mature T conv or mature T conv thymocytes that were generated post BMT. FACs analysis shows the presence of the transferred cells at equal amounts in both mice categories (Figure 5.8 A, B). Interestingly and strikingly, analysis of the transferred cells revealed that a proportion of the transferred mature T conv thymocytes had been peripherally induced to become Tregs as Treg were not transferred at the time of the adoptive transfer (Figure 5.8 C). Interestingly numbers of the Foxp3$^-$ or Foxp3$^+$ T cells was consistent with no significant differences between both categories of mice (Figure 5.8 D).

A
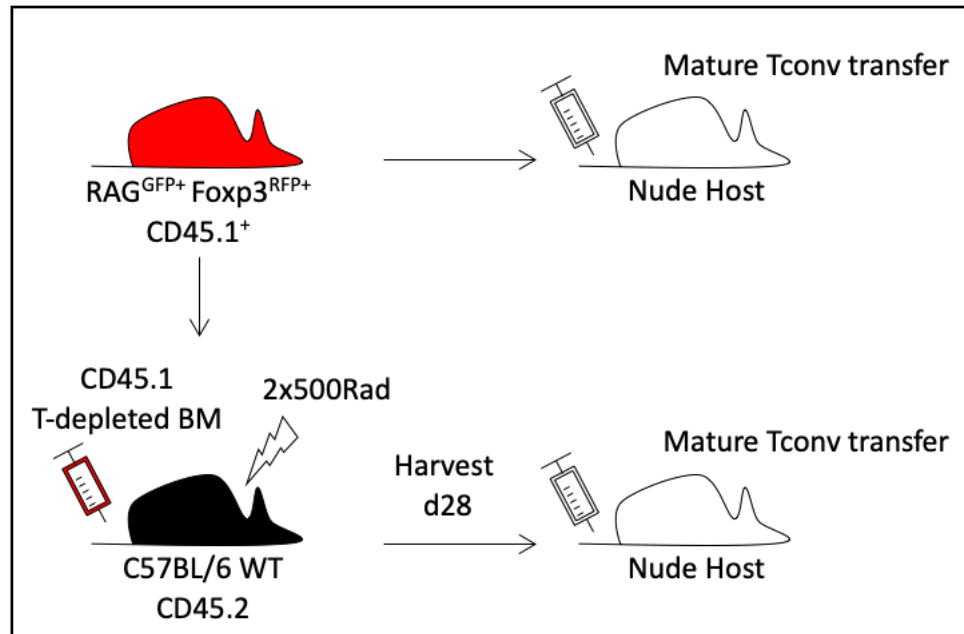
B
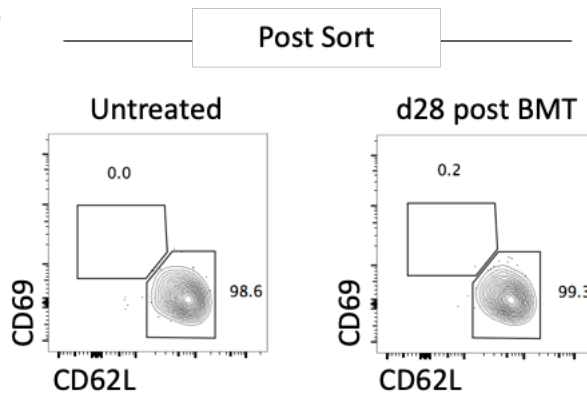
Figure 5.7. Analysis of Self-Tolerance Post BMT.

Mice were placed on Baytril for 1 week prior to use and were subjected to two dose of total body irradiation. A. Bone marrow, congenically marked (CD45.1), obtained from RAG2^{GFP} x Foxp3^{RFP} dual reporter mice was used for immune reconstitution. The thymus was then harvested at d28 post BMT and mechanically digested. Mature T conventional thymocytes were then high speed sorted and intravenously transferred to athymic hosts (nude). Control RAG2^{GFP} x Foxp3^{RFP} dual reporter thymus was also mechanically digested and high speed sorted and transferred into athymic hosts used as controls. B. FACs analysis showing CD69 and CD62L staining of the population that was transferred.
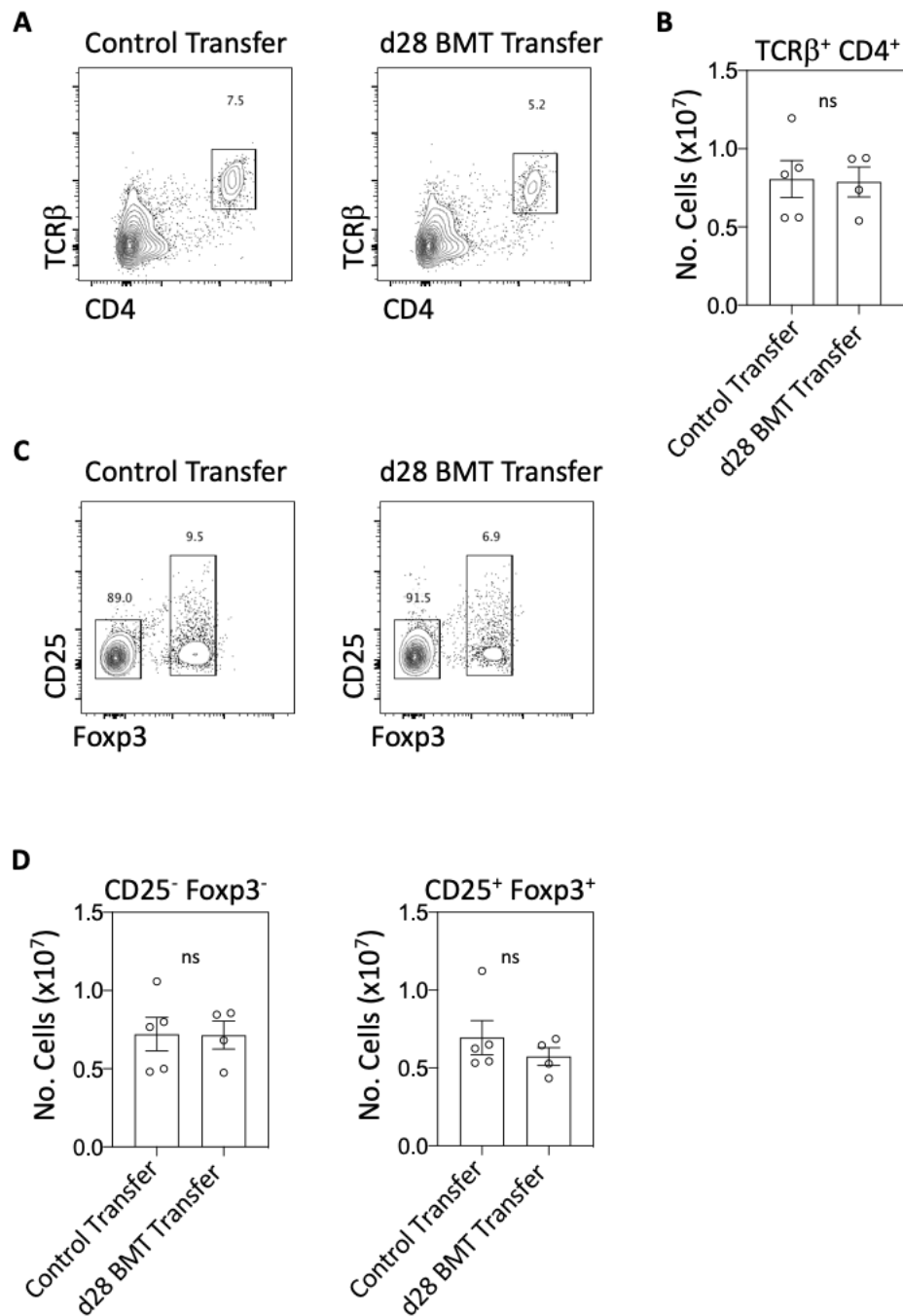
Figure 5.8. Identification of Transferred Cells in Nude Hosts.

Nude Mice received mature CD62L⁺ T conventional thymocytes via intravenous injection. Spleen tissue was harvested and mechanically digested for FACs analysis 4 weeks post transfer. A. Representative FACs plots of TCRβ and CD4 staining in nude hosts. B. Bar graph showing numerical quantification of total CD4⁺ T cells in spleen analysis. C. Representative FACs plots of CD25 and Foxp3 staining in nude hosts. D. Numerical quantification of Tconv and Treg in nude hosts after transfer. Each dot represents one mouse where n=4 for mice receiving BMT cells across two independent experiments and n=5 for mice receiving control cells across two independent experiments. Error bars represent SEM. Unpaired student t test was used for statistical analysis. The level of significance is as follows where non-significant (ns), p<.05 (*), p<.01 (**), p<.001 (***), and p<.0001 (****).

Alongside splenic analysis, blood was collected from the nude mice host via cardiac puncture for serum analysis. Serum was isolated and analysed for presence of autoantibodies. Composite tissue slides that incorporated different tissues (liver, kidney, and stomach) on one slide were used. Following staining, slides were imaged for presence of autoantibodies. It was clearly visualized that slides from mice that received cells from BMC had clear positive staining and the presence of autoantibodies. In contrast, positive staining was largely absent when sera from control mice was used alongside (Figure 5.9 A, B) with only one of the control mice showing any positive staining. Furthermore, that positive staining was only shown in 2 out of the 3 tissues. In contrast, mice that received cells from BMC all had positive staining in stomach and liver tissues. However, only 3 out of the 4 mice had positive staining in the kidney (Figure 5.9 C). Nevertheless, this data suggests that T cells from BMC may be generated where negative selection is compromised, which may then lead to self-reactive immune responses that result in autoantibody production.

To analyse this further, we checked peripheral tissues for the presence of cellular infiltrates. Liver tissue was harvested from nude mice post adoptive transfer and stained with H&E for infiltrate analysis. Whole tissue imaging was performed on the liver tissues and the cellular infiltrates were quantified. Liver tissue from mice that received control cells did not show the abundant presence of cellular infiltrates. In contrast, liver tissue from mice that received cells from BMC had clearly identifiable infiltrates (Figure 5.10 A, B). The number of infiltrates per cm^2 was counted and it was observed that mice receiving cells from BMC had significantly increased numbers of infiltrates (Figure 5.10 C). In sum, the above data shows compromised intrathymic tolerance mechanisms post BMT may mount to the accumulation of mature Tconv

thymocytes, and that, mature Tconv that were adoptively transferred from BMC mice results in symptoms of autoimmunity.
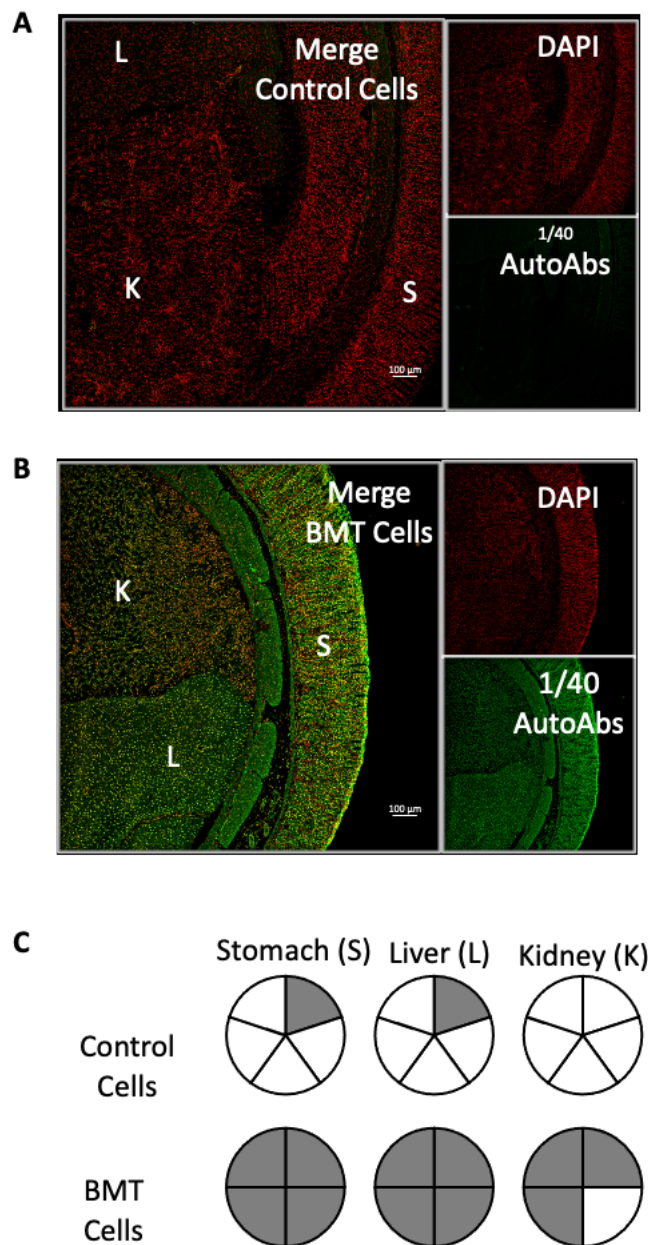
Figure 5.9. Altered Thymic Tolerance Following BMT In Mice Results in Peripheral Autoimmunity.

Nude Mice received mature CD62L$^+$ T conventional thymocytes via intravenous injection. Blood was collected for serum analysis via cardiac puncture 4 weeks post transfer. A. Serum analysis from mice receiving control cells on composite tissue slides. B. Serum analysis from mice receiving BMT cells on composite tissue slides. C. Pie chart identifying and comparing presence of autoantibodies in stomach, liver, and kidney tissues in mice that received either control or BMT cells. N=5 for mice that received control cells and n=4 for mice that received BMT cells across two independent experiments. Slides were left overnight to dry, and pictures were taken the following day. Staining was done alongside a negative and positive control. Staining was done alongside unmanipulated wildtype and unmanipulated nude mice. Staining was done alongside a secondary only control.
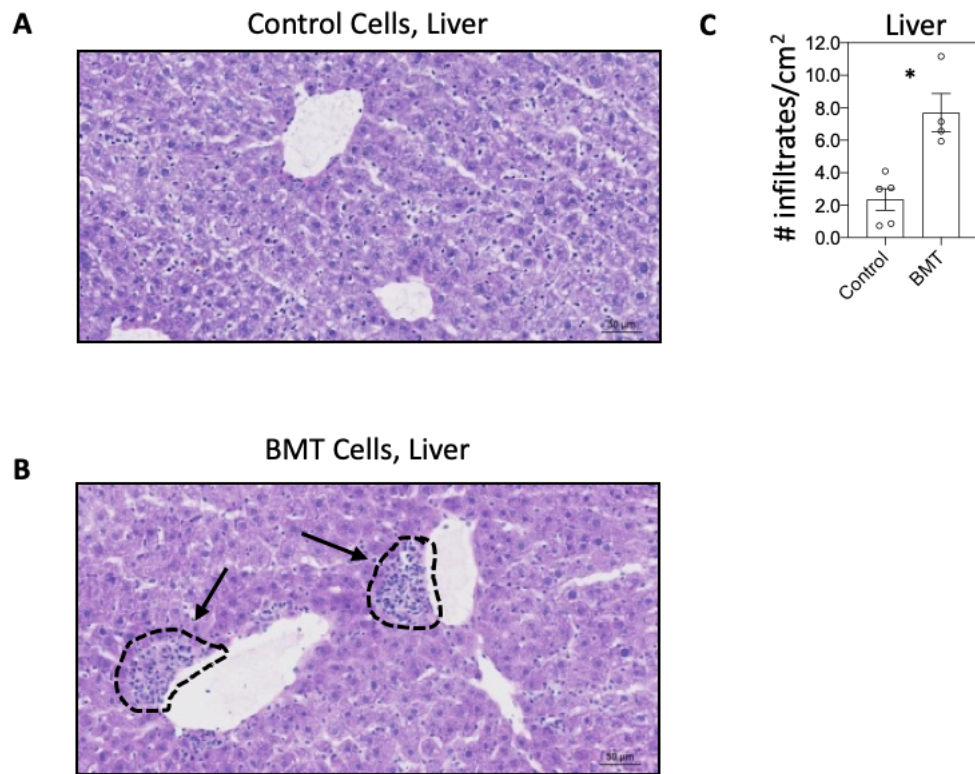
Figure 5.10. Cellular Infiltrates Found in Liver Tissue of Mice Receiving BMT Cells Post Transfer.

Nude Mice received mature CD62L^{+} T conventional thymocytes via intravenous injection. Liver tissue was harvested and frozen and cut for cellular infiltrate analysis 4 weeks post transfer. A. Liver sections from mice receiving control cells. B. Liver sections from mice receiving BMT cells. C. Bar graph comparing the number of infiltrates found in liver tissue of mice that either received control or BMT cells. N=5 for mice that received control cells and n=4 for mice that received BMT cells across two independent experiments. Livers were frozen and cut at 7μm thickness. Sections were approximately 35μm apart. For each mouse three slides were analysed. Each slide contained 3-4 sections. Whole tissue pictures were taken on slide scanner for cellular infiltrate counting.

5.3   Discussion

5.3.1   Imbalanced Restoration of Thymus Function Leads to Symptoms of Autoimmunity

The medullary region of the thymus during thymocyte development fosters a crucial educational step prior to thymocyte egress. Following positive selection in the cortex, newly produced $CD4^+$ and $CD8^+$ thymocytes reside in the medulla to undergo negative selection to ensure non-reactive thymocytes exit into the periphery. As discussed in section 3.3.2, specialized cells that include mTEC and DC localize within the medulla to facilitate antigen presentation and negative selection. Following mTEC and DC analysis, it was shown that post BMT, these cell types do not recover to normal levels through the time course analysis. Furthermore, analysis of thymocytes post BMT shows an accumulation of the mature $CD62L^+$ fraction of developing thymocytes, where proportions are significantly increased. This accumulation of $CD62L^+$ thymocytes was not a result of proliferation, as Ki67 expression was shown to be similar to SP thymocytes in control mice. In addition, when using Rag2GFP expression as molecular timer for newly developing thymocytes (Boursalian *et al.*, 2004), it was apparent that the accumulation in mature thymocytes was not due to increased dwell time in the thymus, as GFP levels were similar to the control. Altogether, our data highlights the rapid regeneration of thymocytes that leads to the intrathymic accumulation of mature SP thymocytes within medullary regions that are lacking specialized cells for the negative selection process.

Based on these observations, we hypothesized that following ablative therapy and immune reconstitution, the negative selection process is failing. To investigate this further, we generated a model to look at antigen-specific clonal deletion post BMT, using endogenous superantigen presentation in a non-TCR transgenic mouse model. Using BALB/c hosts and Kaede$^+$ BALB/c

donors, we generated bone marrow chimeras and investigated the deletion of Vβ⁺ bearing thymocytes. BALB/c mice express mouse mammary tumor virus (MMTV) genes that results in the effective intrathymic deletion of SP4 thymocytes expressing Vβ3, Vβ5 or Vβ11 (Moore *et al.*, 1994). However, post BMT it was apparent that the SP4 thymocytes bearing these 'self-reactive' TCRVβ chains were increased in their intrathymic frequency, and also present within peripheral tissues, suggesting an impairment in negative selection. During negative selection, Bim plays an important role in the apoptosis process as deletion of Bim deficiency resulted in failed deletion of autoreactive cells (Bouillet *et al.*, 2002; Stritesky *et al.*, 2013). Following activation of Bim, apoptosis is initiated through mitochondrial membrane destruction and release of cytochrome C which in turn leads to caspase activation resulting in cell death (Strasser, Cory and Adams, 2011). Flow cytometric analysis using antibodies to detect cleaved Caspase3 as a measure of clonal deletion, has been used previously to detect cells undergoing clonal deletion (Stritesky *et al.*, 2013; Breed, Watanabe and Hogquist, 2019). Using the same approach in mice that received BMT, we found a reduction in the proportion of SP thymocytes that were active Caspase 3⁺, indicating a decreased proportion of cells undergoing negative selection. This observation supports our hypothesis that developing Tconv are not undergoing appropriate negative selection and thus this may at least in part explain the increase in SP thymocytes post BMT.

Tolerance induction to newly developing thymocytes is critical to ensure immune tolerance. The process of negative selection, facilitated by mTEC and DC in the medulla region, ensures that thymocytes acquire tolerance to peripheral self-antigens to avoid development of autoimmune disease. Indeed, it has been shown that the CCR7-dependent migration of thymocytes from cortical to medullary regions establishes central tolerance (Kurobe *et al.*,

2006). Consequently, the failure of thymocytes in medulla localization resulted in peripheral autoimmune disease (Kurobe *et al.*, 2006). Further work has also been conducted to demonstrate that the lack of CCR7 results in autoimmune disease that included increase in autoantibodies in serum levels (Davalos-Misslitz *et al.*, 2007). Although these studies do not directly measure the negative selection impairment in the medulla, CCR7 is required for thymocyte migration from cortical to medullary regions (Ueno *et al.*, 2004), thus indirectly implicating that manifestations of autoimmune disease in CCR7 deficient mice are due to non-localization of thymocytes to the medulla for tolerance induction. Indeed, in a previous study and in a model of aGVHD using OT-II transgenic mice, the reduction in mTEC^hi resulted in decreased negative selection (Dertschnig *et al.*, 2015) as total thymic mOVA expression was reduced which resulted in escape of should be deleted cells. Furthermore, a study has shown that the lack of negative selection resulted in GVHD (Teshima *et al.*, 2003). Here it was suggested through a syngeneic BMT murine model that mice lacking MHCII on thymic epithelium had impaired negative selection. In addition, adoptive transfer of CD4^+ T cells isolated from chimeras that had impaired negative selection into sublethal irradiated hosts developed GVHD (Teshima *et al.*, 2003).

Importantly, our analysis indicates that failures in intrathymic tolerance occur after BMT, the functional consequences of which could include the development of autoimmune disease. To examine this, we performed experiments to analyse peripheral autoimmunity caused by T cells generated in BMT chimeras. After sorting Tconv SP4 thymocytes from BMC, we adoptively transferred these cells into athymic T cell deficient nude mice to assess whether the cells have been tolerized. Four weeks post transfer, and after the analysis of liver tissue, we identified cellular infiltrates from the mice that had received cells from the BMC. When liver cellular

infiltrates were quantified, it was shown that the mice receiving cells from BMC had increased numbers of cellular infiltrates/cm^2. Furthermore, serum analysis on composite tissue slides that included different sections of tissues on one slide revealed positive autoantibodies from the mice that had received cells from BMC.

Collectively, our data shows that post BMT, rapid Tconv regeneration results in accumulation of SP thymocytes at an early timepoint. Failure in negative selection analysis that included Caspase3 revealed that Tconv recovery is taking place in an environment that lacked tolerance mechanisms. Alongside the slow recovery in new Treg generation post BMT, our adoptive transfer experiments show that failures in negative selection may contribute to onset of peripheral autoimmunity as demonstrated by the presence of cellular infiltrates and positive autoantibody staining.

6   CHAPTER 6: GENERAL DISCUSSION

6.1   Thymus Vulnerability to Damage

Migratory T cell progenitors enter the thymus for the generation of a tolerant peripheral T cell pool. This process is achieved through thymocyte interactions with the thymic microenvironment to educate newly developing thymocytes. This process is critical as it ensures that self-reactive T cells do not form part of the peripheral T cell compartment through negative selection and Treg selection (Anderson *et al.*, 2002; Gavanescu *et al.*, 2007; Cowan *et al.*, 2013; Takaba *et al.*, 2015). However, the thymus is susceptible to damage that affects this process. Throughout life, the thymus is prone to age-related thymus involution that can restrict its function. Consequently, the inability to appropriately repopulate the T cell compartment with newly developed naïve T cells can lead to the loss of a diverse TCR repertoire, as well as increase in peripheral memory T cells (Rodewald, 1998), thus hindering the immune response.

Other forms of damage that can affect the thymus include acute or chronic damage such as infection or ablative therapy. Either form of damage can cause severe consequences on development of the new T cell pool. Under conditions where acute damage occurs, the thymus undergoes an endogenous regeneration process to develop new T cells (Dudakov *et al.*, 2012). In contrast, chronic damage causes the thymus to be dependent on donor colonization to produce the cells. This is achieved by adoptively transferring donor cells for reconstitution. Additionally, damage can occur in cases where patients are conditioned prior to transplant thus weaking their T cell immunity. In this case, the reconstitution of the peripheral T cell pool is mainly dependent on thymus function (Mackall *et al.*, 1995, 1996; Roux *et al.*, 2000). However, the reconstitution can be severely delayed as the ablative therapy treatment hinders the process of T cell development (Maury *et al.*, 2001).

6.2   Thymus Regeneration Post SLI

Sub-lethal irradiation (SLI) was used as a model to study the kinetics of thymus recovery following damage. Post SLI, the thymus is significantly reduced in size and is depleted mainly of DP thymocytes, thus proving this model is efficient. Additionally, the thymus undergoes a biphasic recovery, where the first phase involves recovery via an endogenous process. This process is aided by intrathymic radioresistant progenitor cell that is responsible for the first phase of recovery (Takada *et al.*, 1969; Penit and Ezine, 1989). However, a second drop in thymus cellularity is observed that could be explained by colonizing progenitors from the bone marrow. When investigating thymus recovery post SLI, initial outcomes appeared to show the thymus regenerated and recovered its functional capability. This was interpreted by recovery in DP thymocyte numbers as well as in investigating different functions of the thymus. For example, positive selection occurs in the cortical region and when this process was investigated further by the use of OT-1 transgenic mice, it was shown that this process was functioning effectively post SLI. Furthermore, the analysis of cTEC numbers also shows that this compartment is spared, and tissue sections show clearly identifiable cortical regions. Interestingly, tissue sections also showed medullary regions which suggests that post SLI thymic organization is intact. However, and in contrast to the cortex, the medulla appears to be severely affected as numbers of mTEC were significantly reduced (Figure 6.1). With this in mind, Treg selection was analysed as the medulla is required for Treg selection (Cowan *et al.*, 2013). It was apparent that this process is hindered, suggesting that different aspects of the thymic microenvironment do not recover similarly.

Medullary regions facilitate the negative selection process as APCs screen developing thymocytes for self-reactivity. This ensures that a tolerant T cell pool is generated. mTEC and the intrathymic DC compartment were analysed as they have been implicated in this process

(Anderson, Partington and Jenkinson, 1998; Baba, Nakamoto and Mukaida, 2009; Kroger, Wang and Tisch, 2016; Cosway *et al.*, 2017). Surprisingly, following SLI, these two populations did not recover while the thymus was rapidly generating Tconv thymocytes. This could be problematic as thymocytes post irradiation were developing in an environment lacking tolerizing accessory cells (Figure 6.1). The functional capability of the thymic medulla was then investigated through analysis of the deletion of self-antigen specific Vβ bearing thymocytes. The failure to delete MMTV-specific thymocytes post SLI provided evidence to support the notion that although the thymus appeared to recover in terms of its ability to support thymocyte development, functional aspects of the thymus have been severely impaired.

The block of thymocyte egress, through the use of FTY720, resulted in the accumulation of SP thymocytes in the thymus. The controlled increase in dwell time of developing thymocytes post SLI occurred alongside an increase of the TEC compartment. This could be related to increased crosstalk signals between thymocytes and the TEC suggesting that in early phases of recovery, it might prove beneficial to delay thymocyte egress to improve thymus function and to allow developing thymocytes to undergo proper negative selection. Further experiments are required to investigate whether thymocyte blockade that resulted in increased TEC compartment is beneficial to observe improved Treg selection as well as clonal deletion.
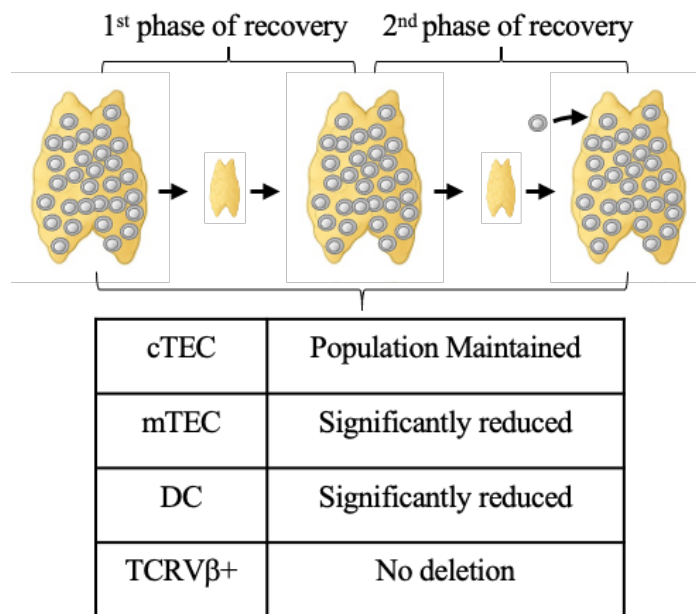
Figure 6.1. Endogenous Thymus Regeneration Post SLI.

Post SLI, the thymus recovers in a biphasic pattern that is initially dependent on intrathymic radioresistant progenitors that are responsible for the first phase of recovery. The second phase of recovery depends on progenitor colonization of the thymus. Differential analysis of thymic epithelium shows that following SLI, cTEC are relatively maintained and able to support positive selection. In contrast, medulla functions are impaired with reduced Treg selection and failure to delete self-antigen specific thymocytes.

6.3 Thymus Regeneration Post BMT

BMT is widely used to establish the immune system and the peripheral T cell compartment post ablative therapy. Mouse models have been exploited to investigate this process and understand the kinetics of immune recovery post ablative therapy. In our BMT model, and in contrast to SLI, thymus recovery was analysed post lethal irradiation and BMT. In this model, thymus regeneration is dependent on donor progenitor colonization to produce new cohorts of T cells. Furthermore, this model allows us to monitor T cell development as well as the peripheral T cell compartment that is generated from donor cells that can be clearly identified through use of congenic markers. Although the thymus is significantly depleted of host cells post lethal irradiation, a small population of SP thymocytes of host origin appear to be radioresistant. However, donor colonization occurs very rapidly with donor SP thymocyte recovery seen as early as d21 post BMT. Interestingly, even after a high dose of irradiation thymus organization is visualized by immunofluorescence suggesting that cortical/medullary organization is spared. However, further investigation into these two compartments revealed that mTEC are highly radiosensitive and are significantly reduced throughout the time course. This has severe effects on medulla function as kinetics of Treg recovery appeared to be slower than Tconv. cTEC on the other hand were found to be constant. The reasons for this differential effect on cTEC/mTEC recovery is not clear. One possibility is that cTEC and mTEC in the adult thymus are maintained and regenerated in different ways, for example by the presence of lineage-specific progenitors, or the expansion of existing lineage-specific mature cells. Further examination is required to determine why cTEC/mTEC recovery is differential.

Following BMT, the peripheral T cell compartment was depleted and required intact thymus function for re-establishment (Figure 6.2). Although the thymus was rapidly generating Tconv by d21, peripheral T cells of donor origin were initially observed at significantly small numbers.

As expected, because Treg selection was reduced in the thymus, peripheral Treg were also reduced. However, numbers of Treg began to rise and this can be attributed to increased proliferation rather than thymic output. Interestingly, peripheral iNKT cells were also reduced which correlates with defects in medulla function to maintain this population (Cowan *et al.*, 2014; White *et al.*, 2014; Lucas *et al.*, 2020) It will be beneficial to investigate this further and determine the localization of thymic iNKT post BMT as iNKT development can be used to measure thymic medulla function.

Similar to what has been observed post SLI, both the mTEC and DC compartments were significantly reduced post BMT. Analysis of clonal deletion revealed that fewer thymocytes were undergoing negative selection, which could be caused by the presence of fewer mTEC and DC. Functional consequences of failed negative selection were revealed by signs of peripheral autoimmunity in nude mice receiving thymocytes generated in BMT mice. As seen with SLI, blockade of thymocyte egress using FTY720 resulted in an increased mTEC population. It could be beneficial to administer FTY720 post BMT to delay thymocyte egress and also investigate whether this also increases the mTEC compartment. Additionally, as mTEC are implicated in DC medulla localization (Lei *et al.*, 2011) it would be interesting to analyse whether the increase in the mTEC compartment enhances the intrathymic DC compartment. Ultimately it would be interesting to determine whether short-term FTY720 treatment may restore the ability of the thymus to support effective intrathymic tolerance mechanisms and reduce the frequency of autoreactive thymocytes that are released post BMT.
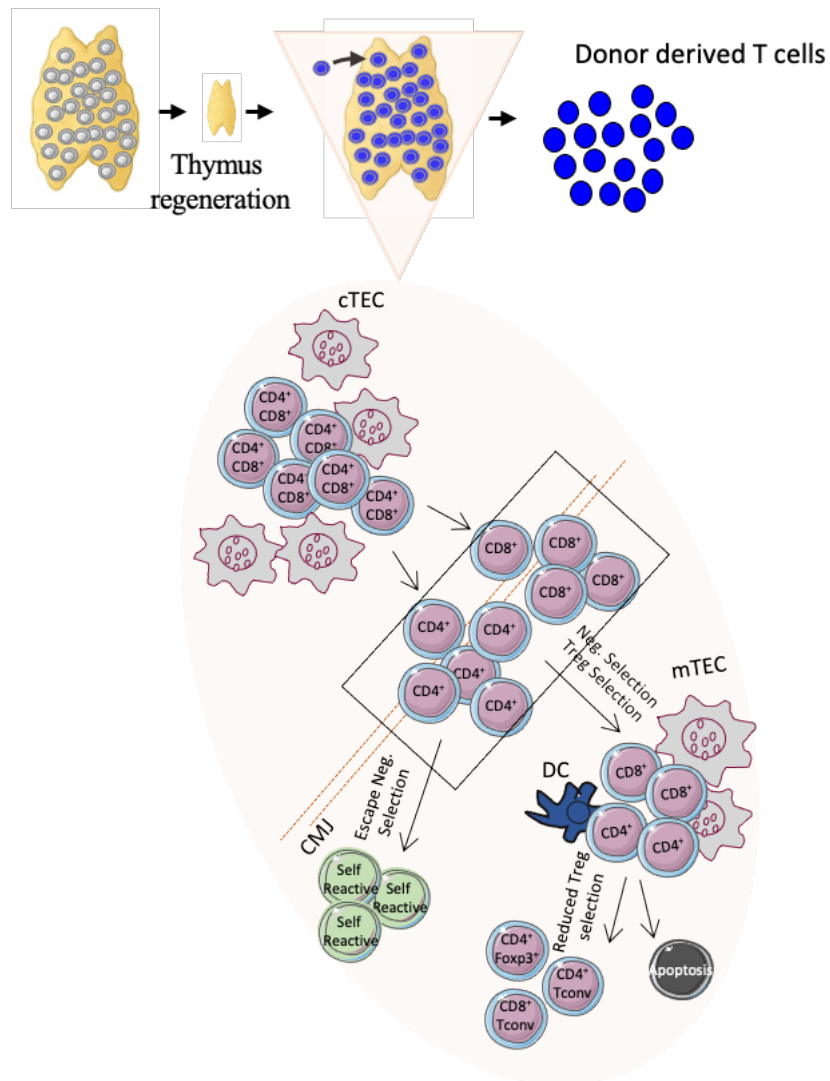
Figure 6.2. Thymus Recovery Post BMT.

Following BMT, thymus recovery is dependent on donor progenitor colonization. Following differential analysis, the cTEC compartment is maintained and able to support thymocyte development, including positive selection. In contrast, in the medulla, both mTEC and DC show impaired recovery. Consequently, Treg selection is reduced and negative selection is impaired. Following impaired intrathymic tolerance, self-reactive Tconv escape into the periphery and result in signs of peripheral autoimmunity.

6.4   Future Work

Both SLI and lethal irradiation have detrimental effects on the thymic microenvironment and its ability to properly repopulate the T cell compartment. The defect in recovery of the thymic epithelium and DC compartment after both acute and chronic thymic damage has resulted in imbalance in T cell reconstitution. As such further examinations are required to improve thymic recovery post damage for therapeutic benefit. Previous studies have shown that alterations to Foxn1 expressions can have a significant impact on thymus involution (Chen, Xiao and Manley, 2009; Zook *et al.*, 2011; Bredenkamp, Nowell and Blackburn, 2014). Furthermore, thymus regeneration mechanisms have been investigated and it has been suggested that thymus regeneration is aided by IL-22 (Dudakov *et al.*, 2012) thus highlighting IL-22 as a potential treatment to improve thymus recovery. Additionally, KGF has been shown to have great potential to improve thymus recovery. Studies that have investigated KGF treatment post BMT also show improved TEC compartment (Min *et al.*, 2002; Rossi *et al.*, 2002; Kelly *et al.*, 2010), which could be beneficial due to the failure in negative selection observed post damage. Collectively, these studies highlight important therapeutic mechanisms that can lead to restore proper thymus function post damage (Figure 6.3). Based on the findings of this thesis, the experiments summarized below would be interesting to further examine thymus function post damage, and how this process might be manipulated.

- Administration of FTY720 post SLI was shown to enhance the mTEC compartment. However, future work is needed to understand whether this treatment can be beneficial to improve the negative selection failure. FTY720 administration post BMT would allow for increased crosstalk signals as well as increased time in the thymus for developing thymocytes to undergo clonal deletion to ensure that self-tolerant T cells are exiting into the periphery (Figure 6.3).

- The failure in negative selection could be explained by the decrease in the TEC and DC compartment. Studies have highlighted the positive effect of KGF administration, and as such it will be interesting to see if KGF treatment improves the mTEC compartment and rescues the negative selection failure (Figure 6.3). Also, if the mTEC compartment is improved, it will be interesting to investigate whether Treg selection and thymic iNKT development is improved.

- The failure of iNKT cell development post BMT is of interest, as it correlates with a reduction in mTEC. As different subsets of iNKT cells (NKT1, NKT2 and NKT17) are controlled by multiple mTEC subsets including tuft cells and $CCL21^+$ $mTEC^{lo}$ (Lucas *et al.*, 2020) it would be interesting to extend analysis of the recovery of the mTEC compartment to study these mTEC subsets.

- Studies have implicated mTEC in DC medulla localization (Lei *et al.*, 2011), via production of the chemokine XCL1. Currently DC localization has not been analysed in this thesis post BMT. It would thus be interesting to determine whether thymic DC are appropriately located in the medulla post BMT, and if this correlates with appropriate levels of XCL1 expression by mTEC.
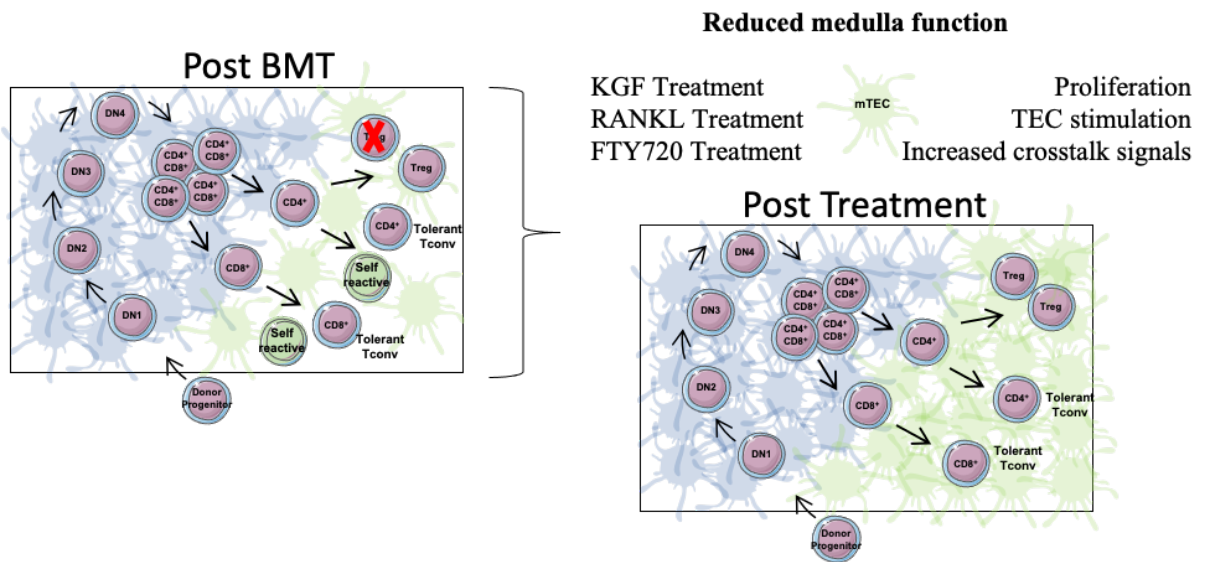
Figure 6.3. Treatment to Improve TEC Recovery.

Following lethal irradiation and BMT, the cTEC population was relatively maintained and able to support thymocyte development. In contrast, the mTEC population sustained a significant reduction. Consequently, key medulla functions were impaired. Studies have utilised treatment regimens to improve TEC recovery following damage. Using KGF and RANKL to target the thymic epithelium as a means of therapeutic treatment could prove beneficial to boost thymic function. Following SLI, treatment of FTY720 to block thymocyte egress resulted in increased TEC numbers. FTY720 treatment post BMT, to increase crosstalk, could prove beneficial to increase TEC numbers and improve medulla function.

In summary, previous work has shown that the thymic microenvironment plays a pivotal role to ensure the education of the developing thymocytes. Post thymic damage, it was shown that Tconv recovery in thymus was achieved early in comparison to Treg generation. Alongside this differential recovery of Tconv and Treg, these processes were occurring under conditions where the presence of tolerising accessory cells (mTEC and DC) were diminished, which correlates with escape from negative selection and resulted in signs of peripheral autoimmunity. Thus, while the primary concern after thymic damage is to rapidly generate new T cells, it may actually prove beneficial to delay this process to ensure all aspects of thymus function are operating in an appropriate manner. Finally, it will be important to investigate further the mechanisms that result in the differential recovery of cTEC and mTEC after damage. By identifying approaches to enhance mTEC recovery, it is anticipated that recovery of medulla function could be restored to ensure effective intrathymic tolerance mechanisms are in place to avoid autoimmunity.

7 **REFERENCES**

<div align="center">**List of References**</div>

Akiyama, T. *et al.* (2008) 'The Tumor Necrosis Factor Family Receptors RANK and CD40 Cooperatively Establish the Thymic Medullary Microenvironment and Self-Tolerance', *Immunity*, 29(3), pp. 423–437. doi: 10.1016/j.immuni.2008.06.015.

Allende, M. L. *et al.* (2004) 'Expression of the Sphingosine 1-Phosphate Receptor, S1P1, on T-cells Controls Thymic Emigration', *Journal of Biological Chemistry*, 279(15), pp. 15396–15401. doi: 10.1074/jbc.M314291200.

Allman, D. *et al.* (2003) 'Thymopoiesis independent of common lymphoid progenitors', *Nature Immunology*, 4(2), pp. 168–174. doi: 10.1038/ni878.

Alves, N. L. *et al.* (2009) 'Characterization of the thymic IL-7 niche in vivo', *Proceedings of the National Academy of Sciences of the United States of America*, 106(5), pp. 1512–1517. doi: 10.1073/pnas.0809559106.

Alves, N. L. *et al.* (2014) 'Serial progression of cortical and medullary thymic epithelial microenvironments', *European Journal of Immunology*, 44(1), pp. 16–22. doi: 10.1002/eji.201344110.

Anderson, G., Partington, K. M. and Jenkinson, E. J. (1998) 'Differential effects of peptide diversity and stromal cell type in positive and negative selection in the thymus.', *Journal of immunology (Baltimore, Md. : 1950)*, 161(12), pp. 6599–603. Available at: http://www.ncbi.nlm.nih.gov/pubmed/9862687.

Anderson, M. S. *et al.* (2002) 'Projection of an immunological self shadow within the thymus by the aire protein', *Science*, 298(5597), pp. 1395–1401. doi: 10.1126/science.1075958.

Aw, D. *et al.* (2008) 'Architectural changes in the thymus of aging mice', *Aging Cell*, 7(2), pp. 158–167. doi: 10.1111/j.1474-9726.2007.00365.x.

Baba, T., Nakamoto, Y. and Mukaida, N. (2009) ' Crucial Contribution of Thymic Sirpα + Conventional Dendritic Cells to Central Tolerance against Blood-Borne Antigens in a CCR2-Dependent Manner ', *The Journal of Immunology*, 183(5), pp. 3053–3063. doi: 10.4049/jimmunol.0900438.

Baik, S. *et al.* (2013) 'Generation of both cortical and Aire+ medullary thymic epithelial compartments from CD205+ progenitors', *European Journal of Immunology*, 43(3), pp. 589–594. doi: 10.1002/eji.201243209.

Baik, S. *et al.* (2016) 'Relb acts downstream of medullary thymic epithelial stem cells and is essential for the emergence of RANK+ medullary epithelial progenitors', *European Journal of Immunology*, 46(4), pp. 857–862. doi: 10.1002/eji.201546253.

Balciunaite, G. *et al.* (2002) 'Wnt glycoproteins regulate the expression of FoxNI, the genes defective in nude mice', *Nature Immunology*, 3(11), pp. 1102–1108. doi: 10.1038/ni850.

Balciunaite, G. *et al.* (2005) 'The role of Notch and IL-7 signaling in early thymocyte proliferation and differentiation', *European Journal of Immunology*, 35(4), pp. 1292–1300. doi: 10.1002/eji.200425822.

Bannard, O., Kraman, M. and Fearon, D. T. (2009) 'Secondary Replicative Function of CD8<sup>+</sup> T Cells That Had Developed an Effector Phenotype', *Science*, 323(5913), pp. 505 LP – 509. doi: 10.1126/science.1166831.

Barnett, A. *et al.* (1999) 'Expression of Mouse Mammary Tumor Virus Superantigen mRNA in the Thymus Correlates with Kinetics of Self-Reactive T-Cell Loss', 73(8), pp. 6634–6645.

Beijleveld, L. J. J., Damoiseaux, J. G. M. C. and Van Breda Vriesman, P. J. C. (1995) 'Differential Effects of X-Irradiation and Cyclosporin-A Administration on the Thymus with Respect to the Generation of Cyclosporin-A-Induced Autoimmunity', *Developmental Immunology*, 4(2), pp. 127–138. doi: 10.1155/1995/18495.

Bendelac, A. (1995) 'Positive selection of mouse NK1+ T cells by CD1-expressing cortical thymocytes', *Journal of Experimental Medicine*, 182(6), pp. 2091–2096. doi: 10.1084/jem.182.6.2091.

Bennett, A. R. *et al.* (2002) 'Identification and characterization of thymic epithelial progenitor cells', *Immunity*, 16(6), pp. 803–814. doi: 10.1016/S1074-7613(02)00321-7.

Benz, C. *et al.* (2008) 'The stream of precursors that colonizes the thymus proceeds selectively through the early T lineage precursor stage of T cell development', *Journal of Experimental Medicine*, 205(5), pp. 1187–1199. doi: 10.1084/jem.20072168.

Bhandoola, A. and Sambandam, A. (2006) 'From stem cell to T cell: One route or many?', *Nature Reviews Immunology*, 6(2), pp. 117–126. doi: 10.1038/nri1778.

Blackburn, C. C. *et al.* (1996) 'The nu gene acts cell-autonomously and is required for differentiation of thymic epithelial progenitors', *Proceedings of the National Academy of Sciences of the United States of America*, 93(12), pp. 5742–5746. doi: 10.1073/pnas.93.12.5742.

Blackburn, C. C. and Manley, N. R. (2004) 'Developing a new paradigm for thymus organogenesis', *Nature Reviews Immunology*, 4(4), pp. 278–289. doi: 10.1038/nri1331.

Bleul, C. C. *et al.* (2006) 'Formation of a functional thymus initiated by a postnatal epithelial progenitor cell', *Nature*, 441(7096), pp. 992–996. doi: 10.1038/nature04850.

Boehm, T., Scheu, S., Pfeffer, K. and Bleul, Conrad C. (2003) 'Thymic medullary epithelial cell differentiation, thymocyte emigration, and the control of autoimmunity require lympho-epithelial cross talk via LTβR', *Journal of Experimental Medicine*, 198(5), pp. 757–769. doi: 10.1084/jem.20030794.

Boehm, T., Scheu, S., Pfeffer, K. and Bleul, Conrad C (2003) 'Thymic Medullary Epithelial Cell Differentiation, Thymocyte Emigration, and the Control of Autoimmunity Require

Lympho–Epithelial Cross Talk via LTβR ', *Journal of Experimental Medicine*, 198(5), pp. 757–769. doi: 10.1084/jem.20030794.

Bolotin, E. *et al.* (1996) 'Enhancement of thymopoiesis after bone marrow transplant by in vivo interleukin-7', *Blood*, 88(5), p. 1887—1894. Available at: http://europepmc.org/abstract/MED/8781449.

Bonasio, R., Scimone, M. Lucila, *et al.* (2006) 'Clonal deletion of thymocytes by circulating dendritic cells homing to the thymus', *Nature Immunology*, 7(10), pp. 1092–1100. doi: 10.1038/ni1385.

Bornstein, C. *et al.* (2018) 'Single-cell mapping of the thymic stroma identifies IL-25-producing tuft epithelial cells', *Nature*, 559(7715), pp. 622–626. doi: 10.1038/s41586-018-0346-1.

Bosco, N. *et al.* (2010) 'Auto-reconstitution of the T-cell compartment by radioresistant hematopoietic cells following lethal irradiation and bone marrow transplantation', *Experimental Hematology*, 38(3), pp. 222–232. doi: 10.1016/j.exphem.2009.12.006.

Bouillet, P. *et al.* (2002) 'BH3-only Bcl-2 family member Bim is required for apoptosis of autoreactive thymocytes', *Nature*, 415(6874), pp. 922–926. doi: 10.1038/415922a.

Bourke, A. P. (1964) '© 1964 Nature Publishing Group', *Nature*, 201, pp. 1212–1213. doi: 10.1038/201834a0.

Boursalian, T. E. *et al.* (2004) 'Continued maturation of thymic emigrants in the periphery', *Nature Immunology*, 5(4), pp. 418–425. doi: 10.1038/ni1049.

Bousso, P. *et al.* (2002) 'Dynamics of thymocyte-stromal cell interactions visualized by two-photon microscopy', *Science*, 296(5574), pp. 1876–1880. doi: 10.1126/science.1070945.

Brandle, D. *et al.* (1992) 'Engagement of the T-cell receptor during positive selection in the thymus down-regulates RAG-1 expression', *Proceedings of the National Academy of Sciences of the United States of America*, 89(20), pp. 9529–9533. doi: 10.1073/pnas.89.20.9529.

Bredenkamp, N., Nowell, C. S. and Clare Blackburn, C. (2014) 'Regeneration of the aged thymus by a single transcription factor', *Development (Cambridge)*, 141(8), pp. 1627–1637. doi: 10.1242/dev.103614.

Breed, E. R., Watanabe, M. and Hogquist, K. A. (2019) 'Measuring Thymic Clonal Deletion at the Population Level', *The Journal of Immunology*, 202(11), pp. 3226–3233. doi: 10.4049/jimmunol.1900191.

Brinkmann, V. *et al.* (2002) 'The immune modulator FTY720 targets sphingosine 1-phosphate receptors', *Journal of Biological Chemistry*, 277(24), pp. 21453–21457. doi: 10.1074/jbc.C200176200.

Burkly, L. *et al.* (1995) 'Expression of relB is required for the development of thymic medulla and dendritic cells', *Nature*, 373(6514), pp. 531–536. doi: 10.1038/373531a0.

Calderón, L. and Boehm, T. (2011) 'Three chemokine receptors cooperatively regulate homing of hematopoietic progenitors to the embryonic mouse thymus', *Proceedings of the National Academy of Sciences*, 108(18), pp. 7517 LP – 7522. doi: 10.1073/pnas.1016428108.

Ceredig, R. and Macdonald, H. R. (1982) 'Phenotypic and functional properties of murine thymocytes . II . Quantitation of host- and donor-derived cytolytic T lymphocyte precursors in regenerating radiation bone marrow chimeras . *The Journal of Immunology*, 128(2), pp. 614–620.

Chen, L., Xiao, S. and Manley, N. R. (2009) 'Foxn1 is required to maintain the postnatal thymic microenvironment in a dosage-sensitive manner', *Blood*, 113(3), pp. 567–574. doi: 10.1182/blood-2008-05-156265.

Chen, W. J. *et al.* (2003) 'Conversion of Peripheral CD4+CD25- Naive T Cells to CD4+CD25+ Regulatory T Cells by TGF-β Induction of Transcription Factor Foxp3', *Journal of Experimental Medicine*, 198(12), pp. 1875–1886. doi: 10.1084/jem.20030152.

Cosway, Emilie J. *et al.* (2017) 'Redefining thymus medulla specialization for central tolerance', *Journal of Experimental Medicine*, 214(11), pp. 3183–3195. doi: 10.1084/jem.20171000.

Cosway, E. J. *et al.* (2018) ' Formation of the Intrathymic Dendritic Cell Pool Requires CCL21-Mediated Recruitment of CCR7 + Progenitors to the Thymus ', *The Journal of Immunology*, 201(2), pp. 516–523. doi: 10.4049/jimmunol.1800348.

Cowan, J. E. *et al.* (2013) 'The thymic medulla is required for Foxp3 [+] regulatory but not conventional CD4 [+] thymocyte development', *The Journal of Experimental Medicine*, 210(4), pp. 675–681. doi: 10.1084/jem.20122070.

Cowan, J. E. *et al.* (2014) 'Differential Requirement for CCR4 and CCR7 during the Development of Innate and Adaptive αβT Cells in the Adult Thymus', *The Journal of Immunology*, 193(3), pp. 1204–1212. doi: 10.4049/jimmunol.1400993.

Cowan, J. E. *et al.* (2019) 'Myc controls a distinct transcriptional program in fetal thymic epithelial cells that determines thymus growth', *Nature Communications*. Springer US, 10(1), pp. 1–14. doi: 10.1038/s41467-019-13465-y.

Davalos-Misslitz, A. C. M. *et al.* (2007) 'Generalized multi-organ autoimmunity in CCR7-deficient mice', *European Journal of Immunology*, 37(3), pp. 613–622. doi: 10.1002/eji.200636656.

Derbinski, J. *et al.* (2001) 'Promiscuous gene expression in medullary thymic epithelial cells mirrors the peripheral self', *Nature Immunology*, 2(11), pp. 1032–1039. doi: 10.1038/ni723.

Dertschnig, S. *et al.* (2015) 'Impaired thymic expression of tissue-restricted antigens licenses

the de novo generation of autoreactive CD4+ T cells in acute GVHD', *Blood*, 125(17), pp. 2720–2723. doi: 10.1182/blood-2014-08-597245.

Desanti, G. E. *et al.* (2012) 'Developmentally Regulated Availability of RANKL and CD40 Ligand Reveals Distinct Mechanisms of Fetal and Adult Cross-Talk in the Thymus Medulla', *The Journal of Immunology*, 189(12), pp. 5519–5526. doi: 10.4049/jimmunol.1201815.

Dudakov, Jarrod A. *et al.* (2012) 'Interleukin-22 drives endogenous thymic regeneration in mice', *Science*, 335(6077), pp. 91–95. doi: 10.1126/science.1218004.

Dudley, E. C. *et al.* (1994) 'T cell receptor β chain gene rearrangement and selection during thymocyte development in adult mice', *Immunity*, 1(2), pp. 83–93. doi: 10.1016/1074-7613(94)90102-3.

Dzhagalov, I. and Phee, H. (2012) 'How to find your way through the thymus: a practical guide for aspiring T cells', *Cellular and Molecular Life Sciences*, 69(5), pp. 663–682. doi: 10.1007/s00018-011-0791-6.

Falk, I. *et al.* (2001) 'Immature thymocytes that fail to express TCRβ and/or TCRγδ proteins die by apoptotic cell death in the CD44-CD25- (DN4) subset', *European Journal of Immunology*, 31(11), pp. 3308–3317. doi: 10.1002/1521-4141(200111)31:11<3308::AID-IMMU3308>3.0.CO;2-5.

Fehling, H. J. *et al.* (1995) 'Crucial role of the pre-T-cell receptor Ŏ gene in development of ap but not ŎŎ T cells', *Nature*, pp. 795–798. doi: 10.1038/375795a0.

Fiorini, E. *et al.* (2008) 'Cutting Edge: Thymic Crosstalk Regulates Delta-Like 4 Expression on Cortical Epithelial Cells', *The Journal of Immunology*, 181(12), pp. 8199–8203. doi: 10.4049/jimmunol.181.12.8199.

Gapin, L. *et al.* (2001) 'NKT cells derive from double-positive thymocytes that are positively selected by CD1d', *Nature Immunology*, 2(10), pp. 971–978. doi: 10.1038/ni710.

Gavanescu, I. *et al.* (2007) 'Loss of Aire-dependent thymic expression of a peripheral tissue antigen renders it a target of autoimmunity', *Proceedings of the National Academy of Sciences of the United States of America*, 104(11), pp. 4583–4587. doi: 10.1073/pnas.0700259104.

Gill, J. *et al.* (2002) 'Generation of a complete thymic microenvironment by MTS24+ thymic epithelial cells', *Nature Immunology*, 3(7), pp. 635–642. doi: 10.1038/ni812.

Godfraind, C., Holmes, K. V and Coutelier, J. P. (1995) 'Thymus involution induced by mouse hepatitis virus A59 in BALB/c mice.', *Journal of virology*, 69(10), pp. 6541–6547. doi: 10.1128/jvi.69.10.6541-6547.1995.

Gordon, J. *et al.* (2001) 'Gcm2 and Foxn1 mark early parathyroid- and thymus-specific domains in the developing third pharyngeal pouch', *Mechanisms of Development*, 103(1–2), pp. 141–143. doi: 10.1016/S0925-4773(01)00333-1.

Gray, D. H. D. *et al.* (2006) 'Developmental kinetics, turnover, and stimulatory capacity of thymic epithelial cells', *Blood*, 108(12), pp. 3777–3785. doi: 10.1182/blood-2006-02-004531.

Gray, D. H. D. *et al.* (2012) 'The BH3-Only Proteins Bim and Puma Cooperate to Impose Deletional Tolerance of Organ-Specific Antigens', *Immunity*. Elsevier Inc., 37(3), pp. 451–462. doi: 10.1016/j.immuni.2012.05.030.

Griffith, A. V. *et al.* (2012) 'Persistent degenerative changes in thymic organ function revealed by an inducible model of organ regrowth', *Aging Cell*, 11(1), pp. 169–177. doi: 10.1111/j.1474-9726.2011.00773.x.

Gui, J. *et al.* (2007) 'The aged thymus shows normal recruitment of lymphohematopoietic progenitors but has defects in thymic epithelial cells', *International Immunology*, 19(10), pp. 1201–1211. doi: 10.1093/intimm/dxm095.

Hadeiba, H. *et al.* (2012) 'Plasmacytoid Dendritic Cells Transport Peripheral Antigens to the Thymus to Promote Central Tolerance', *Immunity*. Elsevier Inc., 36(3), pp. 438–450. doi: 10.1016/j.immuni.2012.01.017.

Hale, J. S. *et al.* (2006) 'Thymic output in aged mice', *Proceedings of the National Academy of Sciences of the United States of America*, 103(22), pp. 8447–8452. doi: 10.1073/pnas.0601040103.

Hamazaki, Y. *et al.* (2007) 'Medullary thymic epithelial cells expressing Aire represent a unique lineage derived from cells expressing claudin', *Nature Immunology*, 8(3), pp. 304–311. doi: 10.1038/ni1438.

Herbin, O. *et al.* (2016) 'Medullary thymic epithelial cells and CD8α+ dendritic cells coordinately regulate central tolerance but CD8α+ cells are dispensable for thymic regulatory T cell production', *Journal of Autoimmunity*. Elsevier Ltd, 75, pp. 141–149. doi: 10.1016/j.jaut.2016.08.002.

Hetzer-Egger, C. *et al.* (2002) 'Thymopoiesis requires Pax9 function in thymic epithelial cells', *European Journal of Immunology*, 32(4), pp. 1175–1181. doi: 10.1002/1521-4141(200204)32:4<1175::AID-IMMU1175>3.0.CO;2-U.

Hikosaka, Y. *et al.* (2008) 'The Cytokine RANKL Produced by Positively Selected Thymocytes Fosters Medullary Thymic Epithelial Cells that Express Autoimmune Regulator', *Immunity*, 29(3), pp. 438–450. doi: 10.1016/j.immuni.2008.06.018.

Honey, K. *et al.* (2002) 'Cathepsin L regulates CD4+ T cell selection independently of its effect on invariant chain: A role in the generation of positively selecting peptide ligands', *Journal of Experimental Medicine*, 195(10), pp. 1349–1358. doi: 10.1084/jem.20011904.

Hu, Z. *et al.* (2017) 'CCR7 Modulates the Generation of Thymic Regulatory T Cells by Altering the Composition of the Thymic Dendritic Cell Compartment', *Cell Reports*, 21(1), pp. 168–180. doi: 10.1016/j.celrep.2017.09.016.

Irla, M. *et al.* (2008) 'Autoantigen-Specific Interactions with CD4+ Thymocytes Control Mature Medullary Thymic Epithelial Cell Cellularity', *Immunity*, 29(3), pp. 451–463. doi: 10.1016/j.immuni.2008.08.007.

James, K. D. *et al.* (2018) 'Endothelial cells act as gatekeepers for LTβRdependent thymocyte emigration', *Journal of Experimental Medicine*, 215(12), pp. 2984–2993. doi: 10.1084/jem.20181345.

Janas, M. L. *et al.* (2010) 'Thymic development beyond β-selection requires phosphatidylinositol 3-kinase activation by CXCR4', *Journal of Experimental Medicine*, 207(1), pp. 247–261. doi: 10.1084/jem.20091430.

Jenkinson, E. J., Kingston, R. and Owen, J. J. T. (1987) 'Importance of IL-2 receptors in intra-thymic generation of cells expressing T-cell receptors', *Nature*, 329(6135), pp. 160–162. doi: 10.1038/329160a0.

Kadish, J. L. and Basch, R. S. (1975) 'Thymic Regeneration after Lethal Irradiation : Evidence for an Intra-Thymic Radioresistant T Cell Precursor Information about subscribing to The Journal of Immunology is online at : THYMIC REGENERATION AFTER LETHAL IRRADIATION : E V I D E N C E FOR A N I', *The Journal of Immunology*, 114, pp. 452–458.

Kelly, R. M. *et al.* (2010a) 'Short-term inhibition of p53 combined with keratinocyte growth factor improves thymic epithelial cell recovery and enhances T-cell reconstitution after murine bone marrow transplantation', *Blood*, 115(5), pp. 1088–1097. doi: 10.1182/blood-2009-05-223198.

Klaus, G. G. B. (1981) 'The effects of cyclosporin A on the immune system', *Immunology Today*, 2(5), pp. 83–87. doi: 10.1016/0167-5699(81)90037-2.

Klein, L. *et al.* (2014) 'Positive and negative selection of the T cell repertoire: What thymocytes see (and don't see)', *Nature Reviews Immunology*. Nature Publishing Group, 14(6), pp. 377–391. doi: 10.1038/nri3667.

Koch, U. *et al.* (2008) 'Delta-like 4 is the essential, nonredundant ligand for Notchl during thymic T cell lineage commitment', *Journal of Experimental Medicine*, 205(11), pp. 2515–2523. doi: 10.1084/jem.20080829.

Kozai, M. *et al.* (2017) 'Essential role of CCL21 in establishment of central self- tolerance in T cells', *Journal of Experimental Medicine*, 214(7), pp. 1925–1935. doi: 10.1084/jem.20161864.

Kroger, C. J., Wang, B. and Tisch, R. (2016) 'Temporal increase in thymocyte negative selection parallels enhanced thymic SIRPα+ DC function', *European Journal of Immunology*, 46(10), pp. 2352–2362. doi: 10.1002/eji.201646354.

Kurobe, H. *et al.* (2006) 'CCR7-dependent cortex-to-medulla migration of positively selected thymocytes is essential for establishing central tolerance', *Immunity*, 24(2), pp. 165–177. doi:

10.1016/j.immuni.2005.12.011.

Lei, Y., Ripen, A. M., Ishimaru, N., Ohigashi, I., Nagasawa, T., Jeker, L. T., Bösl, M. R., Holländer, G. A., Hayashi, Y., De Waal Malefyt, R., *et al.* (2011) 'Aire-dependent production of XCL1 mediates medullary accumulation of thymic dendritic cells and contributes to regulatory T cell development', *Journal of Experimental Medicine*, 208(2), pp. 383–394. doi: 10.1084/jem.20102327.

Lind, E. F. *et al.* (2001) 'Mapping precursor movement through the postnatal thymus reveals specific microenvironments supporting defined stages of early lymphoid development', *Journal of Experimental Medicine*, 194(2), pp. 127–134. doi: 10.1084/jem.194.2.127.

Liu, C. *et al.* (2006) 'Coordination between CCR7- and CCR9-mediated chemokine signals in prevascular fetal thymus colonization', *Blood*, 108(8), pp. 2531–2539. doi: 10.1182/blood-2006-05-024190.

Liu, H. *et al.* (2016) 'Ubiquitin ligase MAR CH 8 cooperates with CD83 to control surface MHC II expression in thymic epithelium and CD4 T cell selection', *Journal of Experimental Medicine*, 213(9), pp. 1695–1703. doi: 10.1084/jem.20160312.

Lopes, N. *et al.* (2017) 'Administration of RANKL boosts thymic regeneration upon bone marrow transplantation', *EMBO Molecular Medicine*, 9(6), pp. 835–851. doi: 10.15252/emmm.201607176.

Lucas, B. *et al.* (2016) 'Lymphotoxin β Receptor Controls T Cell Progenitor Entry to the Thymus', *The Journal of Immunology*, 197(7), pp. 2665–2672. doi: 10.4049/jimmunol.1601189.

Lucas, B. *et al.* (2017) 'Progressive Changes in CXCR4 Expression That Define Thymocyte Positive Selection Are Dispensable for Both Innate and Conventional αβT-cell Development /631/250/1619/554 /631/250/1620/1840 /9 /13 /13/31 /13/51 /64 /64/60 article', *Scientific Reports*, 7(1), pp. 1–11. doi: 10.1038/s41598-017-05182-7.

Lucas, B. *et al.* (2020) 'Diversity in medullary thymic epithelial cells controls the activity and availability of iNKT cells', *Nature Communications*. Springer US, 11(1), pp. 1–14. doi: 10.1038/s41467-020-16041-x.

Luche, H. *et al.* (2011) 'The earliest intrathymic precursors of CD8α+ thymic dendritic cells correspond to myeloid-type double-negative 1c cells', *European Journal of Immunology*, 41(8), pp. 2165–2175. doi: 10.1038/jid.2014.371.

Mackall, C. L. *et al.* (1995) 'Age, thymopoiesis, and CD4+ t-lymphocyte regeneration after intensive chemotherapy', *New England Journal of Medicine*, 332(3), pp. 143–149. doi: 10.1056/NEJM199501193320303.

Mackall, C. L. *et al.* (1996) 'Thymic-independent T cell regeneration occurs via antigen-driven expansion of peripheral T cells resulting in a repertoire that is limited in diversity and prone to skewing.', *Journal of immunology (Baltimore, Md. : 1950)*, 156(12), pp. 4609–16.

Available at: http://www.ncbi.nlm.nih.gov/pubmed/8648103.

Mandala, S. *et al.* (2002) 'Alteration of Lymphocyte Trafficking by Sphingosine-1-Phosphate Receptor Agonists', *Science*, 296(5566), pp. 346 LP – 349. doi: 10.1126/science.1070238.

Masuda, K. *et al.* (2007) ' T Cell Lineage Determination Precedes the Initiation of TCR β Gene Rearrangement ', *The Journal of Immunology*, 179(6), pp. 3699–3706. doi: 10.4049/jimmunol.179.6.3699.

Maury, S. *et al.* (2001) 'Prolonged immune deficiency following allogeneic stem cell transplantation: Risk factors and complications in adult patients', *British Journal of Haematology*, 115(3), pp. 630–641. doi: 10.1046/j.1365-2141.2001.03135.x.

Mayer, C. E. *et al.* (2016) 'Dynamic spatio-temporal contribution of single β5t+ cortical epithelial precursors to the thymus medulla', *European Journal of Immunology*, 46(4), pp. 846–856. doi: 10.1002/eji.201545995.

Mayerova, D. and Hogquist, K. A. (2004) 'Central Tolerance to Self-Antigen Expressed by Cortical Epithelial Cells', *The Journal of Immunology*, 172(2), pp. 851–856. doi: 10.4049/jimmunol.172.2.851.

McCaughtry, T. M. *et al.* (2008) 'Clonal deletion of thymocytes can occur in the cortex with no involvement of the medulla', *Journal of Experimental Medicine*, 205(11), pp. 2575–2584. doi: 10.1084/jem.20080866.

Meredith, M. *et al.* (2015) 'Aire controls gene expression in the thymic epithelium with ordered stochasticity', *Nature Immunology*, 16(9), pp. 942–949. doi: 10.1038/ni.3247.

Miller, J. F. A. P. (1961) 'Immunological Function of the Thymus', *The Lancet*, 278(7205), pp. 748–749. doi: 10.1016/S0140-6736(61)90693-6.

Min, D. *et al.* (2002) 'Protection from thymic epithelial cell injury by keratinocyte growth factor: a new approach to improve thymic and peripheral T-cell reconstitution after bone marrow transplantation', *Blood*, 99(12), pp. 4592–4600. doi: 10.1182/blood.V99.12.4592.

Moore, N. C. *et al.* (1994) 'Differential expression of Mtv loci in MHC class II-positive thymic stromal cells.', *J. Immunol.*, 152, pp. 4826–4831.

Murata, S. *et al.* (2007) 'Regulation of CD8+ T cell development by thymus-specific proteasomes', *Science*, 316(5829), pp. 1349–1353. doi: 10.1126/science.1141915.

Nagamine, K. *et al.* (1997) 'Positional cloning of the APECED gene', *Nature Genetics*, 17(4), pp. 393–398. doi: 10.1038/ng1297-393.

Nakagawa, Y. *et al.* (2012) 'Thymic nurse cells provide microenvironment for secondary T cell receptor α rearrangement in cortical thymocytes', *Proceedings of the National Academy of Sciences of the United States of America*, 109(50), pp. 20572–20577. doi: 10.1073/pnas.1213069109.

Nedjic, J. *et al.* (2008) 'Autophagy in thymic epithelium shapes the T-cell repertoire and is essential for tolerance', *Nature*, 455(7211), pp. 396–400. doi: 10.1038/nature07208.

Nitta, T. *et al.* (2009) 'CCR7-mediated migration of developing thymocytes to the medulla is essential for negative selection to tissue-restricted antigens', *Proceedings of the National Academy of Sciences of the United States of America*, 106(40), pp. 17129–17133. doi: 10.1073/pnas.0906956106.

Nowell, C. S. *et al.* (2011) 'Foxn1 regulates lineage progression in cortical and medullary thymic epithelial cells but is dispensable for medullary sublineage divergence', *PLoS Genetics*, 7(11). doi: 10.1371/journal.pgen.1002348.

Obar, J. J. and Lefranois, L. (2010) 'Memory CD8+ T cell differentiation', *Annals of the New York Academy of Sciences*, 1183, pp. 251–266. doi: 10.1111/j.1749-6632.2009.05126.x.

Oftedal, B. E. *et al.* (2015) 'Dominant Mutations in the Autoimmune Regulator AIRE Are Associated with Common Organ-Specific Autoimmune Diseases', *Immunity*, 42(6), pp. 1185–1196. doi: 10.1016/j.immuni.2015.04.021.

Ohigashi, I. *et al.* (2013) 'Aire-expressing thymic medullary epithelial cells originate from β5t-expressing progenitor cells', *Proceedings of the National Academy of Sciences of the United States of America*, 110(24), pp. 9885–9890. doi: 10.1073/pnas.1301799110.

Ohigashi, I. *et al.* (2015) 'Adult Thymic Medullary Epithelium Is Maintained and Regenerated by Lineage-Restricted Cells Rather Than Bipotent Progenitors', *Cell Reports*. The Authors, 13(7), pp. 1432–1443. doi: 10.1016/j.celrep.2015.10.012.

Otagiri, M. *et al.* (2017) *Janeway ' S 9 Th Edition*, *America*. doi: 10.1007/978-981-10-2116-9.

Penit, C. and Ezine, S. (1989) 'Cell proliferation and thymocyte subset reconstitution in sublethally irradiated mice: Compared kinetics of endogenous and intrathymically transferred progenitors', *Proceedings of the National Academy of Sciences of the United States of America*, 86(14), pp. 5547–5551. doi: 10.1073/pnas.86.14.5547.

Perry, J. S. A. *et al.* (2014) 'Distinct contributions of Aire and antigen-presenting-cell subsets to the generation of self-tolerance in the thymus', *Immunity*. Elsevier Inc., 41(3), pp. 414–426. doi: 10.1016/j.immuni.2014.08.007.

Plotkin, J. *et al.* (2003) 'Critical Role for CXCR4 Signaling in Progenitor Localization and T Cell Differentiation in the Postnatal Thymus', *The Journal of Immunology*, 171(9), pp. 4521–4527. doi: 10.4049/jimmunol.171.9.4521.

Porritt, H. E. *et al.* (2004) 'Heterogeneity among DN1 prothymocytes reveals multiple progenitors with different capacities to generate T cell and non-T cell lineages', *Immunity*, 20(6), pp. 735–745. doi: 10.1016/j.immuni.2004.05.004.

Proietto, A. I. *et al.* (2008) 'Dendritic cells in the thymus contribute to T-regulatory cell

induction', *Proceedings of the National Academy of Sciences of the United States of America*, 105(50), pp. 19869–19874. doi: 10.1073/pnas.0810268105.

Rabasa, C. *et al.* (2015) 'Evidence against a critical role of CB1 receptors in adaptation of the hypothalamic-pituitary-adrenal axis and other consequences of daily repeated stress', *European Neuropsychopharmacology*. Elsevier, 25(8), pp. 1248–1259. doi: 10.1016/j.euroneuro.2015.04.026.

Radtke, F. *et al.* (1999) 'Deficient T cell fate specification in mice with an induced inactivation of Notch1', *Immunity*, 10(5), pp. 547–558. doi: 10.1016/S1074-7613(00)80054-0.

Report, B. D. (1995) 'Positive Selection of Mouse NK1 + T Cells by C131-expressing Cortical Thymocytes By Albert Bendelac', *Cell*, 182(December), pp. 2–7.

Rodewald, H. R. (1998) 'The thymus in the age of retirement', *Nature*, 396(6712), pp. 630–631. doi: 10.1038/25251.

Rosen, H. *et al.* (2003) 'Rapid induction of medullary thymocyte phenotypic maturation and egress inhibition by nanomolar sphingosine 1-phosphate receptor agonist', *Proceedings of the National Academy of Sciences of the United States of America*, 100(19), p. 10907—10912. doi: 10.1073/pnas.1832725100.

Rossi, F. M. V. *et al.* (2005) 'Recruitment of adult thymic progenitors is regulated by P-selectin and its ligand PSGL-1', *Nature Immunology*, 6(6), pp. 626–634. doi: 10.1038/ni1203.

Rossi, S. *et al.* (2002) 'Keratinocyte growth factor preserves normal thymopoiesis and thymic microenvironment during experimental graft-versus-host disease', *Blood*, 100(2), pp. 682–691. doi: 10.1182/blood.V100.2.682.

Rossi, S. W. *et al.* (2006) 'Clonal analysis reveals a common progenitor for thymic cortical and medullary epithelium', *Nature*, 441(7096), pp. 988–991. doi: 10.1038/nature04813.

Rossi, S. W. *et al.* (2007) 'RANK signals from CD4+3- inducer cells regulate development of Aire-expressing epithelial cells in the thymic medulla', *Journal of Experimental Medicine*, 204(6), pp. 1267–1272. doi: 10.1084/jem.20062497.

Roux, E. *et al.* (2000) 'Recovery of immune reactivity after T-cell-depleted bone marrow transplantation depends on thymic activity', *Blood*, 96(6), pp. 2299–2303. doi: 10.1182/blood.v96.6.2299.

Sakaguchi, S. and Sakaguchi, N. (1988) 'Thymus and autoimmunity: Transplantation of the thymus from cyclosporin a-treated mice causes organ-specific autoimmune disease in athymic nude mice', *Journal of Experimental Medicine*, 167(4), pp. 1479–1485. doi: 10.1084/jem.167.4.1479.

Sansom, S. N. *et al.* (2014) 'Population and single-cell genomics reveal the Aire dependency, relief from Polycomb silencing, and distribution of self-antigen expression in thymic epithelia', *Genome Research*, 24(12), pp. 1918–1931. doi: 10.1101/gr.171645.113.

Savino, W. *et al.* (1986) 'Thymic epithelium in AIDS. An immunohistologic study', *American Journal of Pathology*, 122(2), pp. 302–307.

Schlenner, S. M. *et al.* (2010) 'Fate Mapping Reveals Separate Origins of T Cells and Myeloid Lineages in the Thymus', *Immunity*, 32(3), pp. 426–436. doi: 10.1016/j.immuni.2010.03.005.

Scimone, M. L. *et al.* (2006) 'A multistep adhesion cascade for lymphoid progenitor cell homing to the thymus', *Proceedings of the National Academy of Sciences of the United States of America*, 103(18), pp. 7006–7011. doi: 10.1073/pnas.0602024103.

Sekai, M., Hamazaki, Y. and Minato, N. (2014) 'Medullary thymic epithelial stem cells maintain a functional thymus to ensure lifelong central T cell tolerance', *Immunity*. Elsevier Inc., 41(5), pp. 753–761. doi: 10.1016/j.immuni.2014.10.011.

Shah, D. K. and Zúñiga-Pflücker, J. C. (2014) 'An Overview of the Intrathymic Intricacies of T Cell Development', *The Journal of Immunology*, 192(9), pp. 4017–4023. doi: 10.4049/jimmunol.1302259.

Shakib, S. *et al.* (2009) 'Checkpoints in the Development of Thymic Cortical Epithelial Cells', *The Journal of Immunology*, 182(1), pp. 130–137. doi: 10.4049/jimmunol.182.1.130.

Shi, Y. *et al.* (2016) 'LTβR controls thymic portal endothelial cells for haematopoietic progenitor cell homing and T-cell regeneration', *Nature Communications*. Nature Publishing Group, 7, p. 12369. doi: 10.1038/ncomms12369.

Shinkai, Y. *et al.* (1992) 'RAG-2-deficient mice lack mature lymphocytes owing to inability to initiate V(D)J rearrangement', *Cell*, 68(5), pp. 855–867. doi: 10.1016/0092-8674(92)90029-C.

Singer, A. (2002) 'New perspectives on a developmental dilemma: The kinetic signaling model and the importance of signal duration for the CD4/CD8 lineage decision', *Current Opinion in Immunology*, 14(2), pp. 207–215. doi: 10.1016/S0952-7915(02)00323-0.

Stanley, S. K. *et al.* (1993) 'Human Iammunodeficiency Virus Infection of the Human Thymus and Disruption of the Thymic Microenviromnent in the SCID-hu Mouse', *Journal of Experimental Medicine*, 178(4), pp. 1151–1163. doi: 10.1084/jem.178.4.1151.

Strasser, A., Cory, S. and Adams, J. M. (2011) 'Deciphering the rules of programmed cell death to improve therapy of cancer and other diseases', *EMBO Journal*. Nature Publishing Group, 30(18), pp. 3667–3683. doi: 10.1038/emboj.2011.307.

Stritesky, G. L. *et al.* (2013) 'Murine thymic selection quantified using a unique method to capture deleted T cells', *Proceedings of the National Academy of Sciences of the United States of America*, 110(12), pp. 4679–4684. doi: 10.1073/pnas.1217532110.

Sun, Z., Unutmaz, D. and Zou, Y. (2000) 'Requirement for RORγ in Thymocyte Survival and UPKC ∼∼ C ∼ L', 288(June), pp. 4–8.

Szabo, S. J. *et al.* (2000) 'A novel transcription factor, T-bet, directs Th1 lineage commitment', *Cell*, 100(6), pp. 655–669. doi: 10.1016/S0092-8674(00)80702-3.

Takaba, H. *et al.* (2015) 'Fezf2 Orchestrates a Thymic Program of Self-Antigen Expression for Immune Tolerance', *Cell*. Elsevier Inc., 163(4), pp. 975–987. doi: 10.1016/j.cell.2015.10.013.

Takada, A. *et al.* (1969) 'Biphasic pattern of thymus regeneration after whole-body irradiation.', *The Journal of experimental medicine*, 129(3), pp. 445–457. doi: 10.1084/jem.129.3.445.

Teshima, T. *et al.* (2003) 'Impaired thymic negative selection causes autoimmune graft-versus-host disease', *Blood*, 102(2), pp. 429–435. doi: 10.1182/blood-2003-01-0266.

Thomas, D. E. *et al.* (1957) 'INTRAVENOUS INFUSION OF BONE MARROW IN PATIENTS RECEIVING RADIATION AND CHEMOTHERAPY', *The New England Journal of Medicine*.

Thomas, E. D. *et al.* (1977) 'One hundred patients with acute leukemia treated by chemotherapy, total body irradiation, and allogeneic marrow transplantation', *Blood*, 49(4), pp. 511–533. doi: 10.1182/blood.V49.4.511.511.

Tormo, A. *et al.* (2017) 'Interleukin-21 promotes thymopoiesis recovery following hematopoietic stem cell transplantation', *Journal of hematology & oncology*, 10(1), p. 120. doi: 10.1186/s13045-017-0490-3.

Trampont, P. C. *et al.* (2010) 'CXCR4 acts as a costimulator during thymic B-selection', *Nature Immunology*. Nature Publishing Group, 11(2), pp. 162–170. doi: 10.1038/ni.1830.

Ueno, T. *et al.* (2004) 'CCR7 signals are essential for cortex-medulla migration of developing thymocytes', *Journal of Experimental Medicine*, 200(4), pp. 493–505. doi: 10.1084/jem.20040643.

Uldrich, A. P. *et al.* (2006) 'Antigen Challenge Inhibits Thymic Emigration', *The Journal of Immunology*, 176(8), pp. 4553–4561. doi: 10.4049/jimmunol.176.8.4553.

URSO, P. and CONGDON, C. C. (1957) 'The Effect of the Amount of Isologous Bone Marrow Injected on the Recovery of Hematopoietic Organs, Survival and Body Weight after Lethal Irradiation Injury in Mice', *Blood*, 12(3), pp. 251–260. doi: 10.1182/blood.v12.3.251.251.

Vignali, D. A. A., Collison, L. W. and Workman, C. J. (2008) 'How regulatory T cells work', *Nature Reviews Immunology*, 8(7), pp. 523–532. doi: 10.1038/nri2343.

Wang, C. Y. *et al.* (1999) 'Cloning of Aire, the mouse homologue of the autoimmune regulator (AIRE) gene responsible for autoimmune polyglandular syndrome Type 1 (APS1)', *Genomics*, 55(3), pp. 322–326. doi: 10.1006/geno.1998.5656.

Wang, H. and Hogquist, K. A. (2018) 'CCR7 defines a precursor for murine iNKT cells in thymus and periphery', *eLife*, 7, pp. 1–20. doi: 10.7554/eLife.34793.

Weih, F. *et al.* (1995) 'Multiorgan inflammation and hematopoietic abnormalities in mice with a targeted disruption of RelB, a member of the NF-κB/Rel family', *Cell*, 80(2), pp. 331–340. doi: 10.1016/0092-8674(95)90416-6.

Weinberg, K. *et al.* (2001) 'Factors affecting thymic function after allogeneic hematopoietic stem cell transplantation', *Blood*, 97(5), pp. 1458–1466. doi: 10.1182/blood.V97.5.1458.

Wekerle, H., Ketelsen, U.-P. and Ernst, M. (1980) 'THYMIC NURSE CELLS L y m p h o e p i t h e l i a l Cell Complexes in M u r i n e T h y m u s e s : Morphological a n d Serological Characterization * BY HARTMUT WEKERLE , UWE-PETER KETELSEN , AND MARTIN ERNST From the Max-Planck-Institut filr Immunbiologi', 151(April), pp. 925–944.

White, A. J. *et al.* (2010) 'Lymphotoxin Signals from Positively Selected Thymocytes Regulate the Terminal Differentiation of Medullary Thymic Epithelial Cells', *The Journal of Immunology*, 185(8), pp. 4769–4776. doi: 10.4049/jimmunol.1002151.

White, A. J. *et al.* (2014) 'An Essential Role for Medullary Thymic Epithelial Cells during the Intrathymic Development of Invariant NKT Cells', *The Journal of Immunology*, 192(6), pp. 2659–2666. doi: 10.4049/jimmunol.1303057.

White, A. J. *et al.* (2017) 'A type 2 cytokine axis for thymus emigration', *Journal of Experimental Medicine*, 214(8), pp. 2205–2216. doi: 10.1084/jem.20170271.

Wu, L. and Shortman, K. (2005) 'Heterogeneity of thymic dendritic cells', *Seminars in Immunology*, 17(4), pp. 304–312. doi: 10.1016/j.smim.2005.05.001.

Wu, W. *et al.* (2017) 'Epithelial LTβR signaling controls the population size of the progenitors of medullary thymic epithelial cells in neonatal mice', *Scientific Reports*. Nature Publishing Group, 7(February), pp. 1–11. doi: 10.1038/srep44481.

Xiao, S. *et al.* (2017) 'Sublethal Total Body Irradiation Causes Long-Term Deficits in Thymus Function by Reducing Lymphoid Progenitors', *The Journal of Immunology*, 199(8), pp. 2701–2712. doi: 10.4049/jimmunol.1600934.

Xing, Y. *et al.* (2016) 'Late stages of T cell maturation in the thymus involve NF-κB and tonic type i interferon signaling', *Nature Immunology*. Nature Publishing Group, 17(5), pp. 565–573. doi: 10.1038/ni.3419.

Yagi, H. *et al.* (2000) 'Immunosuppressant FTY720 inhibits thymocyte emigration', *European Journal of Immunology*, 30(5), pp. 1435–1444. doi: 10.1002/(SICI)1521-4141(200005)30:5<1435::AID-IMMU1435>3.0.CO;2-O.

Zhang, S. L. *et al.* (2014) 'Chemokine treatment rescues profound T-lineage progenitor homing defect after bone marrow transplant conditioning in mice', *Blood*, 124(2), pp. 296–

304. doi: 10.1182/blood-2014-01-552794.

Zhu, J. and Paul, W. E. (2008) 'CD4 T cells: Fates, functions, and faults', *Blood*, 112(5), pp. 1557–1569. doi: 10.1182/blood-2008-05-078154.

Zhu, X. *et al.* (2007) 'Lymphohematopoietic progenitors do not have a synchronized defect with age-related thymic involution', *Aging Cell*, 6(5), pp. 663–672. doi: 10.1111/j.1474-9726.2007.00325.x.

Zinkernagel, R. M. *et al.* (1980) 'On the immunocompetence of H-2 incompatible irradiation bone marrow chimeras', *Journal of Immunology*, 124(5), pp. 2356–2365.

Zlotoff, D. A. *et al.* (2010) 'CCR7 and CCR9 together recruit hematopoietic progenitors to the adult thymus', *Blood*, 115(10), pp. 1897–1905. doi: 10.1182/blood-2009-08-237784.

Zlotoff, D. A. *et al.* (2011) 'Delivery of progenitors to the thymus limits T-lineage reconstitution after bone marrow transplantation', *Blood*, 118(7), pp. 1962–1970. doi: 10.1182/blood-2010-12-324954.

Zoller, A. L., Schnell, F. J. and Kersh, G. J. (2007) 'Murine pregnancy leads to reduced proliferation of maternal thymocytes and decreased thymic emigration', *Immunology*, 121(2), pp. 207–215. doi: 10.1111/j.1365-2567.2006.02559.x.

Zook, E. C. *et al.* (2011) 'Overexpression of Foxn1 attenuates age-associated thymic involution and prevents the expansion of peripheral CD4 memory T cells', *Blood*, 118(22), pp. 5723–5731. doi: 10.1182/blood-2011-03-342097.

Zubkova, I., Mostowski, H. and Zaitseva, M. (2005) 'Up-Regulation of IL-7, Stromal-Derived Factor-1α, Thymus-Expressed Chemokine, and Secondary Lymphoid Tissue Chemokine Gene Expression in the Stromal Cells in Response to Thymocyte Depletion: Implication for Thymus Reconstitution', *The Journal of Immunology*, 175(4), pp. 2321–2330. doi: 10.4049/jimmunol.175.4.2321.

Zúñiga-Pflücker, J. C. and Kruisbeek, A. M. (1990) 'Intrathymic radioresistant stem cells follow an IL-2/IL-2R pathway during thymic regeneration after sublethal irradiation.', *The Journal of Immunology*, 144(10), pp. 3736 LP – 3740. Available at: http://www.jimmunol.org/content/144/10/3736.abstract.